PERFORMANCE ANALYSIS OF BAND-LIMITED DS-CDMA SYSTEMS OVER GENERALIZED-*K* FADING CHANNELS

HAIDER MEHDI

2010

NANYANG TECHNOLOGICAL UNIVERSITY

PERFORMANCE ANALYSIS OF BAND-LIMITED DS-CDMA SYSTEMS OVER GENERALIZED-*K* FADING CHANNELS

HAIDER MEHDI

SCHOOL OF ELECTRICAL AND ELECTRONIC ENGINEERING

2010

PERFORMANCE ANALYSIS OF BAND-LIMITED DS-CDMA SYSTEMS OVER GENERALIZED-*K* FADING CHANNELS

HAIDER MEHDI

School of Electrical and Electronic Engineering

A thesis submitted to the Nanyang Technological University
in partial fulfillment of the requirement for the degree of
Doctor of Philosophy

2010

Statement of Originality

I hereby certify that content of this dissertation is the result of work done by me and has not been submitted for a higher degree to any other University.

_____ _____

Date Haider Mehdi

Acknowledgements

I take this opportunity to express my sincere gratitude to my supervisor Dr. Teh Kah Chan for his invaluable support and outstanding technical guidance during the course of my degree. I am grateful to Dr. Li Kwok Hung for providing generous help and excellent guidance throughout my research. Working with them was a wonderful experience. I am very grateful for their time and patience dedicated to my research and dissertation. I am deeply impressed with their enthusiasm for research, creative thinking, and organizational skills. Their technical expertise together with their patience has been a model for me to follow.

During my time at the Nanyang Technological University (NTU), I met numerous students and faculty who have made my Ph.D. experience all more rewarding, and to them I owe my thanks. I have not only learned valuable theoretical skills in wireless communications, but also inspirational ways to solve problems and enthusiasm in searching new ideas. It has been a privilege and great pleasure working with them. Finally, I would like to thank my family, for all their encouragement and patience.

Table of Contents

Summary

Direct-sequence spread-spectrum (DS-SS) has attracted considerable attention and has been adopted by many wireless communication vendors. Well-known communication systems employing DS-SS are based on the code-division multiple-access (CDMA) technique, such as global positioning system (GPS), wideband CDMA (WCDMA) system, etc. In practice, wireless channels are commonly modeled as a mixture of fading and shadowing. Various composite models have been reported in the literature. These models are based on lognormal distributions. The main disadvantage of these models is that they are mathematically complicated to analyze. Hence, the lognormal shadowing was approximated by a gamma shadowing leading to the *K* distribution and its generalized version, i.e., generalized-*K* distribution. This versatile distribution is useful in evaluating the performance of composite channels with simplicity and mathematical tractability. The BER performance of DS-CDMA systems has been extensively studied during the last two decades. However, most of the reported work is focused on DS-CDMA systems with rectangular pulse-shaping, while in practice, band-limited pulse shapes are adopted. Therefore, the performance analysis of band-limited systems is of considerable interest, and has gained some interest in the recently published literature.

The aim of this research is to analyze the BER performance of band-limited DS-CDMA systems over composite small-scale fading and shadowing channels. We consider generalized-*K* distribution in our BER analysis. We study conventional matched-filter based systems as well as decorrelator based multiuser detection systems. We consider both flat and frequency-selective multipath fading channels. Systems with

single-dimensional technique based on multipath diversity as well as two-dimensional scheme based on the combination of space and multipath diversity are considered. We present analytical BER expressions as a function of multiple-access interference (MAI), multitone jamming (MTJ) due to narrowband interference source, and the shadowing and fading parameters of the wireless channels.

In recent literature, there has been interest in the transmit diversity techniques in order to combat multipath fading and interference conditions. Such diversity schemes are commonly incorporated in the form of multiple transmitter and receiver antennas and are known as multiple-input multiple-output (MIMO) diversity schemes. We analyze MIMO systems based on the recently introduced space-time spreading scheme with two transmitter and multiple receiver antennas. We consider fast as well as slow frequency-selective multipath fading channels. The corresponding analytical BER expressions of space-time DS-CDMA systems with decorrelator based receivers are presented.

In our numerical analysis, we consider two types of band-limited pulse shapes, namely, spectrum raised cosine (SRC) and Beaulieu-Tan-Damen (BTD) pulses. From the numerical results, we observe that the systems with BTD pulse show better BER performance as compared to the ones with SRC pulse. We further observe that the presence of MTJ and MAI introduces an irreducible noise floor at high signal-to-noise ratio (SNR) levels. We also observe that the systems with two-dimensional diversity outperform the ones with single-dimensional diversity. From our BER analysis, we demonstrate that by incorporating generalized-K distribution, various scenarios of shadowing and fading can be easily analyzed.

List of Abbreviations

AM	Amplitude modulation
AWGN	Additive white Gaussian noise
BER	Bit-error rate
BPSK	Binary phase-shift keying
BTD	Beaulieu–Tan–Damen
CDMA	Code-division multiple-access
CF	Characteristic function
CLT	Central limit theorem
DS-CDMA	Direct-sequence code-division multiple-access
DS-SS	Direct-sequence spread-spectrum
EGC	Equal-gain combining
FH-SS	Frequency-hopping spread-spectrum
FIR	Finite impulse response
GA	Gaussian approximation
GPS	Global positioning system
GSM	Global systems for mobile communications
MAI	Multiple-access interference
MGF	Moment generating function
MIMO	Multiple-input multiple-output
MIP	Multipath intensity profile
MMSE	Minimum mean-squared error

MRC	Maximal-ratio combining
MTJ	Multitone jamming
MUD	Multiuser detection
NRZ	Non-return-to-zero
PDF	Probability density function
PG	Processing gain
PN	Pseudo-noise
PSD	Power spectral density
SC	Selection combining
SINR	Signal-to-interference-plus-noise ratio
SISO	Single-input single-output
SNR	Signal-to-noise power ratio
SRC	Spectrum raised-cosine
STBC	Space-time block code
STC	Space-time coding
STTC	Space-time trellis code
SJR	Signal-to-jamming power ratio
TCM	Trellis coded modulation
TDL	Tapped-delay line
WCDMA	Wideband code-division multiple-access
WLAN	wireless local area networks

List of Figures

Chapter 1

Introduction

The aim of this chapter is to give an overview of this research and the fundamental motivation behind it. Following that, we will present some of the main contributions of this research. Finally in the last section, we conclude this chapter with an outline of the thesis.

1.1 Background and Motivation

Wireless communication is one of the fastest growing technologies in recent years that has impacted our daily lives. The demand to accommodate high number of users, high data rates and mobility has spurred the introduction of services, products, and standards based on techniques like direct-sequence code-division multiple-access (DS-CDMA) systems, i.e., wireless local area networks (WLAN) [1], [2], global positioning system (GPS) [3], and cellular communication systems such as wideband CDMA (WCDMA) [4], [5] and cdma 2000 [6], [7]. DS-CDMA has many features that make it suitable for a secure and reliable communication system over a wireless channel. These features include good antijamming performance, its ability to combat multipath fading of the radio link, low power spectral density (PSD) level, privacy due to the use of unknown random spreading codes and multiple-access communication. An important parameter in the DS-CDMA scheme is the spreading factor or processing gain (PG), which is the ratio of the transmission bandwidth to the information bandwidth [6]. The processing gain plays a

key role in determining the number of users that can be supported in a system, the amount of multipath effect reduction, and the difficulty to jam the signal [6]. Increasing customer demand for high-speed services such as internet, video and multimedia traffic has resulted in more research towards such new technologies to accommodate these requirements. It has emerged as the predominant radio access technology for the regional and global wireless standards.

The DS-CDMA technology is designed to support simultaneous high data rate users [9]. However, impairments like additive white Gaussian noise (AWGN), multipath fading, multiple-access interference (MAI) and intentional or unintentional jamming may cause performance degradation. The randomness of wireless channels resulting from fading can be exploited to enhance performance through various diversity-combining techniques. There are a variety of diversity-combining techniques available and the most commonly used techniques are maximal-ratio combining (MRC) and equal-gain combining (EGC) [8]. Communication systems employ these combining techniques by either exploiting multipath diversity or the combination of both multipath and spatial schemes, i.e., two-dimensional diversity to improve signal-to-interference-plus-noise ratio (SINR) [8]. Moreover, various receivers based on multiuser detection (MUD) techniques have been studied in the literature to effectively combat MAI [6], [10]-[12]. Multiuser detection can substantially enhance the receiver performance and increase the capacity of DS-CDMA systems by exploiting the underlying structure of spreading waveforms of user signals. Instead of treating MAI as noise as in a conventional matched-filter receiver, MUD performs a joint detection of all the users' signals. The most commonly incorporated multiuser detector is the linear decorrelating detector [10], [11]. The linear

multiuser detectors are well established and studied due to their linear nature and ease of obtaining analytical results.

In a DS-CDMA system, the signaling waveform affects not only the spectral occupancy, but also the bit-error rate (BER) performance of the system [13]. This is because the statistical properties of the MAI depend on the actual shape of the signaling waveform. In [14], various time-limited signaling waveforms have been examined under the assumption that the channel bandwidth is infinite. Since the bandwidth of any practical system is limited, it is more useful to study and compare different signaling waveforms under some bandwidth constraints. For example, in CDMA IS-95 standard, the signaling waveforms are band-limited [15]. Practical DS-CDMA systems such as IS-95 and WCDMA implement pulse (or waveform) shaping to improve spectral efficiency and reduce out-of-band radio interference. WCDMA, for example, uses a spectrum raised-cosine (SRC) pulse [16]. Thus, a practical band-limited DS-CDMA system normally involves band-limitation filtering or pulse-shaping filtering to restrict out-of-band radiation [17]. Therefore, the performance analysis of band-limited systems is of considerable interest and has gained some attention recently [15]-[17]. Despite the fact that band-limited DS-CDMA systems are studied with some bandwidth constraint, they belong to the family of broadband systems. The use of large transmission bandwidths introduces some challenges. In particular, the successful deployment of these systems requires that they coexist with a variety of narrowband interfering signals [18], [19].

The aim of this research is to present the BER performance analysis of band-limited DS-CDMA systems over composite shadowing and small-scale fading channels. In order

to include such conditions in our BER analysis, we incorporate recently proposed generalized-*K* distribution due to its simplicity and mathematical tractability [20]. Additional wireless channel scenarios include multitone jamming (MTJ) caused by an intentional or unintentional jammer, MAI and AWGN.

1.2 Objective and Contributions

In this research, our objective is to present the analytical BER performance analysis of band-limited DS-CDMA systems over composite shadowing and fading wireless channels. We present analytical BER expressions for these systems under various channel fading and shadowing conditions by incorporating the recently proposed generalized-*K* model [20]. The generalized-*K* model has the advantages of simplicity, accuracy and mathematical tractability when compared with other distributions [20], [21]. It is known from the previous work that for the band-limited DS-CDMA systems, the main focus has been towards the scenarios with MAI and AWGN [15]. Therefore in this work, we analyze such band-limited systems with various pulse shapes in the presence of MTJ, MAI and AWGN.

The main contributions of this project are as follows. We first present analytical BER expressions for the space diversity, multipath diversity and the combination of two, i.e., two-dimensional diversity schemes with conventional matched-filter based systems. Two types of band-limited pulse shapes, namely, spectrum raised-cosine (SRC) [6] and Beaulieu–Tan–Damen (BTD) [22] are incorporated in our numerical analyses. Our analytical BER analysis can also be generalized to any type of band-limited pulse shape. We incorporate both EGC and MRC based systems. From our numerical analysis, we also observe that by incorporating the generalized-*K* model, we can easily analyze various

small scale fading and shadowing conditions of a wireless channel with ease and mathematical tractability. We also observe that the systems with BTD pulse shape show better performance as compared to the systems with SRC pulse shape. We further observe that the presence of MTJ and MAI produces an irreducible noise floor at high values of signal-to-noise power ratio (SNR). Our numerical analysis shows that by incorporating a two-dimensional diversity scheme, we can significantly improve BER performance as compared with multipath diversity alone. We also observe that by increasing the number of diversity branches, the gap between BER plots of the SRC and BTD based systems increases.

We further extend our BER analysis for the case of multiuser detection based systems. We consider linear decorrelator-based systems over a frequency selective multipath fading channel. Both single and two-dimensional diversity schemes are employed. We incorporate both EGC and MRC based systems. From our numerical analysis, we observe that the decorrelator-based systems outperform the ones without it for both type of pulses, i.e., SRC and BTD.

After studying the system with single transmitter antenna per user with single or multiple antennas at the receiver side, we then extend our analysis to the case of multiple-input multiple-output (MIMO) systems. We incorporate space-time spreading transmit diversity scheme based on space-time block code (STBC) technique, with 2-transmitter and multiple receiver antennas [23]. We consider decorrelator and minimum mean-squared error (MMSE) based MUD schemes. Both slow and fast fading conditions are analyzed. We also consider flat and frequency-selective multipath fading channels. From the numerical analysis, we observe that this space-time spreading based temporal and

spatial diversity technique can exploit both temporal and spatial diversity to enhance system SINR. We also observe that the systems under fast fading conditions show better BER performance than the ones under slow fading conditions.

1.3 Thesis Outline

The thesis is organized as follows. Chapter 2 provides some theoretical background studies of the related topics, such as band-limited systems, generalized-K fading model, MTJ and MIMO systems based on the space-time transmit diversity scheme. Chapter 3 presents the BER analysis of asynchronous band-limited DS-CDMA systems. Space diversity over a flat-fading environment and multipath as well as two-dimensional diversity scheme over frequency-selective multipath channel is studied. BTD and SRC band-limited pulse shapes are considered in the numerical analysis. In Chapter 4, we extend the BER analysis in Chapter 3 to the case of decorrelator-based schemes. In Chapter 5, we first discuss the synchronous band-limited DS-CDMA systems over flat-fading channels with space-time transmit diversity scheme. We consider both slow and fast fading conditions. We then extend the BER analysis in Chapter 5 for the case of asynchronous systems over frequency-selective multipath channels. Finally, Chapter 6 gives the final conclusion and future research work.

Chapter 2

Theoretical Background

Direct-sequence code-division multiple-access (DS-CDMA) systems have good ability to combat interference and fading [6] as well as the capability of multiple access. Due to these attractive features, band-limited DS-CDMA has been proposed as the major multiple-access method in the third-generation wireless communication standards [15]. However, most of the reported theoretical works focused on DS-CDMA systems with rectangular pulse-shaping, while in practice, for example in the CDMA IS-95 standard, the band-limited pulse shapes are considered. Therefore, the performance analysis of band-limited systems is of significant interest [16]. In this chapter, we provide some theoretical backgrounds of band-limited DS-CDMA systems over an AWGN channel. We then describe the generalized-K fading distribution in the following section. Next, we provide brief details about the multitone jamming (MTJ) model. Finally, in the last section of this chapter, an introduction to the multiple-input multiple-output (MIMO) based space-time spreading scheme is provided.

2.1 Overview of Band-limited DS-CDMA Systems

In DS-CDMA systems, data bits are spread by the pseudo-random code or pseudo-noise (PN) signal, which has a higher rate than the original signal [6]. The signal is then modulated and transmitted through the specified medium. Binary phase-shift keying (BPSK) is widely used as the digital modulation scheme for DS-CDMA systems. We will

consider BPSK as the modulation technique in this work. Once the modulated signal is received at the receiver, the signal is demodulated using a BPSK demodulator. This is then multiplied with the locally generated PN sequence. If the locally generated PN sequence is correlated with the one that was used in the transmitter, the original signal can be recovered. A DS-CDMA system can either be synchronous or asynchronous [6]. The uplink signal is often asynchronous in practice, while the downlink is synchronous [6]. In this chapter, we consider an asynchronous band-limited binary DS-CDMA system with K_u users over an AWGN channel. The received signal can be written as [15]

$$s(t) = \sum_{k=1}^{K_u} A_k \cos\left(2\pi f_S t + \theta_k\right) \sum_{n=-\infty}^{\infty} d_{\lfloor n/N \rfloor}^{(k)} c_n^{(k)} h\left(t - \tau_k - nT_C\right) + n(t) \tag{2.1}$$

where $n(t)$ is the AWGN term with two-sided power spectral density (PSD) $N_0/2$, $\lfloor z \rfloor$ indicates the integer portion of z, $d_{\lfloor n/N \rfloor}^{(k)} \in \{+1,-1\}$ is the k-th user's equiprobable data bit of duration T_b, T_C is the chip duration and $c_n^{(k)} \in \{+1,-1\}$ is the n-th chip of the k-th user's random spreading sequence. In (2.1), A_k is the amplitude of the k-th user's transmitted signal, f_S is the carrier frequency and the spreading factor is given by $N = T_b/T_C$. The random variables τ_k and θ_k represent time delay and carrier phase of the k-th user, and are uniformly distributed over $[0,T_C]$ and $[0,2\pi]$, respectively [15]. The received baseband chip pulse is denoted by $h(t)$ and it satisfies the energy constraint of $\int_{-\infty}^{\infty} |h(t)|^2 dt = T_C$. The received signal is then passed through the correlator structure, as shown in Fig. 2.1. It consists of a down-converter, a matched filter $H^*(f)$, a sampler, despreader and finally a summer, to give the final decision statistic. In Fig. 2.1, the

function $H^*(f)$ is the complex conjugate of $H(f)$ where $H(f)$ is the Fourier transform of $h(t)$. Without loss of generality, we assume that the transmitted bit is "+1" and user $k = 1$ is the desired user, with $\tau_1 = 0$ and $\theta_1 = 0$. In Fig. 2.1, the decision statistic of the correlator for our desired user is expressed as y^1, which can be expressed as [15]

$$y^1 = A_1 T_b + \Xi + \eta \tag{2.2}$$

where η is a zero-mean Gaussian random variable with variance [17]

$$\sigma_\eta^2 = N_0 \times N \int_{-\infty}^{\infty} |h(t)|^2 dt = N_0 T_b \tag{2.3}$$

and Ξ is the MAI component given by $\Xi = \sum_{k=2}^{K_u} \Xi_k$, where the term Ξ_k is defined as [15]

$$\Xi_k = A_k \cos(\theta_k) T_C \times \sum_{u=0}^{N-1} \sum_{n=-\infty}^{\infty} c_u^{(1)} b_n^{(k)} g\left((u-n)T_C - \tau_k\right). \tag{2.4}$$

The function $g(t)$ in (2.4) is the band-limited Nyquist pulse shape given by $g(t) = F^{-1}\left(|H(f)|^2 / T_C\right)$, where $F^{-1}(.)$ denotes the inverse Fourier transform operator. Also, $h(t) = F^{-1}\left(\sqrt{T_C G(f)}\right)$, where $G(f)$ is the Fourier transform of $g(t)$, and $b_n^{(k)} \in \{+1, -1\}$ is defined as $b_n^{(k)} = c_n^{(k)} d_{\lfloor n/N \rfloor}^{(k)}$ for $k = 2, \ldots, K_u$.

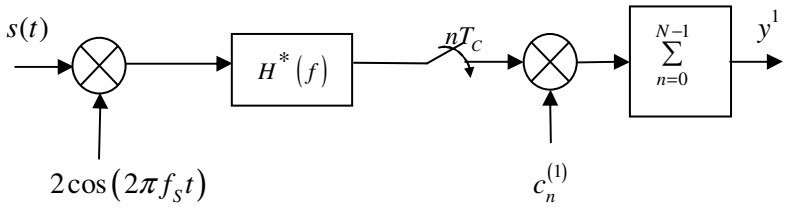

Figure 2.1: Correlator structure for an asynchronous band-limited DS-CDMA system.

In this research, we consider two types of band-limited pulse shapes for the numerical analysis, namely, the well-known spectrum raised cosine (SRC) [6] and newly proposed Beaulieu-Tan-Damen (BTD) [22] pulse. However, our BER analysis is valid for any type of band-limited pulse shape. The time functions of these pulses are defined as [6], [15], [22]

$$g_{SRC}(t) = \frac{\sin(\pi t/T_C)}{\pi t/T_C} \times \frac{\cos(\pi\beta t/T_C)}{1-4(\beta t/T_C)^2}$$

and

$$g_{BTD}(t) = \frac{\sin(2\pi Bt)}{2\pi Bt} \times \frac{4A\pi t\sin(2\pi B\beta t)+2A^2\cos(2\pi B\beta t)-A^2}{A^2+4(\pi t)^2},$$

respectively, where $\beta \in [0,1]$ is the excess bandwidth of the pulse, $B = 1/(2T_C)$ and $A = \ln(2)/(\beta B)$. In Figs. 2.2 and 2.3, the time and frequency domain characteristics, respectively, are presented for both types of pulse shapes. In [22], it was shown with the help of receiver eye diagrams that the BTD pulse has a more open receiver eye and a smaller probability of error in the presence of symbol timing error for the same excess bandwidth. In [15], BER analysis of asynchronous band-limited DS-CDMA systems with both types of pulses in the presence of MAI over Nakagami fading channels was performed and discussed. In [15], it has been shown for the MAI that

$$\gamma = \frac{2}{\beta}\left[1-\frac{1}{T_C^3}\int_{-\infty}^{\infty}\left|H(f)\right|^4 df\right]. \tag{2.5}$$

It can be observed that expression (2.5) depends on the frequency domain characteristics of the band-limited pulse shape. The effects of γ on the BER performance with respect to MAI will be discussed with the help of analytical expressions in the subsequent chapter.

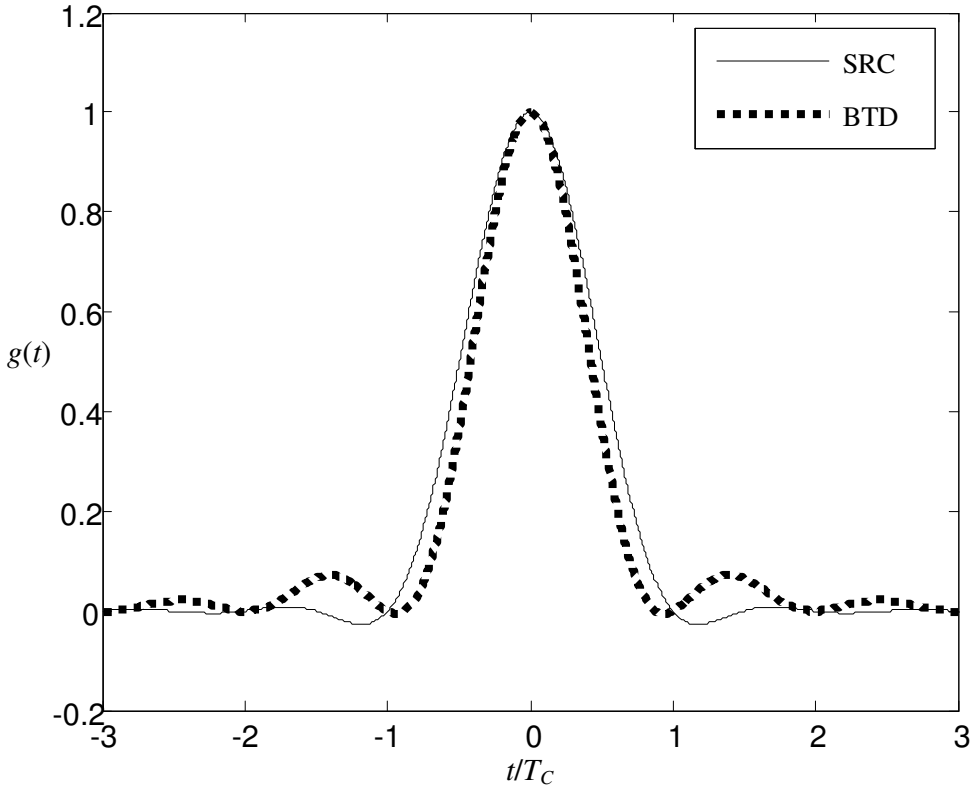

Figure 2.2: Time-domain characteristics of SRC and BTD pulses for an excess bandwidth of $\beta = 1$.

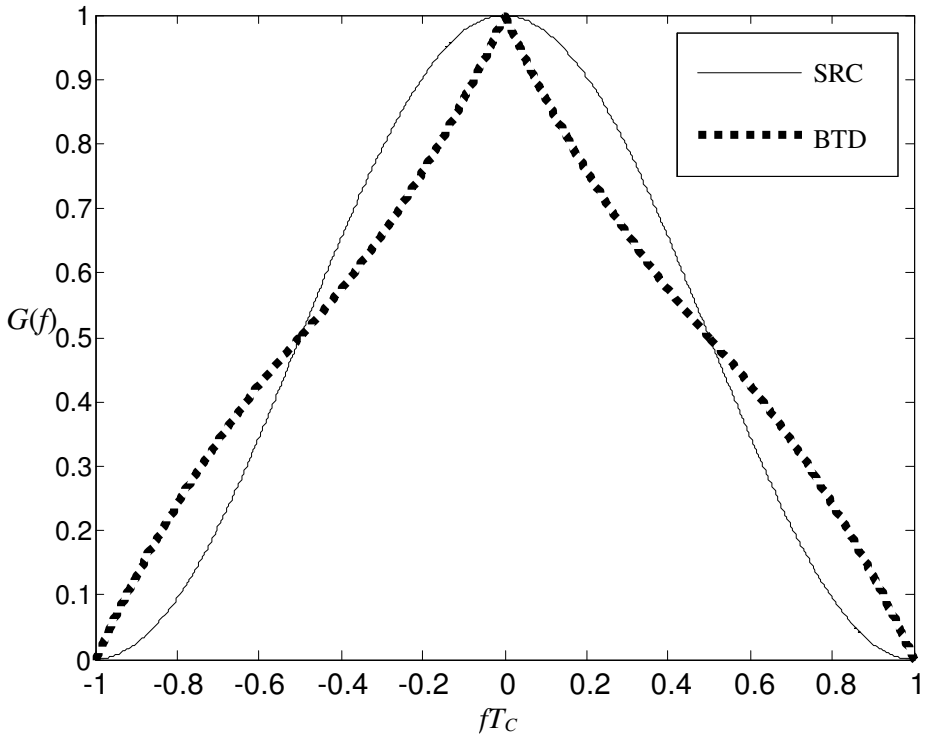

Figure 2.3: Frequency-domain characteristics of SRC and BTD pulses for an excess bandwidth of $\beta = 1$.

The spectrum expressions of these pulse shapes are given by [6], [15], [22]

$$G_{SRC}(f) = \begin{cases} T_C, & 0 \le |f| \le B(1-\beta) \\ \dfrac{T_C}{2}\left\{1+\cos\left(\dfrac{\pi T_C}{\beta}\left(|f|-(1-\beta)/2T_C\right)\right)\right\}, & B(1-\beta) \le |f| \le B(1+\beta) \\ 0, & |f| > B(1+\beta) \end{cases}$$

and

$$G_{BTD}(f) = \begin{cases} T_C, & 0 \le |f| \le B(1-\beta) \\ T_C \exp\{A(B(1-\beta)-|f|)\}, & B(1-\beta) \le |f| \le B \\ T_C - T_C \exp\{A(|f|-B(1+\beta))\}, & B \le |f| \le B(1+\beta) \\ 0, & |f| > B(1+\beta) \end{cases}$$

respectively.

2.2 Multipath Fading

Fading refers to the distortion that a carrier-modulated signal experiences over certain propagation media [8]. In wireless communications, multipath is the propagation phenomenon that results in radio signals reaching the receiving antenna by two or more paths. Causes of multipath effects include ionospheric reflection and refraction, and the reflection from terrestrial objects such as mountains and buildings [6]. As a result, the receiver receives the superposition of multiple copies of the transmitted signal, each traversing through a different path. Each signal copy experiences different attenuation, delay and phase shift while traveling from the source to the receiver. This can result in either constructive or destructive interference, amplifying or attenuating the signal power seen at the receiver. Mathematically, fading is usually modeled as a time-varying random change in the amplitude and phase of the transmitted signal [24].

Fading can be either flat or frequency-selective, depending upon the coherence bandwidth [6] of the system. Coherence bandwidth is a statistical measurement of the range of frequencies over which the channel can be considered ‘flat’. In other words, it is the approximate maximum bandwidth over which various frequencies of a signal are likely to experience comparable amplitude fading. In flat fading, the coherence bandwidth of the channel is larger than the bandwidth of the signal. In frequency-selective fading, the coherence bandwidth of the channel is smaller than the bandwidth of the signal [6], [8]. Hence, different frequency components of the signal may experience different amount of fading. Fading can also be described in terms of distances, i.e., whether the observation of the fluctuations in the envelope of a signal has been made over short or long distances. For a wireless channel, the former case will show rapid fluctuations in the

signal's envelope, while the latter will give a slowly varying and averaged view. For this reason, the first scenario is called small-scale fading, and the second scenario is referred to as shadowing [8]. Furthermore, with respect to the time variation of the channel characteristics, if the channel variations are faster than the symbol rate, the channel is a fast-fading channel; otherwise, it is a slow-fading channel.

A frequency-selective channel can be modeled as a finite impulse response (FIR) filter implemented with the tapped-delay line (TDL) model [6]. This TDL model consists of evenly spaced tap coefficients, each representing one resolved multipath. In this research, we assume a negative exponentially decaying multipath intensity profile (MIP) for the multipath gains given by [8]

$$\mathfrak{A}_{k,l} = \mathfrak{A}_{k,1} \exp\left(-\eta_k (l-1)\right) \tag{2.6}$$

for $\eta_k \geq 0$ and $l = 1, \ldots, L_p$. In (2.6), $\mathfrak{A}_{k,l} = \mathrm{E}\left(X_{k,l}^2\right)$ where $\mathrm{E}(.)$ is the expectation operator and $X_{k,l}$ is the random fading variable of the *k*-th user in the *l*-th multipath. From (2.6), we observe that the parameter $\mathfrak{A}_{k,l}$ is the average fading power of the *k*-th user's *l*-th resolvable multipath with respect to the first resolvable path's power, i.e., $\mathfrak{A}_{k,1}$. Also in (2.6), η_k is the rate of average power decay factor for the *k*-th user and L_p is the total number of resolvable paths. In this research, we assume η_k to have a common value for all users. Therefore, in our subsequent BER analysis we will use η instead of η_k. Fundamentally, fading causes poor BER performance in communication systems. The effects of fading can be combated by using diversity-combining techniques at the receiver. Modulation schemes such as DS-CDMA are well suited to utilize multipath diversity to provide robustness against fading conditions [24].

2.2.1 Generalized-*K* Model

Multipath fading is introduced due to the constructive and destructive combination of randomly delayed, reflected, scattered and diffracted signal components, while shadowing affects the link quality with slow variation of the mean level [8]. In many cases, multipath fading and shadowing occur simultaneously. This composite propagation environment consists of multipath fading superimposed by lognormal shadowing, resulting in lognormal based fading models, such as Rayleigh-, Ricean-, or Nakagami-lognormal fading channels [8]. However, such lognormal based fading models are analytically very difficult to handle and therefore rather complicated mathematical expressions have been derived for the performance of digital communication systems [25], [26]. An alternative approach is to employ the gamma distribution, which is mathematically a more versatile and accurate model to describe fading shadowing phenomena [27]. Based upon the gamma distribution, several generalized distributions have been proposed to serve useful composite fading channel models, e.g., the *K* distribution [28], [29], the generalized-*K* distribution [20], [21], [28], and the generalized-gamma distribution [30], [31]. Among them, the generalized-*K* distribution, which includes the *K* distribution as a special case, accurately approximates a great variety of fading and/or shadowing models [20], [28].

Based upon the Nakagami-*m* distribution, the author in [20] derived the probability density function (PDF) of the generalized-*K* distribution. The multipath fading observed in wireless systems is often modeled using the Nakagami-*m* distribution because it can account for various types of small-scale fading distributions depending on the value of *m* [8]. The probability density function (PDF) of the Nakagmai-*m* distribution is [8]

$$f_X(x) = \frac{2m^m x^{2m-1} e^{-\frac{m}{\bar{y}}x^2}}{\Gamma(m)\,\bar{y}^m}, \quad \text{for } x > 0 \tag{2.7}$$

where $\Gamma(.)$ is the gamma function, $m \in [0.5, \infty)$ is the Nakagami-*m* parameter and $\bar{y}$ is the average power given by $\mathrm{E}(X^2)$. In (2.7), $m = 1$ corresponds to Rayleigh statistics of the fading variable and $m > 1$ corresponds to Rician statistics. Values of *m* lower than 1 corresponds to severe fading. Such short term fading conditions modeled using the Nakagami-*m* distribution assumes that the average power received is fixed. In the absence of shadowing, the average power in (2.7) is deterministic. When shadowing or long term fading is present, $\bar{y}$ becomes a random variable. Thus, under conditions when shadowing also exists, (2.7) can be rewritten by conditioning the random fading variable as [20]

$$f_{X|\bar{Y}}\left(x|\bar{y}\right) = \frac{2m^m x^{2m-1} e^{-\frac{m}{\bar{y}}x^2}}{\Gamma(m)\,\bar{y}^m}, \quad \text{for } x > 0 \text{ and } \bar{y} > 0 \tag{2.8}$$

Also, the PDF of the fading variable in combined fading and shadowing is [20]

$$f_X(x) = \int_0^\infty f_{X|\bar{Y}}\left(x|\bar{y}\right) f_{\bar{Y}}\left(\bar{y}\right)\, d\bar{y} \tag{2.9}$$

where $f_{\bar{Y}}\left(\bar{y}\right)$ is the PDF of $\bar{y}$. The randomness of the average power is described as long term fading or shadowing and it is generally modeled in terms of a lognormal distribution for the average power [8]. Since shadowing and fading occur simultaneously, the Rayleigh-lognormal, and the Nakagami-lognormal models have been used to describe shadowed fading channels. All these models are hampered by the complicated mathematical form for the PDF. The gamma PDF is justified because the two-parameter

gamma PDF can be used as an approximate form of several probability density functions [20]. Therefore, $f_{\bar{Y}}\left(\bar{y}\right)$ can be expressed as

$$f_{\bar{Y}}\left(\bar{y}\right) = \frac{\left(\bar{y}\right)^{M-1} e^{-\frac{\bar{y}}{\bar{y}_0}}}{\Gamma\left(M\right)\bar{y}_0^{M}}, \quad \text{for } \bar{y} > 0 \tag{2.10}$$

where M is the order of the gamma PDF and $\bar{y}_0$ is a measure of the mean power. Finally, with the help of (2.9) and (2.10), the PDF of generalized-K distribution $f_X\left(x\right)$ is [20]

$$f_X\left(x\right) = \frac{b^{M+m} x^{M+m-1}}{2^{M+m-2}\Gamma\left(M\right)\Gamma\left(m\right)} K_{M-m}\left(bx\right), \quad \text{for } x > 0 \tag{2.11}$$

where $K_{M-m}(.)$ is the modified Bessel function of order $M-m$. The parameter b in (2.11) is given as $b = \sqrt{4m/\bar{y}_0}$ [20]. Various combinations of composite shadowing and fading conditions can be easily analyzed with the help of the generalized-K distribution. Note that in (2.11), m and M, respectively, are the small-scale fading and shadowing parameters of the generalized-K distribution. In (2.11), parameters M and m reflect the shadowing and small-scale fading severity of the wireless channel, respectively. The parameters M and m together describe the amount of fading (AF) in a wireless channel. The amount of fading is a measure of the severity of the fading effects [8]. When $m \rightarrow \infty$ and $M \rightarrow \infty$, $AF = 0$, we have a channel without any small-scale fading or shadowing effects. Small values of m and M correspond to the channel with severe fading and shadowing conditions. On the other hand, when $m \rightarrow \infty$ and $M \rightarrow \infty$, it will approach a channel without any fading or shadowing conditions. Also, as $M \rightarrow \infty$, it causes the absence of the shadowing effects in the wireless channel. Thus, making the wireless channel completely dependent on m and we have a pure Nakagami-m fading channel.

Hence, when $M \to \infty$ and $m = 1$, we have Rayleigh type channel. Similarly, when $M \to \infty$ and $m > 1$, we have Rician type characteristics for the wireless channel [20]. Under such condition, the relationship between the Rician K-factor and parameter m is given as [8]

$$K_{Rician} = \frac{\sqrt{m^2 - m}}{m - \sqrt{m^2 - m}}, \quad m \geq 1. \tag{2.12}$$

In (2.12), K_{Rician} is the Rician K-factor. Also, the n-th moment of the generalized-K random variable X can be expressed as [20]

$$\mathrm{E}\left(X^n\right) = \frac{\Gamma\left(M + \frac{n}{2}\right)\Gamma\left(m + \frac{n}{2}\right)}{\Gamma(M)\Gamma(m)}\left(\frac{2}{b}\right)^n. \tag{2.13}$$

Expression (2.13) can be used to find the relationships between the shadowing parameter M and various moments of the channel random fading variable X. Furthermore, by setting $n = 2$ in (2.13), we can obtain the relationship between parameter b and the second moment of X, i.e., $b = \sqrt{4Mm/\Omega}$, where $\Omega = \mathrm{E}\left(X^2\right)$ is the second moment of the random fading variable X [20]. It has been discussed in [6] and [21] that under practical conditions the path loss at a particular location is random and distributed log-normally. However, as discussed previously, log-normal based shadowing model gives mathematically complicated composite models [20]. Hence, as described in (2.10), gamma PDF was employed to approximate the log-normal shadowing. The parameter M is thus introduced as the order of the gamma PDF. In our subsequent BER analysis, we will incorporate generalized-K distribution to include shadowing and small-scale fading effects. The severity of composite shadowing and small-scale fading effects are varied with the values of both shadowing and small-scale fading parameters, i.e., M and m,

respectively. In Fig. 2.4, the variation in the PDF shape of generalized-*K* distribution can be observed for various values of *m* and *M*.

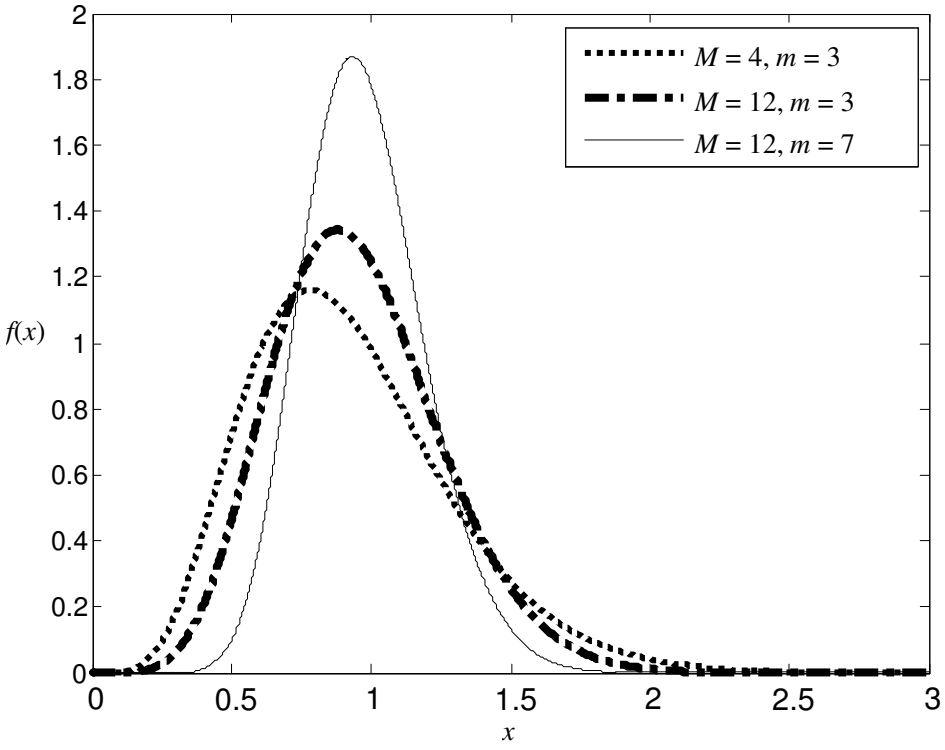

Figure 2.4: Generalized-*K* probability density functions for different values of *M* and *m*.

2.3 Multitone Jamming

DS-CDMA systems have wide transmission bandwidths [6]. Therefore, they are always susceptible to narrowband interference. Since the bandwidth of a DS-CDMA signal is much wider than that of narrowband interference or jammer, therefore narrowband interference can be approximated as multitone jamming (MTJ) [19]. Multitone jamming (MTJ) model is usually used to represent one or more interfering tones in the frequency band of a DS-CDMA system. Multitone jamming may arise from communication systems like frequency-hopping spread-spectrum (FH-SS) systems [32] and systems incorporating amplitude modulation (AM) or angle modulation. The MTJ term can be expressed as [6]

$$I(t) = \sum_{i=1}^{J} \alpha_i \cos\left(2\pi f_i t + \varphi_i\right) \tag{2.14}$$

where $J \geq 1$ represents the total number of independent jamming tones. The parameters α_i, f_i and φ_i are the amplitude, frequency, and random phase of the *i*-th jamming tone, respectively. The parameter φ_i is assumed to be uniformly distributed over $[0, 2\pi]$.

2.4 MIMO Space-Time Spreading Scheme

With applications such as video conferencing, extensive web browsing and live video streaming, future wireless systems become extremely demanding in terms of their requirements for high data rates and improved signal quality. Wireless communication systems that employ multiple transmitter and/or receiver antennas, known as multiple-input multiple-output (MIMO) systems have been shown to offer higher data rates and improved signal reliability than single-input single-output (SISO) systems [33]. A major phenomenon limiting the performance of wireless systems is multipath fading. Transmitter diversity techniques are widely proposed as a way to improve the performance of a system with a limited number of receiver antennas as in the case of mobile users where unit size and power are two major limitations. Space-time coding (STC) techniques based on MIMO are known to provide spatial diversity [34]. Two major classes of STC are, space-time trellis code (STTC) which is a generalization of trellis coded modulation (TCM) to multiple transmitter antennas [34], and space-time block code (STBC) [35] which is generalization of Alamouti's transmit diversity scheme [36] to multiple transmitter antennas. The application of STC with DS-CDMA, referred to as space-time spreading, was first introduced in [37]. In that work, the authors investigated

the performance of a new space-time spreading technique for DS-CDMA systems over quasi-static Rayleigh fading channels. The proposed space-time spreading technique was examined in a single-user DS-CDMA system where no multiuser interference was considered. In this research, we consider the space-time spreading scheme that was proposed in [23] and combines MIMO with multiuser access in a simple and effective way in the presence of MTJ over a generalized-K channel. Similar to [23], the system under consideration employs $L_T = 2$ antennas at the transmitter side and L_A antennas at the receiver side. The space-time spreading scheme in [23] can be described as follows. If we let d_1 and d_2 be the input bits of a user to the space-time encoder at the transmitter side, then each data symbol is modulated using two spreading codes, i.e., s_i, $i = 1, 2$. The encoder produces codewords $d_1 s_1 + d_2 s_2$ and $d_1 s_2 - d_2 s_1$ to be transmitted from antennas 1 and 2, respectively, during the first transmission period. In the second transmission period, these codewords are switched with respect to the antenna order. At the receiver side, each antenna has two correlators matched to each spreading sequence for the despreading purpose.

Chapter 3

BER Analysis of Diversity-Combining Receivers over Flat and Frequency-Selective Multipath Fading Channels

There are a variety of diversity-combining techniques available and the most frequently used ones are maximal-ratio combining (MRC) and equal-gain combining (EGC) [6]. The performance of these diversity-combining schemes in DS-CDMA systems has been studied in the literature [8]. In this chapter, we analyze the BER performance of MRC and EGC based techniques for asynchronous band-limited DS-CDMA systems. We study the BER performance of such diversity receivers under various scenarios of channel fading, shadowing, MAI, MTJ, and AWGN. In Section 3.1, we present an overview of the previous work and the contribution of our work. In Section 3.2, we present the BER analysis of band-limited systems over flat-fading channels with MRC and EGC based diversity systems. In Section 3.3, we present the BER analysis over frequency-selective multipath fading channels with single and two-dimensional techniques. Numerical results and discussions are presented in Section 3.4 with two types of band-limited pulse shapes, i.e., SRC [6] and BTD [22]. Finally, conclusions are drawn in Section 3.5.

3.1 Introduction

In this chapter, we investigate the BER performance of asynchronous band-limited DS-CDMA systems with various types of diversity-combining receivers over generalized-*K* fading channels. The effects of slow flat and frequency-selective fading are considered with conventional matched-filter detection technique. In the literature, various diversity techniques have been discussed and the most commonly used ones are MRC and EGC [38]. In MRC, each signal branch is multiplied by a weight factor that is proportional to the signal amplitude, such that more emphasis is placed on stronger components and less on weaker ones when the outputs of the correlators are summed before making symbol decision [6]. Thus, MRC requires the desired user's channel information. In EGC, each signal branch is weighted with the same factor, irrespective of the received signal amplitude [38]. Multi-dimensional diversity schemes involving the combination of two or more conventional means of realizing diversity (e.g., space and multipath) to provide better performance have recently received a good deal of attention [8]. For example, in the context of wideband CDMA, multi-dimensional diversity schemes are implemented in the form of two-dimensional RAKE receivers, consisting of an array of antennas, each followed by a conventional RAKE receiver [8].

Performance of various diversity schemes in wireless channels has been well studied in the literature [6]. Diversity receptions for DS-CDMA systems have been studied using various modulation techniques over a range of fading channels such as Rayleigh fading with lognormal shadowing, Rician fading and Nakagami fading [39]. In these works, non-return-to-zero (NRZ) pulse shapes were considered. However, as previously pointed out in Chapters 1 and 2, a practical DS-CDMA system usually employs pulse-shaping

filtering to restrict out-of-band radiation [40], [41]. In [42]-[43], the authors analyzed the BER performance of band-limited DS-CDMA systems with selection combining (SC), EGC and MRC over Nakagami fading channels. In [44], performance evaluation of a DS-CDMA system over frequency-selective Nakagami fading channels with RAKE combining was considered with various band-limited and time-limited pulses.

In this chapter, we study the BER performance of asynchronous band-limited DS-CDMA systems over generalized-K fading channels with various diversity-combining receivers. We incorporate generalized-K model in order to study the effects of composite shadowing and fading effects on the BER performance of the system. We analyze EGC and MRC based receivers for the space-diversity schemes over flat-fading channels as well as for the case of multipath frequency-selective fading channels. We consider both the single-dimensional and two-dimensional multipath diversity-combining schemes in our analyses. A two-dimensional diversity-combining scheme is a combination of two conventional means of realizing diversity, i.e., space and multipath [8]. Conventional matched-filter based system, random spreading, BPSK modulation scheme, asynchronous timing and independent generalized-K fading variables are assumed. In [40]-[44], only MAI and AWGN were considered. However, a DS-CDMA based system, because of its inherent wideband nature and coexistence with various narrowband systems, can be jammed by narrowband interference or MTJ [45]. Techniques based on the Gaussian approximation (GA) [15] are employed for the BER performance analyses. Therefore, MTJ and MAI are assumed to follow Gaussian distribution [6]. We consider Gaussian approximation because of its simplicity and thus, it leads to mathematically tractable BER expressions for the system and channel model that are incorporated in this research. Our

analytical and numerical results are valid for arbitrary number of diversity branches and arbitrary value of generalized-*K* fading parameters. In this chapter, we derive analytical BER expressions for asynchronous band-limited DS-CDMA systems employing conventional matched-filter based systems over generalized-*K* fading channels. Both shadowing and small-scale fading effects are incorporated in the BER analysis. Diversity schemes based on MRC and EGC are considered in order to combat fading effects. Numerical results are presented and analyzed by employing two types of band-limited pulse shapes, namely, spectrum raised-cosine (SRC) and Beaulieu–Tan–Damen (BTD).

3.2 Diversity Combining in Flat Fading

3.2.1 System Model

We consider an asynchronous band-limited DS-CDMA system with MTJ and AWGN over a generalized-*K* flat-fading channel. We assume K_u active users in the system. A unified representation of space diversity model with two types of diversity receptions, namely, EGC and MRC, is shown in Fig. 3.1a. The detailed model of the *l*-th correlator is shown in Fig. 3.1b. The receiver can combine receptions from L_A independent space diversity branches. The *l*-th branch received signal after co-phasing can be written as [15], [43]

$$s_l(t) = \sum_{k=1}^{K_u} A_k X_{k,l} \cos\left(2\pi f_S t + \theta_{k,l}\right) \sum_{n=-\infty}^{\infty} d_{\lfloor n/N \rfloor}^{(k)} c_n^{(k)} h\left(t - \tau_k - nT_C\right) + I_l(t) + n_l(t) \qquad (3.1)$$

where $I_l(t)$ is the MTJ term and $n_l(t)$ is the AWGN term with two-sided power spectral density (PSD) $N_0/2$. In (3.1), $d_{\lfloor n/N \rfloor}^{(k)} \in \{+1, -1\}$ is the *k*-th user's equiprobable data bit

of duration T_b, $\lfloor z \rfloor$ indicates the integer portion of z, and $c_n^{(k)} \in \{+1,-1\}$ is the n-th chip of the k-th user's random spreading sequence. Furthermore, spreading factor is given by $N = T_b/T_C$ where T_C is the chip duration, A_k is the amplitude of the k-th user's transmitted signal and f_S is the carrier frequency. The received baseband chip pulse is denoted by $h(t)$ and it satisfies the energy constraint of $\int_{-\infty}^{\infty} |h(t)|^2 dt = T_C$. The random variables τ_k and $\theta_{k,l}$ represent time delay and phase of the k-th user in the l-th diversity branch, and are uniformly distributed over $[0, T_C]$ and $[0, 2\pi]$, respectively [15]. The k-th user's independent fading amplitude in the l-th diversity branch, $X_{k,l}$, follows the generalized-K distribution [20]. We assume $k = 1$ as our desired user with $\tau_1 = 0$ and $\theta_{1,l} = 0$. In Fig. 3.1a, the output from the correlator of the l-th space diversity branch is represented as y_l^1. The output from the l-th correlator stage when we employ EGC or MRC is represented as $y_{EGC,l}^1$ and $y_{MRC,l}^1$, respectively. In addition, the variables y_{EGC}^1 and y_{MRC}^1 represent the outputs from the diversity-combining stage for EGC or MRC, respectively. The parameter ∂_l in Fig. 3.1b is the diversity reception weight parameter for the l-th branch [42]. Note that $\partial_l = 1$ for EGC, while $\partial_l = X_{1,l}$ for MRC [43]. The MTJ term in (3.1) can be expressed as [19]

$$I_l(t) = \sum_{i=1}^{J} \alpha_i \lambda_{l,i} \cos\left(2\pi f_i t + \varphi_{l,i}\right) \tag{3.2}$$

where $J \geq 1$ represents the total number of independent jamming tones. The parameters α_i and f_i are the amplitude and frequency of the i-th jamming tone, respectively. The

parameters $\lambda_{l,i}$ and $\varphi_{l,i}$ are the independent generalized-K fading variable and random phase of the i-th jamming tone, respectively. The parameter $\varphi_{l,i}$ is assumed to be uniformly distributed over $[0, 2\pi]$. Without loss of generality, we assume that bit "+1" is being transmitted. The decision statistic of the received signal at the l-th space diversity branch can be expressed as [42]

$$y_l^1 = D_l + \Xi_l + \hat{I}_l + \eta_l \tag{3.3}$$

where $D_l = \partial_l A_1 T_b X_{1,l}$, η_l is a zero-mean Gaussian random variable with variance of [17]

$$\sigma_{l,\eta}^2 = \partial_l^2 N_0 \times N \int_{-\infty}^{\infty} |h(t)|^2 dt = \partial_l^2 N_0 T_b. \tag{3.4}$$

In (3.3), Ξ_l is the MAI component and is given by $\Xi_l = \sum_{k=2}^{K_u} \Xi_{k,l}$ where [15]

$$\Xi_{k,l} = \partial_l A_k X_{k,l} T_C \cos(\theta_{k,l}) \sum_{u=0}^{N-1} \sum_{n=-\infty}^{\infty} c_u^{(1)} b_n^{(k)} g((u-n)T_C - \tau_k). \tag{3.5}$$

The function $g(.)$ in (3.5) denotes the band-limited Nyquist pulse shape [15] as discussed in Section 2.1 and the parameter $b_n^{(k)} \in \{+1, -1\}$ in (3.5) is defined as $b_n^{(k)} = c_n^{(k)} d_{\lfloor n/N \rfloor}^{(k)}$ where $\lfloor z \rfloor$ indicates the integer portion of z, and $k = 2, \ldots K_u$.

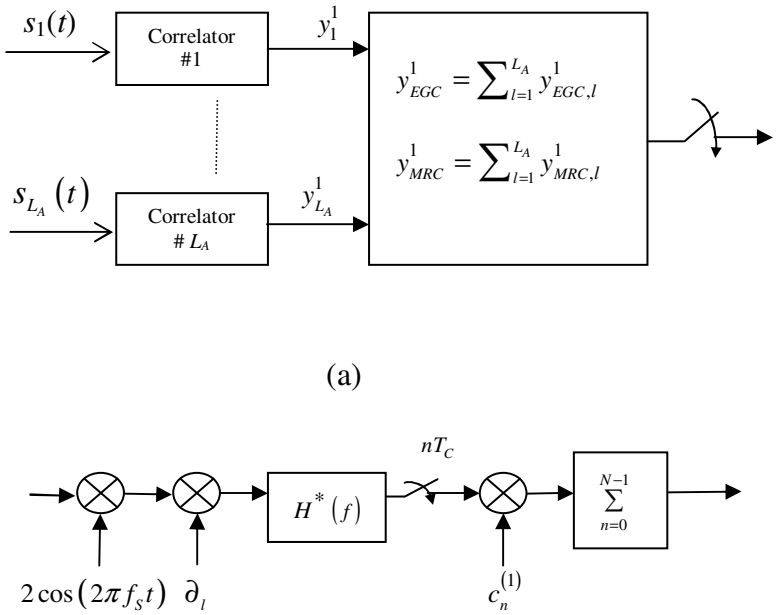

(a)

(b)

Figure 3.1: Receiver block diagram: (a) Space diversity model with L_A correlators and diversity-combining techniques, (b) Block diagram of the l-th space diversity branch correlator.

3.2.2 BER Analysis for Equal-Gain Combining

The BER performance of an L_A branch EGC receiver for the band-limited DS-CDMA system is analyzed in this section. The EGC-based system coherently combines the signals from L_A space diversity branches, to form the final decision statistic y_{EGC}^1 [42]. We assume that bit "+1" is being transmitted. The probability of bit error of the EGC-based system can be written as [43]

$$P_e = \Pr\left(y_{EGC}^1 = D_{EGC,L_A} + \Xi_{EGC,L_A} + \hat{I}_{EGC,L_A} + \eta_{EGC,L_A} < 0\right) \quad (3.6)$$

where $D_{EGC,L_A} = \sum_{l=1}^{L_A} D_l$, $\Xi_{EGC,L_A} = \sum_{l=1}^{L_A} \Xi_l$, $\hat{I}_{EGC,L_A} = \sum_{l=1}^{L_A} \hat{I}_l$ and $\eta_{EGC,L_A} = \sum_{l=1}^{L_A} \eta_l$,

where D_l, Ξ_l, $\hat{I}_l$ and η_l are the data, MAI, MTJ and AWGN components in the l-th branch of the receiver, respectively. The characteristic function (CF) with Gaussian approximation (GA) approach is adopted here to obtain the final BER expression. The CF of the AWGN component is given as [17]

$$\Phi_\eta(\omega) = \exp\left(-\omega^2\sigma_\eta^2/2\right) \tag{3.7}$$

where

$$\sigma_\eta^2 = N_0 \times N\int_{-\infty}^{\infty}\left|h(t)\right|^2 dt = N_0 T_b. \tag{3.8}$$

The CF of the MAI component is

$$\Phi_\Xi(\omega) = \exp\left(-\omega^2\sigma_\Xi^2/2\right). \tag{3.9}$$

Now, by assuming large values of K_u and N, the MAI component is assumed to follow Gaussian distribution with zero mean and variance σ_Ξ^2 [15]. In (3.9), the variance σ_Ξ^2 of the MAI component is [15]

$$\begin{aligned}\sigma_\Xi^2 &= \frac{1}{2}N\left[1-\gamma\beta/2\right]T_C^2\sum_{k=2}^{K_u}A_k^2\mathrm{E}\left(X_k^2\right)\\ &= 2N\left[1-\gamma\beta/2\right]T_C^2\sum_{k=2}^{K_u}A_k^2\frac{M_k m_k}{b_k^2}\end{aligned} \tag{3.10}$$

where $\gamma = \frac{2}{\beta}\left[1-\frac{1}{T_C^3}\int_{-\infty}^{\infty}\left|H(f)\right|^4 df\right]$ and $b_k = \sqrt{4M_k m_k/\mathrm{E}\left(X_k^2\right)}$, M_k and m_k are the generalized-K distribution parameters for the k-th $\left(k=2,\ldots K_u\right)$ MAI component. Moreover, we assume that various random fading variables of the MAI component are

independent of each other. With the help of (3.10), the overall unconditional CF of the Gaussian distributed MAI component is [42], [43]

$$\Phi_{\Xi}(\omega) = \prod_{k=2}^{K_u} \Phi_{\Xi_k}(\omega)$$

$$= \prod_{k=2}^{K_u} \exp\left(-\omega^2 N \left[1 - \gamma\beta/2\right] T_C^2 A_k^2 \frac{M_k m_k}{b_k^2} \right). \tag{3.11}$$

Next, we consider the MTJ component in (3.3) which can be expressed as [6], [17], [38]

$$\hat{I}_l = \sum_{i=1}^{J} \alpha_i \lambda_{l,i} \sum_{n=0}^{N-1} c_n^{(1)} \int_{-\infty}^{\infty} h\left(t - nT_c\right) \cos\left(2\pi \Delta f_i t + \varphi_{l,i}\right) dt. \tag{3.12}$$

In (3.12), the parameter Δf_i is defined as $\Delta f_i = f_i - f_S$ where f_S is the system carrier frequency and f_i is frequency of the i-th jamming tone, respectively. By considering large N and by invoking the central limit theorem (CLT) [6], we can view MTJ component as a Gaussian random variable with zero mean and a variance given as [6], [15], [38]

$$\sigma_{\hat{I}}^2 = \frac{1}{2} N T_C \sum_{i=1}^{J} \left(\alpha_i^2 \frac{\left[H\left(\Delta f_i\right)\right]^2}{T_C} \mathrm{E}\left(\lambda_{l,i}^2\right) \right)$$

$$= \frac{1}{2} T_b \sum_{i=1}^{J} \alpha_i^2 G\left(\Delta f_i\right) \mathrm{E}\left(\lambda_{l,i}^2\right)$$

$$= 2T_b \sum_{i=1}^{J} \left(\frac{\alpha_i^2 G\left(\Delta f_i\right) M_{(i)} m_{(i)}}{b_{(i)}^2} \right) \tag{3.13}$$

where $M_{(i)}$, $m_{(i)}$ and $b_{(i)} = \sqrt{4 M_{(i)} m_{(i)} / \mathrm{E}\left(\lambda_{l,i}^2\right)}$ are the generalized-K fading parameters of the i-th jamming tone. Also, we assume various random fading variables of the MTJ component to be independent of each other. With the help of (3.13), the CF of the Gaussian distributed MTJ term is [6]

$$\Phi_{\hat{I}}(\omega) = \exp\left(-\omega^2 T_b \sum_{i=1}^{J} \frac{\alpha_i^2 G(\Delta f_i) M_{(i)} m_{(i)}}{b_{(i)}^2}\right)$$

$$= \prod_{i=1}^{J} \exp\left(-\omega^2 T_b \frac{\alpha_i^2 G(\Delta f_i) M_{(i)} m_{(i)}}{b_{(i)}^2}\right). \tag{3.14}$$

Finally, the CF of $D_l = A_1 T_b X_{1,l}$ in (3.3) can be obtained as [46]

$$\Phi_{l,D}(\omega) = \mathrm{E}\left\{\exp\left(j\omega X_{1,l} A_1 T_b\right)\right\}$$

$$= \frac{{b_{l,D}}^{M_{l,D}+m_{l,D}}}{2^{M_{l,D}+m_{l,D}-2}\Gamma\left(m_{l,D}\right)\Gamma\left(M_{l,D}\right)}$$

$$\times \int_0^{\infty} x^{M_{l,D}+m_{l,D}-1} K_{M_{l,D}-m_{l,D}}\left(b_{l,D}x\right)\exp\left(j\omega x A_1 T_b\right)dx$$

$$= \frac{\sqrt{\pi}\,2^{2-2m_{l,D}}\,{b_{l,D}}^{2M_{l,D}}\Gamma\left(2M_{l,D}\right)\Gamma\left(2m_{l,D}\right)}{\Gamma\left(M_{l,D}\right)\Gamma\left(m_{l,D}\right)\Gamma\left(\Theta_{l,D}\right)}$$

$$\times \frac{\mu^{M_{l,D}}\,{}_2F_1\left(2M_{l,D}, \mathfrak{M}_{l,D}; \Theta_{l,D}; -\mu_{l,D}\right)}{\left[{b_{l,D}}^2 + \left(A_1 T_b \omega\right)^2\right]^{M_{l,D}}} \tag{3.15}$$

where $j = \sqrt{-1}$, $\Gamma(.)$ is the gamma function and ${}_2F_1(.)$ is the hypergeometric function given as [46]

$${}_2F_1(a,b;c;z) = \sum_{n=0}^{\infty} \frac{(a)_n (b)_n}{(c)_n} \frac{z^n}{n!},$$

where $(.)_n$ is the Pochhammer symbol [46]. In (3.15), the parameters $b_{l,D}$, $m_{l,D}$, and $M_{l,D}$ are the generalized-*K* distribution parameters for the random variable D_l. Note that in (3.15),

$$\Theta_{l,D} = M_{l,D} + m_{l,D} + 1/2, \tag{3.16}$$

$$\mathfrak{M}_{l,D} = M_{l,D} - m_{l,D} + 1/2 \tag{3.17}$$

and

$$\mu_{l,D} = \exp\left[j2\tan^{-1}\left(A_1 T_b \omega / b_{l,D}\right)\right]. \tag{3.18}$$

The final BER expression for the EGC case can be obtained by using the inversion formula as [43], [47]

$$P_e \approx \frac{1}{2} - \frac{1}{\pi}\int_0^{\infty} \frac{\Phi_{L_A,\eta}(\omega)\Phi_{L_A,\Xi}(\omega)\Phi_{L_A,\hat{I}}(\omega)\Im\left(\Phi_{L_A,D}(\omega)\right)}{\omega} d\omega \tag{3.19}$$

where $\Im(z)$ denotes the imaginary component of z. Moreover, the integration in (3.19) can be solved by incorporating any suitable numerical technique. In (3.19), the characteristic functions are [8]

$$\Phi_{L_A,D}(\omega) = \prod_{l=1}^{L_A} \Phi_{l,D}(\omega)$$

$$= \prod_{l=1}^{L_A} \frac{\sqrt{\pi}\, 2^{2-2m_{l,D}}\, {b_{l,D}}^{2M_{l,D}}\, \Gamma\left(2M_{l,D}\right)\Gamma\left(2m_{l,D}\right)}{\Gamma\left(M_{l,D}\right)\Gamma\left(m_{l,D}\right)\Gamma\left(\Theta_{l,D}\right)}$$

$$\times \frac{\mu^{M_{l,D}}\, {}_2F_1\left(2M_{l,D}, \mathfrak{M}_{l,D}; \Theta_{l,D}; -\mu_{l,D}\right)}{\left[{b_{l,D}}^2 + \left(A_1 T_b \omega\right)^2\right]^{M_{l,D}}}, \tag{3.20}$$

$$\Phi_{L_A,\Xi}(\omega) = \prod_{l=1}^{L_A}\Phi_{\Xi}(\omega)$$

$$= \prod_{l=1}^{L_A}\prod_{k=2}^{K_u}\exp\left(-\omega^2 N\left[1-\gamma\beta/2\right]T_C^2 A_k^2 \frac{M_k m_k}{b_k^2}\right)$$

$$= \left[\prod_{k=2}^{K_u}\exp\left(-\omega^2 N\left[1-\gamma\beta/2\right]T_C^2 A_k^2 \frac{M_k m_k}{b_k^2}\right)\right]^{L_A}$$

$$= \prod_{k=2}^{K_u}\exp\left(-\omega^2 L_A N\left[1-\gamma\beta/2\right]T_C^2 A_k^2 \frac{M_k m_k}{b_k^2}\right), \qquad (3.21)$$

$$\Phi_{L_A,\hat{I}}(\omega) = \prod_{l=1}^{L_A}\Phi_{\hat{I}}(\omega)$$

$$= \prod_{l=1}^{L_A}\prod_{i=1}^{J}\exp\left(-\omega^2 T_b \frac{\alpha_i^2 G(\Delta f_i) M_{(i)} m_{(i)}}{b_{(i)}^2}\right)$$

$$= \left[\prod_{i=1}^{J}\exp\left(-\omega^2 T_b \frac{\alpha_i^2 G(\Delta f_i) M_{(i)} m_{(i)}}{b_{(i)}^2}\right)\right]^{L_A}$$

$$= \prod_{i=1}^{J}\exp\left(-\omega^2 L_A T_b \frac{\alpha_i^2 G(\Delta f_i) M_{(i)} m_{(i)}}{b_{(i)}^2}\right) \qquad (3.22)$$

and

$$\begin{aligned}\Phi_{L_A,\eta}(\omega) &= \prod_{l=1}^{L_A}\exp\left(-\omega^2\sigma_\eta^2/2\right)\\ &= \prod_{l=1}^{L_A}\exp\left(-\omega^2 N_0 T_b/2\right)\\ &= \left[\exp\left(-\omega^2 N_0 T_b/2\right)\right]^{L_A}\\ &= \exp\left(-\omega^2 L_A N_0 T_b/2\right).\end{aligned} \tag{3.23}$$

From (3.19), we observe that by using the generalized-*K* distribution shadowing and fading effects can be incorporated in the BER analysis without much extra computational complexity.

3.2.3 BER Analysis for Maximal-Ratio Combining

The probability of bit error based on the final decision statistic for the MRC case is [43]

$$P_e = \Pr\left(y_{MRC}^1 = D_{MRC,L_A} + \Xi_{MRC,L_A} + \hat{I}_{MRC,L_A} + \eta_{MRC,L_A} < 0\right) \tag{3.24}$$

where $D_{MRC,L_A} = A_1 T_b X_M$ and $X_M = \sum_{l=1}^{L_A} X_{1,l}^2$. The random variables Ξ_{MRC,L_A}, I_{MRC,L_A} and η_{MRC,L_A} represent the MAI, MTJ and AWGN components, respectively. We observe from (3.24) that the weighted outputs from the L_A space diversity branches are coherently combined before the decision stage. Based on the approach presented in Section 3.2.2, by using Gaussian approximation, the variance expressions of AWGN, MAI, and MTJ components are [43]

$$\sigma_{L_A,\eta}^2 = X_M N_0 \times N\int_{-\infty}^{\infty}\left|h(t)\right|^2 dt = X_M N_0 T_b, \tag{3.25}$$

$$\sigma^2_{L_A,\Xi} = 2X_M N\left[1-\gamma\beta/2\right]T_C^2\sum_{k=2}^{K_u} A_k^2\frac{M_k m_k}{b_k^2} \tag{3.26}$$

and

$$\sigma^2_{L_A,\hat{I}} = 2T_b X_M \sum_{i=1}^{J}\frac{\alpha_i^2 G\left(\Delta f_i\right)M_{(i)}m_{(i)}}{b^2_{(i)}}, \tag{3.27}$$

respectively. Based on (3.24), the conditional BER expression for the MRC case is [43]

$$P_e\left(\gamma_l\right) \approx Q\left(\sqrt{\frac{\left(A_1T_b\right)^2 X_M}{N_0T_b+V_\Xi+V_\Upsilon}}\right)$$

$$= Q\left(\sqrt{\sum_{l=1}^{L_A}2\gamma_l}\right) \tag{3.28}$$

where $Q(x)$ is the Gaussian Q function [6] which can also be represented as [8]

$$Q(x) = \frac{1}{\pi}\int_0^{\pi/2}\exp\left(-\frac{x^2}{2\sin^2\theta}\right)d\theta, \qquad \text{for } x\geq 0. \tag{3.29}$$

In (3.28), $V_\Xi = \sigma^2_{L_A,\Xi}/X_M$, $V_\Upsilon = \sigma^2_{L_A,\hat{I}}/X_M$, and $2\gamma_l$ represents the output signal-to-interference-plus-noise ratio (SINR) at the l-th branch of the diversity receiver with $\gamma_l = CX^2_{0,l}$, where

$$C = \frac{\left(A_1T_b\right)^2}{2\left(N_0T_b+V_\Xi+V_\Upsilon\right)}. \tag{3.30}$$

Now, by using the modified form of the Gaussian Q function, we can express (3.28) as

$$P_e\left(\gamma_l\right) \approx \frac{1}{\pi}\int_0^{\pi/2}\exp\left(-\frac{\sum_{l=1}^{L_A}\gamma_l}{\sin^2\theta}\right)d\theta$$

$$= \frac{1}{\pi}\int_0^{\pi/2}\prod_{l=1}^{L_A}\exp\left(-\frac{\gamma_l}{\sin^2\theta}\right)d\theta. \tag{3.31}$$

Using the moment generating function (MGF) based approach, the unconditional BER expression can be written as [8]

$$P_e \approx \frac{1}{\pi}\int_0^{\pi/2}\prod_{l=1}^{L_A}\overline{\chi_l}\left(b_{l,D},M_{l,D},m_{l,D},\theta\right)d\theta. \tag{3.32}$$

The integral in (3.32) can be solved with the help of numerical technique. In (3.32), the parameter $\overline{\chi_l}\left(b_{l,D},M_{l,D},m_{l,D},\theta\right)$ is given as [8], [46]

$$\overline{\chi_l}\left(b_{l,D},M_{l,D},m_{l,D},\theta\right) = \int_0^{\infty}\exp\left(-\frac{Cx^2}{\sin^2\theta}\right)f_{X_{l,D}}\left(x\right)dx$$

$$= \left(\frac{b_{l,D}\sin\theta}{2\sqrt{C}}\right)^{M_{l,D}+m_{l,D}-1}\times\exp\left(\frac{b_{l,D}^2\sin^2\theta}{8\times C}\right)$$

$$\times W_{-\frac{1}{2}\left(M_{l,D}+m_{l,D}-1\right),\frac{1}{2}\left(M_{l,D}-m_{l,D}\right)}\left(\frac{b_{l,D}^2\sin^2\theta}{4\times C}\right). \tag{3.33}$$

In (3.33), $W_{x,y}\left(z\right)$ is the Whittaker function and is defined as [46]

$$W_{x,y}\left(z\right)=\frac{\exp\left(-z/2\right)z^x}{\Gamma\left(\frac{1}{2}-x+y\right)}\int_0^{\infty}t^{-x+y-\frac{1}{2}}\left(1+\frac{t}{z}\right)^{x+y-\frac{1}{2}}\exp\left(-t\right)dt. \tag{3.34}$$

Also, $f_{X_{l,D}}\left(x\right)$ is the generalized-K distribution of the desired user's random fading variable. It can be seen from (3.19) and (3.32) that the BER performance of EGC and MRC, respectively, can be computed for any arbitrary values of L_A and the generalized-K

distribution parameters. Also, by using the generalized-*K* model, we can study the composite effects of shadowing and fading on BER performance with mathematical tractability and simplicity.

In the followings, we will consider a special scenario of the MRC based space diversity systems in the absence of shadowing effects, i.e., when $M \to \infty$. Under such conditions, the generalized-*K* fading channel can be described as a Nakagami-*m* fading channel [20]. We further assume random fading variables of the desired user's signal in various branches of the receiver are independent and identically distributed. Under such conditions and with the help of [43], the probability density function of the random fading variable $X_M = \sum_{l=1}^{L_A} X_{1,l}^2$ can be expressed as

$$f_{X_M}(x) = \frac{1}{\Gamma(mL_A)} \left(\frac{m}{\mathrm{E}\left(X_1^2\right)} \right)^{mL_A} \exp\left(\frac{-m}{\mathrm{E}\left(X_1^2\right)} \right) x^{mL_A - 1}, \qquad \text{for } x > 0.$$

By using the expression of $f_{X_M}(x)$, the unconditional BER expression is given as [43]

$$P_e \approx \int_0^\infty Q\left(\sqrt{2CX_M}\right) f_{X_M}(x)\, dx$$

$$= \frac{\Gamma\left(mL_A + \frac{1}{2}\right)}{2\sqrt{\pi} mL_A \Gamma(mL_A)} \times \left[\frac{m}{C\ \mathrm{E}\left(X_1^2\right)} \right]^{mL_A}$$

$$\times {}_2F_1\left(mL_A, mL_A + \frac{1}{2}; mL_A + 1; \frac{-m}{C\ \mathrm{E}\left(X_1^2\right)} \right) \tag{3.35}$$

where C in (3.35) follows the same definition as in (3.30), i.e., $C = \dfrac{\left(A_1 T_b\right)^2}{2\left(N_0 T_b + V_\Xi + V_\Upsilon\right)}$, and m is the small-scale fading parameter. The simplified BER expression in (3.35) is valid for arbitrary number of branches as well as arbitrary values of parameter m.

3.3 Diversity-Combining over Multipath Frequency-Selective Fading Channels

3.3.1 Single-Dimensional Diversity with EGC

In this section, we consider an asynchronous DS-CDMA band-limited communication system with MTJ and AWGN over a frequency-selective generalized-K fading channel. The received signal is [6]

$$r_l(t) = \sum_{k=1}^{K_u} \sum_{l=1}^{L_p} A_k X_{k,l} \cos\left(2\pi f_S t + \theta_{k,l}\right) \sum_{n=-\infty}^{\infty} d_{\lfloor n/N \rfloor}^{(k)} c_n^{(k)} h\left(t - \tau_k - lT_C - nT_C\right) + I_l(t) + n_l(t) \tag{3.36}$$

where $I_l(t)$ and $n_l(t)$ are the MTJ and AWGN components, respectively. In (3.34), L_p is the total number of resolvable paths and $X_{k,l}$ denotes the independent random fading variable for the k-th user in the l-th multipath. We assume a negative exponentially decaying multipath intensity profile (MIP) given by [8]

$$\mathfrak{A}_{k,l} = \mathfrak{A}_{k,1} \exp\left(-\eta\ (l-1)\right) \tag{3.37}$$

for $\eta \geq 0$ and $l = 1, \ldots, L_p$, where $\mathfrak{A}_{k,l}$ is the average signal strength relative to the first resolvable multipath component, i.e., $\mathfrak{A}_{k,1}$, η is the rate of average power decay for the

system. In this research, we assume η to have a common value for all users. The multipath fading variables are assumed to be independent of each other. The multipath receiver consists of a bank of L_r filters, matched to the delayed versions of the user's random signature waveform, where $L_r \le L_p$. The BER performance of an L_r branch EGC receiver for the band-limited DS-CDMA system is analyzed in this section. The EGC based system coherently combines the signals from L_r multipath diversity branches, to form the final decision statistic $Z_{1,EGC}$ [42]. The probability of bit error based on the decision statistic for the EGC based system can be written as [6]

$$Z_{1,EGC} = D_{1,EGC} + I_{MAI,EGC} + I_{SI,EGC} + I_{MTJ,EGC} + I_{\eta,EGC} \tag{3.38}$$

where $D_{1,EGC}$, $I_{SI,EGC}$, $I_{MAI,EGC}$, $I_{MTJ,EGC}$ and $I_{\eta,EGC}$ are the desired data, self-interference, MAI, MTJ and Gaussian noise components, respectively. Note that $D_{1,EGC} = \sum_{l=1}^{L_r} D_l = \sum_{l=1}^{L_r} A_1 T_b X_{1,l}$, $I_{SI,EGC} = \sum_{l=1}^{L_r} I_{SI,EGC,l}$, $I_{MAI,EGC} = \sum_{l=1}^{L_r} I_{MAI,EGC,l}$, $I_{MTJ,EGC} = \sum_{l=1}^{L_r} I_{MTJ,EGC,l}$ and $I_{\eta,EGC} = \sum_{l=1}^{L_r} I_{\eta,EGC,l}$, where $I_{SI,EGC,l}$, $I_{MAI,EGC,l}$, $I_{MTJ,EGC,l}$ and $I_{\eta,EGC,l}$ are the self-interference, MAI, MTJ and AWGN components in the l-th branch of the receiver, respectively. The characteristic function (CF) with Gaussian approximation (GA) approach is adopted here. The variance expressions of the MAI and self-interference components are [44]

$$\sigma^2_{MAI,EGC} = \frac{NT_C^2}{2}\left[1-\gamma\beta/2\right] q\left(L_p,\eta\right) \sum_{k=2}^{K_u} A_k^2 \mathfrak{A}_{k,1} \tag{3.39}$$

and

$$\sigma^2_{SI,EGC} = \frac{NT_C^2 A_1^2 \mathfrak{A}_{1,1}}{2}\left[q\left(L_p,\eta\right)-1\right], \tag{3.40}$$

respectively. In (3.39) and (3.40), the parameter $q\left(L_p,\eta\right)$ is defined as [44]

$$q\left(L_p,\eta\right) = \sum_{l=1}^{L_p}\exp\left(-\eta\left(l-1\right)\right) = \left[\frac{1-\exp\left(-\eta L_p\right)}{1-\exp\left(-\eta\right)}\right] \tag{3.41}$$

and $\mathfrak{A}_{1,l} = \mathfrak{A}_{1,1}\exp\left(-\eta\ \left(l-1\right)\right)$ for $\eta \geq 0$ and $l = 1,\ldots,L_p$. The CF of the self-interference component is

$$\Phi_{SI,EGC}\left(\omega\right) = \exp\left(-\omega^2\frac{NT_C^2 A_1^2 \mathfrak{A}_{1,1}}{4}\left[q\left(L_p,\eta\right)-1\right]\right). \tag{3.42}$$

Similarly, the CF of the MAI component is given as

$$\Phi_{MAI,EGC}\left(\omega\right) = \prod_{k=2}^{K_u}\exp\left(-\omega^2\frac{NT_C^2}{4}\left[1-\gamma\beta/2\right]q\left(L_p,\eta\right)A_k^2\mathfrak{A}_{k,1}\right). \tag{3.43}$$

The characteristic functions of the MTJ, Gaussian noise and the data term for the *l*-th diversity branch have the same form as the one shown in Section 3.2.2. Now, by assuming that all the fading variables are independent of each other, the final BER expression for the EGC case can be obtained by using the inversion formula as [42], [47]

$$P_e \approx \frac{1}{2}-\frac{1}{\pi}\int_0^{\infty}\frac{\Phi^{L_r}_{\eta,EGC}\left(\omega\right)\Phi^{L_r}_{SI,EGC}\left(\omega\right)\Phi^{L_r}_{MAI,EGC}\left(\omega\right)\Phi^{L_r}_{MTJ,EGC}\left(\omega\right)\Im\left(\Phi_D\left(\omega\right)\right)}{\omega}d\omega \tag{3.44}$$

The integral in (3.44) can be solved by using any suitable numerical technique. In (3.44), the characteristic functions of the data, MAI, MTJ, self-interference and Gaussian noise terms are

$$\Phi_D(\omega) = \prod_{l=1}^{L_r} \Phi_{l,D}(\omega)$$

$$= \prod_{l=1}^{L_r} \frac{\sqrt{\pi} 2^{2-2m_{1,l}} {b_{1,l}}^{2M_{1,l}} \Gamma(2M_{1,l}) \Gamma(2m_{1,l})}{\Gamma(M_{1,l}) \Gamma(m_{1,l}) \Gamma(\Theta_{1,l})}$$

$$\times \frac{\mu^{M_{1,l}} {}_2F_1(2M_{1,l}, \mathfrak{M}_{1,l}; \Theta_{1,l}; -\mu_{1,l})}{\left[{b_{1,l}}^2 + (A_1 T_b \omega)^2 \right]^{M_{1,l}}}, \tag{3.45}$$

$$\Phi_{MAI,EGC}^{L_r}(\omega) = \prod_{k=2}^{K_u} \exp\left(-\omega^2 L_r \frac{NT_C^2}{4} \left[1 - \gamma\beta/2 \right] q(L_p, \eta) A_k^2 \mathfrak{A}_{k,1} \right), \tag{3.46}$$

$$\Phi_{MTJ,EGC}^{L_r}(\omega) = \prod_{i=1}^{J} \exp\left(-\omega^2 L_r T_b \frac{\alpha_i^2 G(\Delta f_i) M_{(i)} m_{(i)}}{b_{(i)}^2} \right), \tag{3.47}$$

$$\Phi_{SI,EGC}^{L_r}(\omega) = \exp\left(-\omega^2 L_r \frac{NT_C^2 A_1^2 \mathfrak{A}_{1,1}}{4} \left[q(L_p, \eta) - 1 \right] \right) \tag{3.48}$$

and

$$\Phi_{\eta,EGC}^{L_r}(\omega) = \exp\left(-\omega^2 L_r N_0 T_b / 2 \right), \tag{3.49}$$

respectively.

3.3.2 Single-Dimensional Diversity with MRC

We incorporate MRC as the diversity-combining technique in this section. The individual matched-filter output is appropriately delayed in order to coherently combine the L_r diversity paths. Assuming that bit "+1" is transmitted, the final decision statistic is [43]

$$Z_{1,MRC} = D_{1,MRC} + I_{MAI,MRC} + I_{SI,MRC} + I_{MTJ,MRC} + I_{\eta,MRC} \tag{3.50}$$

where $D_1 = A_1 T_b \sum_{l=1}^{L_r} X_{1,l}^2$. In (3.50), the terms $I_{MAI,MRC}$, $I_{SI,MRC}$, $I_{MTJ,MRC}$, and $I_{\eta,MRC}$ represent the MAI, self-interference, MTJ, and Gaussian noise, respectively. Now, under

the assumption of random spreading sequences with large value of N and with the help of central limit theorem, $I_{MAI,MRC}$, $I_{SI,MRC}$, $I_{MTJ,MRC}$, and $I_{\eta,MRC}$ can be approximated as Gaussian random variables with zero mean and variances of [6], [41], [44]

$$\sigma^2_{MAI,MRC} = \frac{NT_C^2}{2}[1-\gamma\beta/2]q\left(L_p,\eta\right)\sum_{k=2}^{K_u}A_k^2\Omega_{k,1}\sum_{l=1}^{L_r}X^2_{1,l}, \tag{3.51}$$

$$\sigma^2_{SI,MRC} = \frac{NT_C^2A_1^2\Omega_{1,1}}{2}\left[q\left(L_p,\eta\right)-1\right]\sum_{l=1}^{L_r}X^2_{1,l}, \tag{3.52}$$

$$\sigma^2_{MTJ,MRC} = 2T_b\sum_{i=1}^{J}\frac{\alpha_i^2G\left(\Delta f_i\right)M_{(i)}m_{(i)}}{b^2_{(i)}}\sum_{l=1}^{L_r}X^2_{1,l} \tag{3.53}$$

and

$$\sigma^2_{\eta,MRC} = N_0T_b\sum_{l=1}^{L_r}X^2_{1,l}, \tag{3.54}$$

respectively. The BER expression based on the Gaussian approximation approach and conditioned on the set of fading magnitudes is given as [44]

$$P_e\left(\gamma_l\right) \approx Q\left(\sqrt{\frac{\left(A_1T_b\right)^2\sum_{l=1}^{L_r}X^2_{1,l}}{N_0T_b+V_{MAI}+V_{SI}+V_{MTJ}}}\right)$$

$$= Q\left(\sqrt{\sum_{l=1}^{L_r}2\gamma_l}\right) \tag{3.55}$$

where $V_{MAI,MRC} = \sigma^2_{MAI}\Big/\sum_{l=1}^{L_r}X^2_{1,l}$, $V_{SI} = \sigma^2_{SI,MRC}\Big/\sum_{l=1}^{L_r}X^2_{1,l}$, $V_{MTJ} = \sigma^2_{MTJ,MRC}\Big/\sum_{l=1}^{L_r}X^2_{1,l}$, and $2\gamma_l$ represents the output SINR of the multipath receiver with $\gamma_l = C_RX^2_{l,1}$, where

$$C_R = \frac{\left(A_1T_b\right)^2}{2\left(N_0T_b+V_{MAI}+V_{SI}+V_{MTJ}\right)}. \tag{3.56}$$

Now, based on the assumption that all the random variables $X_{1,l}$ are independent of each other, the unconditional BER expression can be obtained with the help of MGF based approach as [6], [44]

$$P_e \approx \frac{1}{\pi}\int_0^{\pi/2}\prod_{l=1}^{L_r}\overline{\chi_l}\left(\mathfrak{A}_{1,l}, M_{1,l}, m_{1,l}, \theta\right) d\theta \tag{3.57}$$

where $\overline{\chi_l}\left(\mathfrak{A}_{1,l}, M_{1,l}, m_{1,l}, \theta\right)$ can be obtained as [46]

$$\overline{\chi_l}\left(\mathfrak{A}_{1,l}, M_{1,l}, m_{1,l}, \theta\right) = \left(\frac{\sqrt{M_{1,l}m_{1,l}}\times\sin\theta}{\sqrt{\mathfrak{A}_{1,l}C_R}}\right)^{M_{1,l}+m_{1,l}-1}\exp\left(\frac{M_{1,l}m_{1,l}\sin^2\theta}{2\mathfrak{A}_{1,l}C_R}\right)$$

$$\times W_{-\left(M_{1,l}+m_{1,l}-1\right)/2,\left(M_{1,l}+m_{1,l}\right)/2}\left(\frac{M_{1,l}m_{1,l}\sin^2\theta}{\mathfrak{A}_{1,l}C_R}\right). \tag{3.58}$$

The integral in (3.57) can be solved by using any numerical technique.

3.3.3 Two-Dimensional Diversity with EGC

In this section, we will extend the analysis of Section 3.3.1 to the case of a two-dimensional diversity system, i.e., space and multipath [8]. A two-dimensional diversity scheme can be viewed as a composite microscopic plus macroscopic diversity designed to provide improved performance over a fading channel [8]. A unified representation of space diversity model with two types of diversity receptions, namely, EGC and MRC, is shown in Fig. 3.2a. The detailed model of the l_A-th multipath correlators bank is shown in Fig. 3.2b. We consider a two-dimensional diversity system consisting of an array of L_A antennas or space diversity branches each followed by a L_r finger multipath receiver. Now, by assuming that all the fading variables are independent of each other, the final

BER expression for the EGC case can be obtained by using the inversion formula as [42], [47]

$$P_e \approx \frac{1}{2} - \frac{1}{\pi}\int_0^{\infty} \frac{\Phi_{\eta,EGC}(\omega)\Phi_{SI,EGC}(\omega)\Phi_{MAI,EGC}(\omega)\Phi_{MTJ,EGC}(\omega)\Im\left(\Phi_D(\omega)\right)}{\omega} d\omega. \quad (3.59)$$

The integration in (3.59) can be found by using any numerical technique. Also, in (3.59), MAI, MTJ, self-interference and noise components are assumed to follow Gaussian distribution. In (3.59), the characteristic functions of the data, MAI, MTJ, self-interference and Gaussian noise terms are given as

$$\Phi_D(\omega) = \prod_{l_A=1}^{L_A}\prod_{l=1}^{L_r}\Phi_{1,l_A,l}(\omega)$$

$$= \prod_{l_A=1}^{L_A}\prod_{l=1}^{L_r}\frac{\sqrt{\pi}\,2^{2-2m_{1,l_A,l}}\, b_{1,d,l}{}^{2M_{1,l_A,l}}\,\Gamma\left(2M_{1,l_A,l}\right)\Gamma\left(2m_{1,l_A,l}\right)}{\Gamma\left(M_{1,l_A,l}\right)\Gamma\left(m_{1,l_A,l}\right)\Gamma\left(\Theta_{1,l_A,l}\right)}$$

$$\times \frac{\mu^{M_{1,l_A,l}}\,{}_2F_1\left(2M_{1,l_A,l},\mathfrak{M}_{1,l_A,l};\Theta_{1,l_A,l};-\mu_{1,l_A,l}\right)}{\left[b_{1,l_A,l}{}^2+\left(A_1T_b\omega\right)^2\right]^{M_{1,l_A,l}}}, \quad (3.60)$$

$$\Phi_{MAI,EGC}(\omega) = \prod_{k=2}^{K_u}\exp\left(-\omega^2 L_A L_r \frac{NT_C^2}{4}\left[1-\gamma\beta/2\right]q\left(L_p,\eta\right)A_k^2\mathfrak{A}_{k,1}\right), \quad (3.61)$$

$$\Phi_{MTJ,EGC}(\omega) = \prod_{i=1}^{J}\exp\left(-\omega^2 L_A L_r T_b \frac{\alpha_i^2 G\left(\Delta f_i\right)M_{(i)}m_{(i)}}{b_{(i)}^2}\right), \quad (3.62)$$

$$\Phi_{SI,EGC}(\omega) = \exp\left(-\omega^2 L_A L_r \frac{NT_C^2A_0^2\mathfrak{A}_{1,1}}{4}\left[q\left(L_p,\eta\right)-1\right]\right) \quad (3.63)$$

and,

$$\Phi_{\eta,EGC}(\omega) = \exp\left(-\omega^2 L_A L_r N_0 T_b/2\right), \tag{3.64}$$

respectively.

In Fig. 3.2, the received signal $r_{l_A}(t)$ in the l_A-th spatial branch is defined in (3.36). The output from the l_A-th stage when we employ EGC or MRC is represented as Z_{1,EGC,l_A} and Z_{1,MRC,l_A}, respectively. The parameter ∂_l in Fig. 3.2b is the diversity reception weight parameter for the l-th multipath diversity branch. Note that $\partial_l = 1$ for EGC, while $\partial_l = X_{1,l}$ for MRC.

3.3.4 Two-Dimensional Diversity with MRC

We consider MRC as the diversity-combining scheme in this section. For the independent fading case, we can extend the BER analysis in (3.57) to the two-dimensional diversity system as [8]

$$P_e \approx \frac{1}{\pi}\int_0^{\pi/2}\prod_{l_A=1}^{L_A}\prod_{l=1}^{L_r}\overline{\chi_{l_A,l}}\left(\mathfrak{A}_{1,l_A,l}, M_{1,l_A,l}, m_{1,l_A,l}, \theta\right) d\theta \tag{3.65}$$

where the function $\overline{\chi_{l_A,l}}\left(\mathfrak{A}_{1,l_A,l}, M_{1,l_A,l}, m_{1,l_A,l}, \theta\right)$ can be obtained as [46]

$$\begin{aligned}\overline{\chi_{l_A,l}}\left(\mathfrak{A}_{1,l_A,l}, M_{1,l_A,l}, m_{1,l_A,l}, \theta\right) &= \left(\frac{\sqrt{M_{1,l_A,l}m_{1,l_A,l}}\times\sin\theta}{\sqrt{\mathfrak{A}_{1,l_A,l}C_R}}\right)^{M_{1,l_A,l}+m_{1,l_A,l}-1} \\ &\times \exp\left(\frac{M_{1,l_A,l}m_{1,l_A,l}\sin^2\theta}{2\times\mathfrak{A}_{1,l_A,l}C_R}\right) \\ &\times W_{-\left(M_{1,l_A,l}+m_{1,l_A,l}-1\right)/2,\left(M_{1,l_A,l}+m_{1,l_A,l}\right)/2}\left(\frac{M_{1,l_A,l}m_{1,l_A,l}\sin^2\theta}{\mathfrak{A}_{1,l_A,l}C_R}\right).\end{aligned} \tag{3.66}$$

The integration in (3.65) can be solved by using numerical technique. It should also be noted that in (3.66) $W_{x,y}(.)$ is the Whittaker function defined in (3.34) and [46].

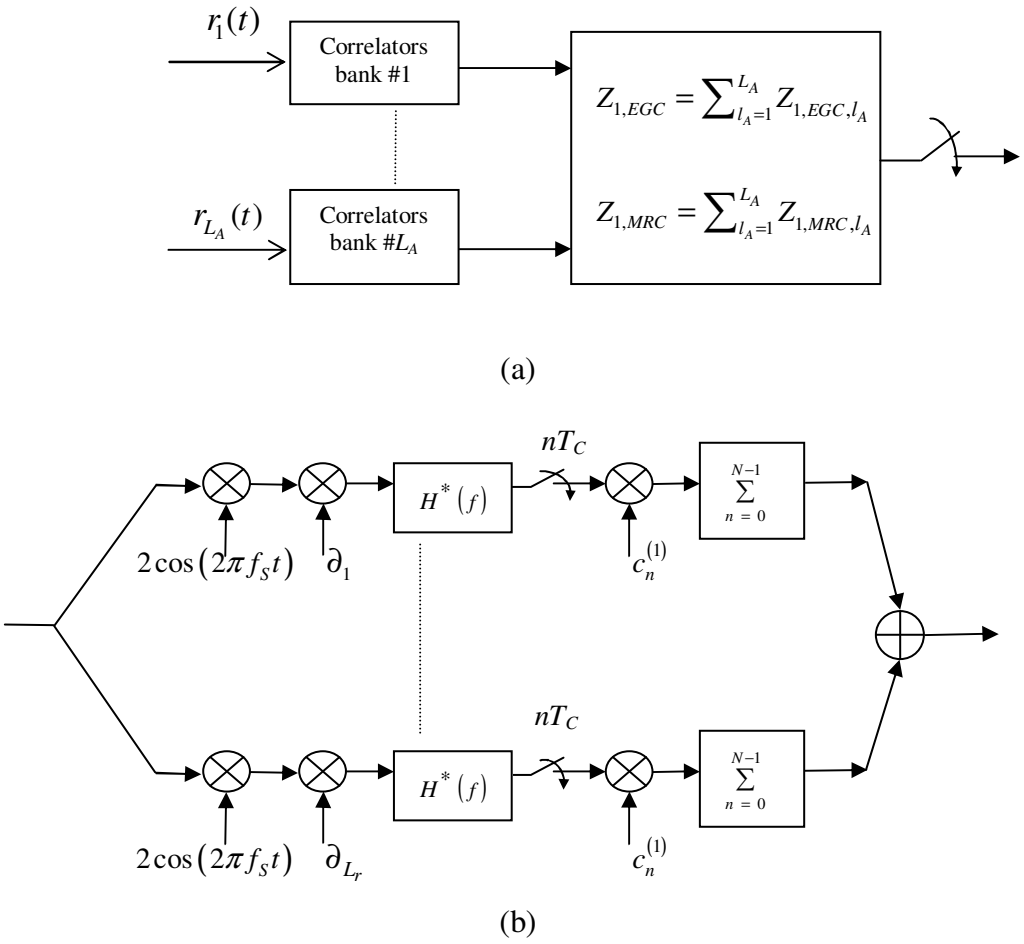

Figure 3.2: Receiver block diagram of a two-dimensional diversity system: (a) Block diagram with L_A multipath correlators banks, (b) Block diagram of the l_A -th bank of multipath correlators.

Now, due to the complexity of the problem considered in this chapter, the final BER expressions presented cannot be further simplified analytically. Therefore, such BER expressions can be solved by using numerical techniques. However, with the help of our theoretical BER expressions, various scenarios of small-scale fading, shadowing and interference for the band-limited DS-CDMA systems can be analyzed. Also, with the help of our BER expressions, we can study the performance of system under low BER ranges, where simulation is time consuming.

3.4 Numerical Results and Discussions

In this section, we present numerical results based on the BER expressions presented in Sections 3.2 and 3.3. The BER results with SRC and BTD pulses are presented under various conditions of small-scale fading and shadowing. The effects of AWGN, MTJ and MAI are also considered. In our analytical and simulation results, we assume $\beta = 1$, i.e., excess bandwidth to be 100%. However, our BER analysis is applicable for any $\beta \in [0,1]$. We also assume perfect power control, although our results can also be extended to non-uniform power cases. A processing gain of $N = 31$ is assumed for the system with random spreading sequences with BPSK modulation scheme. However, our BER expressions can incorporate any value of N. Based on the analysis in [20], we consider $M = 4$ in order to incorporate shadowing effects, whereas for negligible shadowing effects, M is set to 12. We assume that the total jamming power is uniformly distributed among all jamming tones. We consider $J = 3$ jamming tones in our numerical analysis with shadowing parameter fixed at $M_{(i)} = 12$ for $i = 1$, 2 and 3. The small-scale fading parameters for the three jamming tones are set at $m_{(1)} = 2$, $m_{(2)} = 1$ and $m_{(3)} = 4$. We also fix the shadowing parameter for other users at $M_k = 12$ and the small-scale fading parameter at $m_k = 3$, for $k = 2,\ldots, K_u$. For the case of frequency-selective fading case, we assume the total number of resolvable multipaths to be $L_p = 10$ and $\eta = 0.2$. Furthermore, in our simulations, we also assume to have perfect knowledge of various channel fading parameters in order to incorporate MRC, and all fading variables are assumed to be fixed for a bit duration in order to have a coherent reception. In addition, fading variables of all K_u users are assumed to be independent of each other and vary

independently from one bit to another. The jamming tones are assumed to be uniformly distributed over the spectrum of the desired user and the total jamming power is assumed to be equally distributed among all jamming tones. In Figs. 3.3 to 3.12, we present BER performance of flat-fading systems incorporating space diversity scheme based on MRC and EGC techniques. In Figs. 3.13 to 3.21, we present BER performance over frequency-selective multipath fading channels. The multipath receiver incorporates both MRC and EGC based techniques to combat fading. We compare the BER performance of systems with single-dimensional and two-dimensional diversity combining schemes.

In Fig. 3.3, analytical and simulation results are presented for EGC and MRC based systems. Only systems with BTD pulse are considered. We assume $K_u = 11$ and the total signal-to-jamming power ratio (SJR) is fixed at -10 dB. We observe a close match between the simulation and analytical results. It validates the BER expressions presented in Section 3.2. Note that the slight deviation between analytical and simulation results is due to the fact that we have used Gaussian approximation in our analysis. We also observe that the systems with MRC outperform the ones with EGC in the presence of MAI and MTJ. Furthermore, we also observe flattening of the BER plots as E_b/N_0 value increases, due to the jamming effects of MAI and MTJ. In Fig. 3.4, we compare the BER performance of EGC and MRC based systems under shadowing conditions while keeping other channel parameters fixed. From the figure, we observe that under shadowing conditions, system BER performance degrades due to the worsening of system SINR. As described in [20], when the value of M increases, the shadowing effect of the wireless channel diminishes. In Fig. 3.5, we compare the BER performance when the number of space diversity branches is increased from $L_A = 2$ to $L_A = 4$.

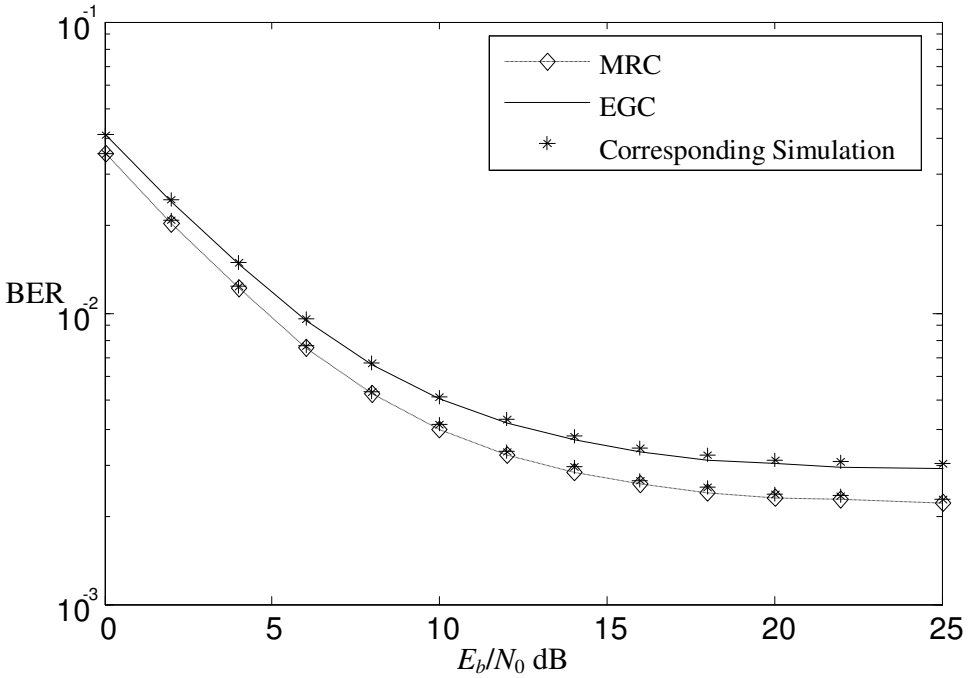

Figure 3.3: BER performance of EGC and MRC based systems with BTD pulse, K_u =11, $m_{l,D}$ = 3, $M_{l,D}$ =4, L_A = 3 and SJR = -10 dB.

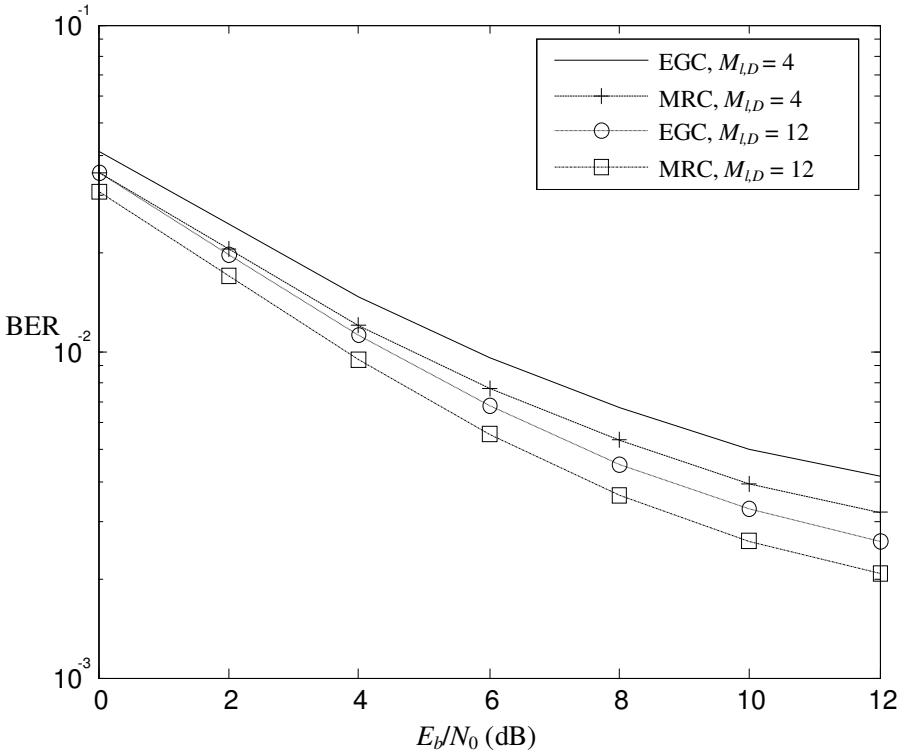

Figure 3.4: BER performance of EGC and MRC systems with BTD pulse and various shadowing conditions, K_u =11, $m_{l,D}$ = 3, L_A = 3 and SJR = -10 dB.

We observe that the BER performance is improved when the number of space diversity branches is increased. This is due to improved SINR conditions. We further observe that the BER plots do not show noticeable increase in the slopes with the increase of the diversity branches. This is due to the presence of interference contributed by MTJ and MAI, causing the flattening effect of the BER plots at higher values of E_b/N_0, where E_b is the bit energy.

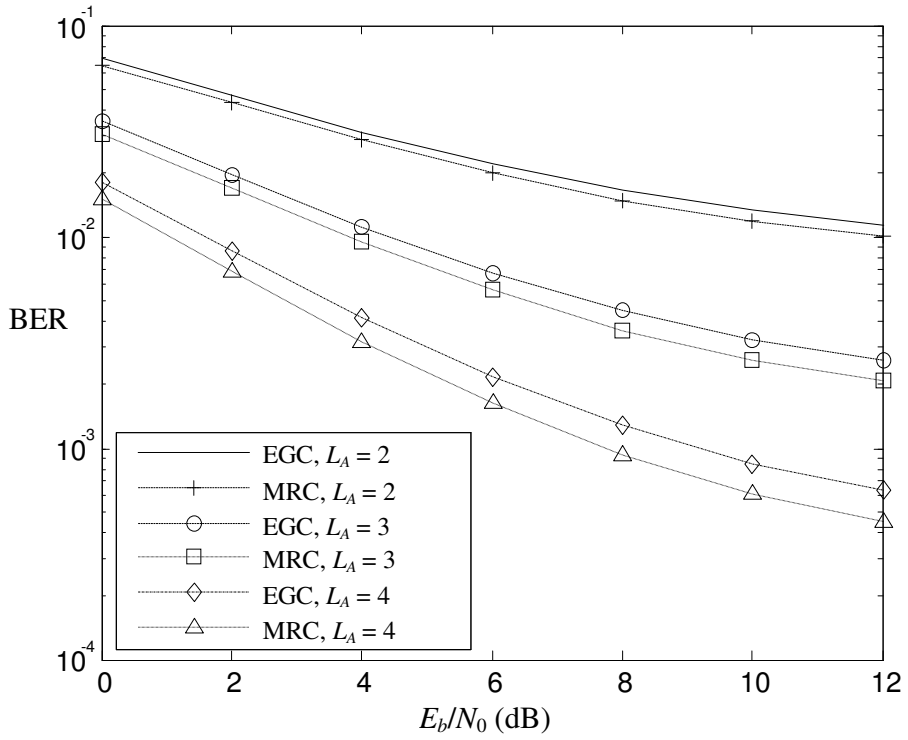

Figure 3.5: BER performance of band-limited systems employing BTD pulse, $K_u = 11$, $m_{l,D} = 3$, $M_{l,D} = 12$ and SJR = -10 dB.

In Fig. 3.6, BER performance of space diversity systems with various combinations of small-scale fading and shadowing is shown. From Fig. 3.6, it is clear that for the smaller values of M and m, the BER performance is degraded. However, as the values of M and m increase, improvement in BER performance is observed due to less severe fading and shadowing conditions of the wireless channel.

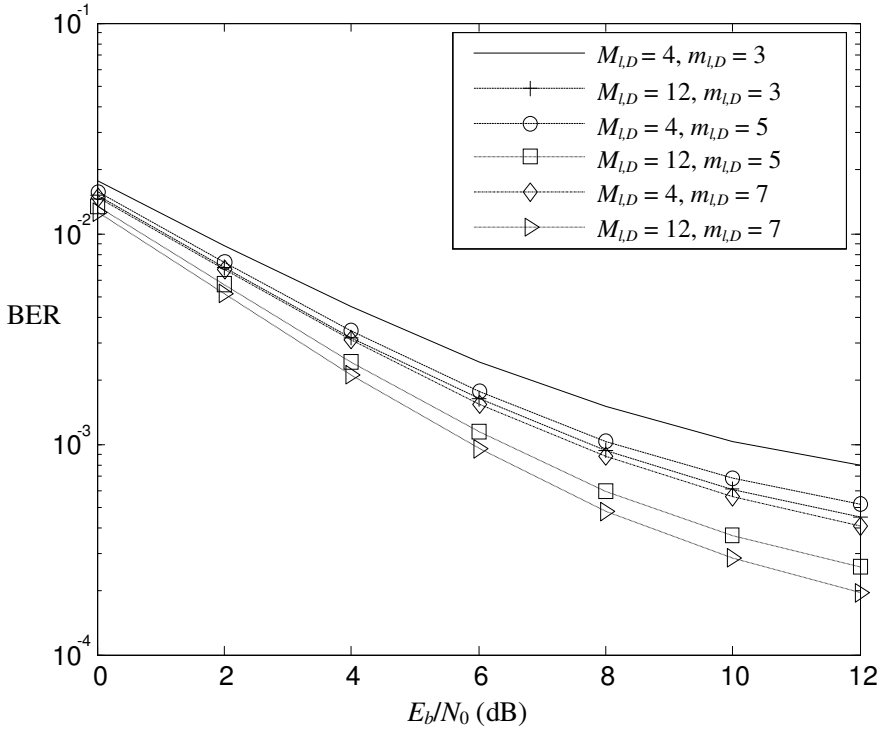

Figure 3.6: BER performance of MRC combining technique and BTD pulse shape, K_u =11, L_A = 4 and SJR = -10 dB.

In Fig. 3.7, we present the BER performance with BTD and SRC pulses for L_A = 4 diversity branches. We include both diversity-combining schemes, i.e., EGC and MRC. It can be observed that the systems with BTD pulses show better BER performance than the ones with SRC pulses for both diversity-combining schemes. The superior BER performance shown by the BTD based systems is due to the fact that the BTD pulse has better correlation properties as compared to SRC pulse [15]. It can be observed that the BTD based systems demonstrate an improvement of approximately 1 dB in E_b/N_0 at the BER value of 10^{-3}.

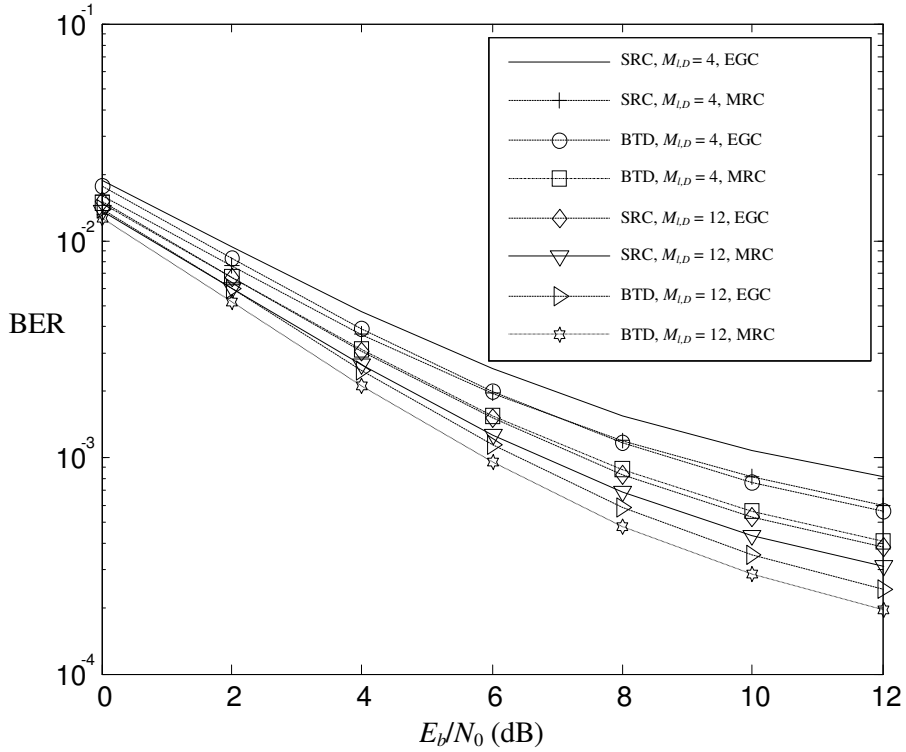

Figure 3.7: BER results of EGC and MRC based receivers with SRC and BTD pulses, K_u =11, $m_{l,D}$ = 7, L_A = 4, and SJR= -10 dB.

In Fig. 3.8, we compare the BER performance of band-limited DS-CDMA systems employing both types of pulses under various SJR conditions. From Fig. 3.8, we observe that the BER performance degrades as the total jamming power is increased. We also observe that at higher value of shadowing parameter, i.e., M = 12, all systems show better BER performance due to less severe shadowing effects. Furthermore, under similar conditions of jamming and interference, BTD based systems show better performance than that of SRC based systems. In Fig. 3.9, we plot BER performance of both diversity-combining techniques versus the number of users. We fix SJR at -5 dB and consider L_A = 3 space diversity branches. We only consider BTD pulse shape. From Fig. 3.9, we observe that the BER performance is degraded when the number of users is increased due to higher MAI level.

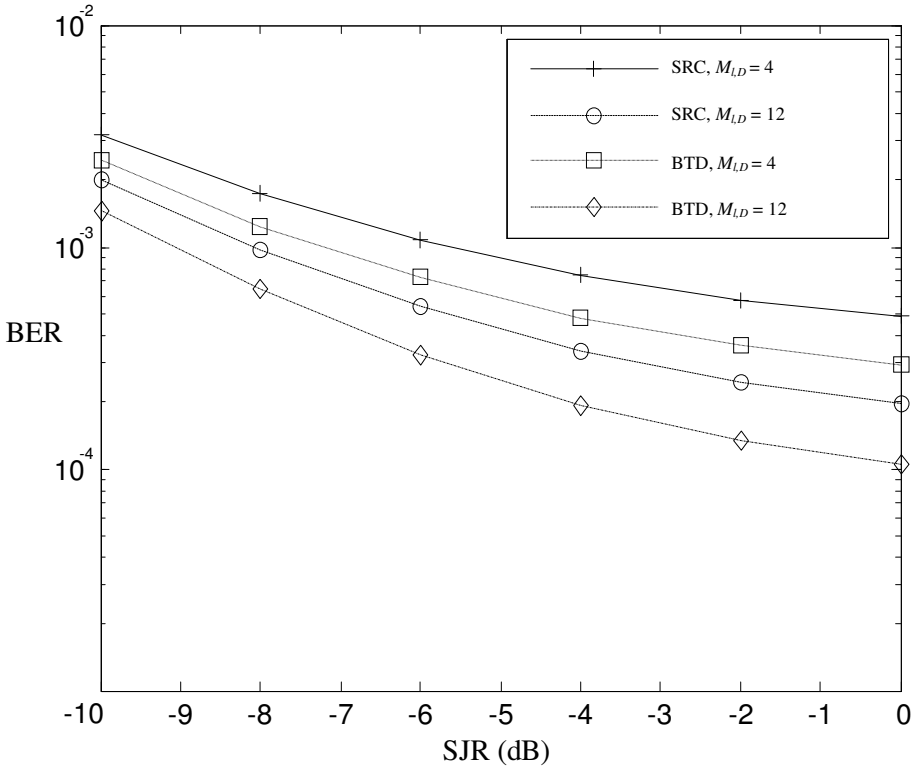

Figure 3.8: BER analysis of MRC based space diversity scheme with various SJR conditions, $K_u = 11$, $m_{l,D} = 7$, $L_A = 3$ and $E_b/N_0 = 10$dB.

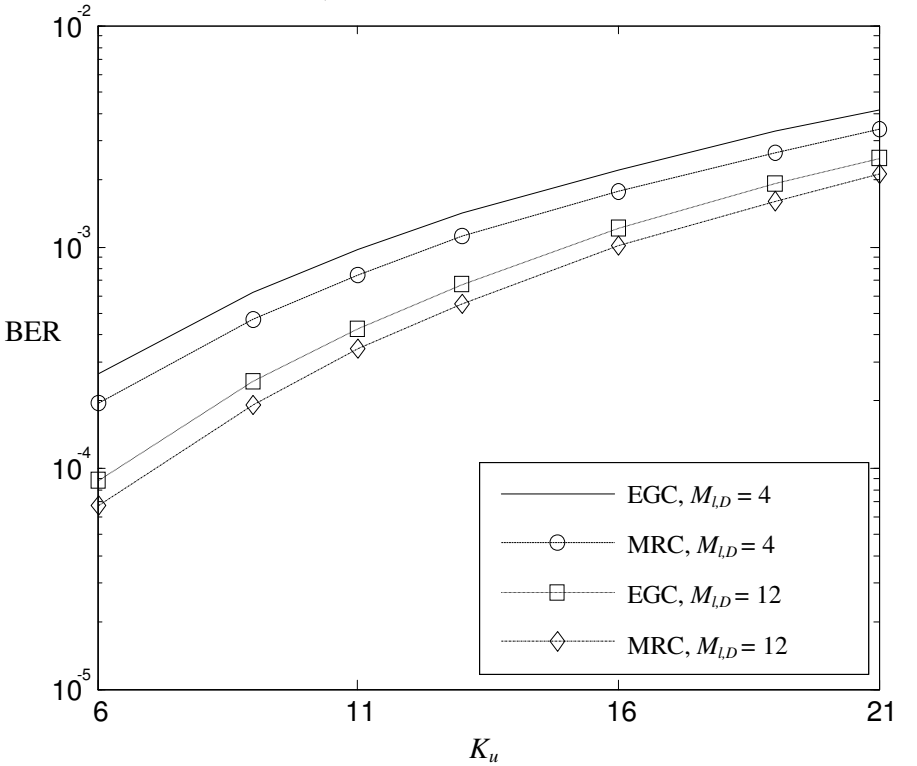

Figure 3.9: BER performance of EGC and MRC based systems with BTD pulse, $m_{l,D} = 5$, $L_A = 3$, $E_b/N_0 = 10$ dB and SJR = -5 dB.

In Fig. 3.10, we compare the BER performance of band-limited systems employing BTD pulse shape under various system loads and jamming power conditions. We observe that BER performance degrades as we increase the total jamming and MAI power. This is because the SINR condition deteriorates with the increase in the interference power contributed by both MTJ and MAI components.

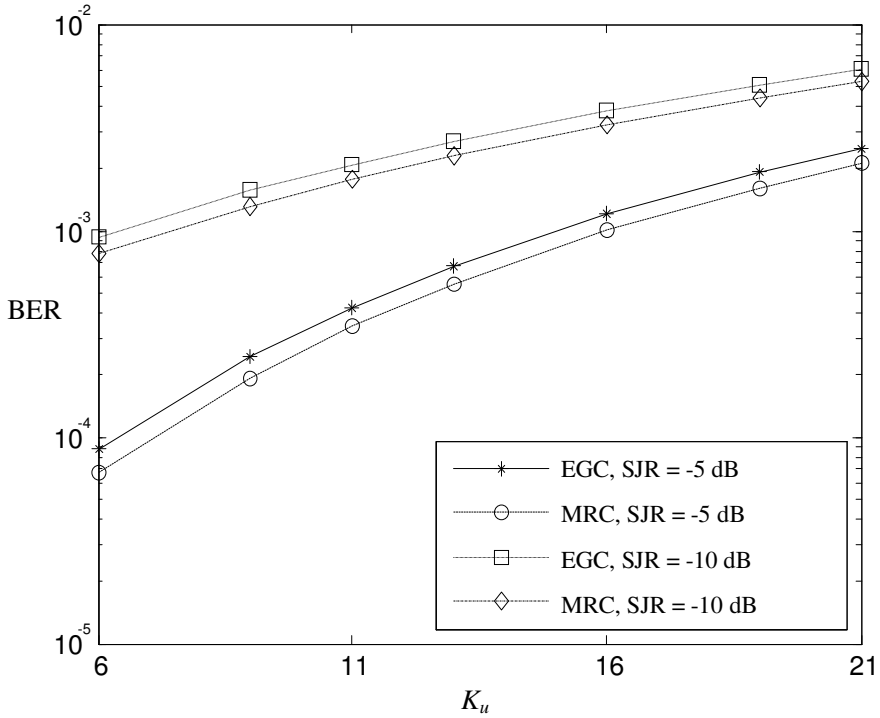

Figure 3.10: Performance of band-limited systems with EGC and MRC, BTD pulse, $m_{l,D} = 5$, $L_A = 3$ and $E_b/N_0 = 10$ dB.

In Fig. 3.11, we study the effect of the number of diversity branches on the BER performance of MRC based system. We fix SJR at -5 dB and incorporate BTD pulse shape. We observe that BER performance is improved as we increase the number of diversity branches from 2 to 3. This is because the system SINR is improved as we increase the number of diversity branches. In Fig. 3.12, BER results are presented for the case of DS-CDMA system with $K_u = 1$ to $K_u = 31$. We also consider various conditions of shadowing and small-scale fading.

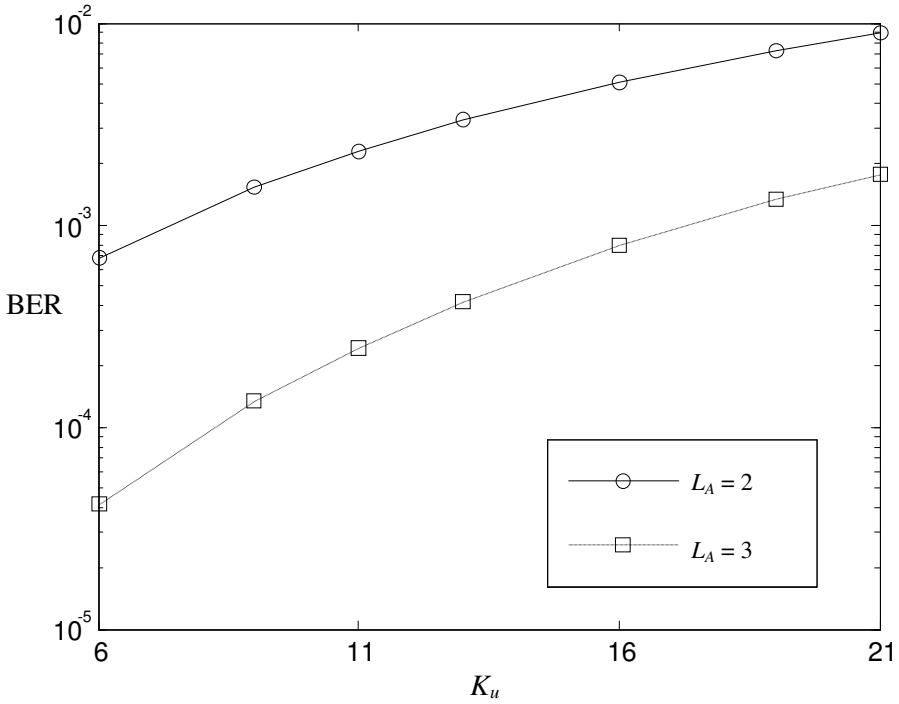

Figure 3.11: BER performance of MRC based systems, BTD pulse, $m_{l,D} = 7$, $M_{l,D} = 12$, $E_b/N_0 = 10$ dB and SJR = -5 dB.

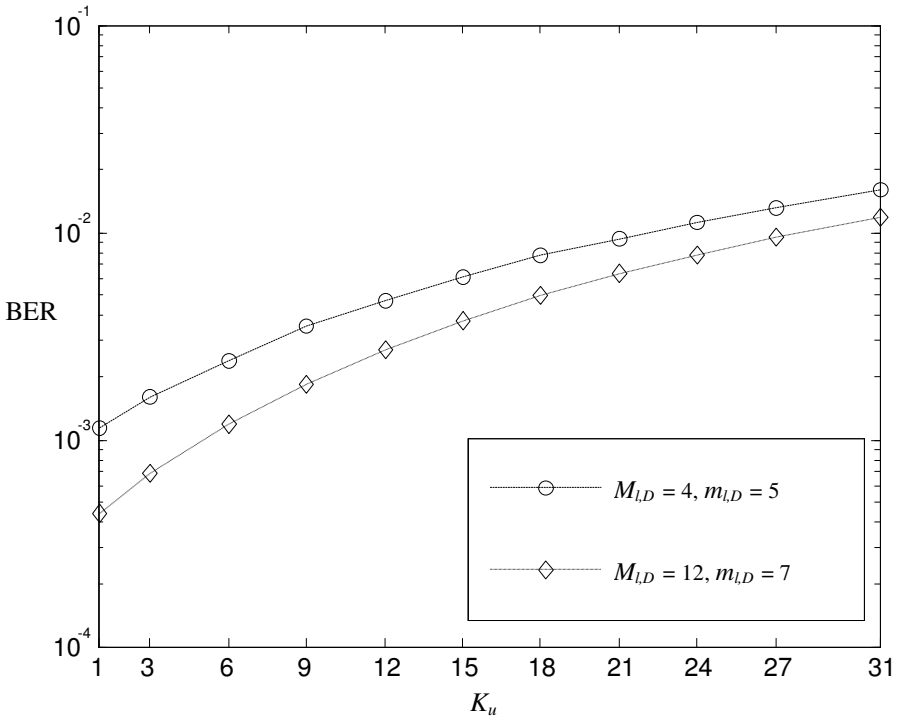

Figure 3.12: BER performance of MRC based systems, BTD pulse, $E_b/N_0 = 16$ dB and SJR = -12 dB.

From the figure, we observe flattening of BER plots as the MAI power in the system increases, i.e., K_u increases. Furthermore, we also observe that the system BER performance improves with higher values of M and m, i.e., less severe shadowing and fading conditions.

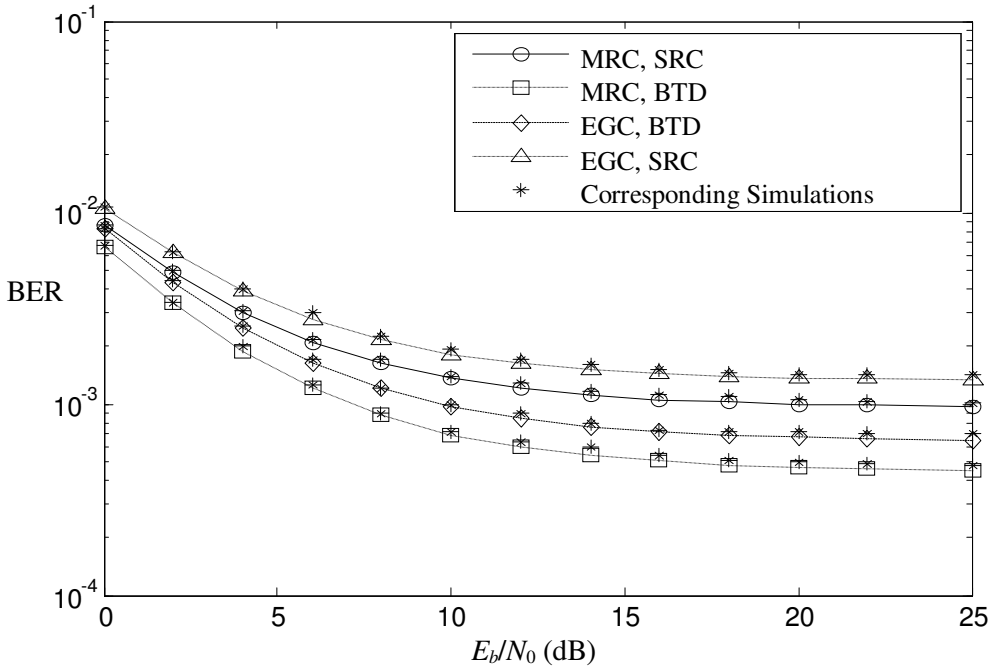

Figure 3.13: Comparison of analytical and simulation results over frequency-selective multipath channels with K_u =11, L_r = 5, L_A = 2, $m_{1,l}$ = 7, $M_{1,l}$ = 12 and SJR= -5 dB.

In Fig. 3.13, analytical and simulation results are presented for EGC and MRC based systems over frequency-selective multipath channels. The close match between both analytical and simulation results validates the BER expressions presented in Section 3.3. Also, the slight deviation between analytical and simulation results is due to the Gaussian approximation. Furthermore, flattening of BER plots is observed as E_b/N_0 value is increased. This is due to reason is the increase in the jamming power of the interference components, i.e., self-interference, MAI and MTJ. We also observe that the MRC-based

system outperforms the one with EGC. In Fig. 3.14, we compare the BER performance of systems incorporating both SRC and BTD pulses with two-dimensional diversity. We consider both EGC and MRC based systems. From Fig. 3.14, we observe that the systems with BTD pulses and MRC based combining technique outperform the ones incorporating EGC and SRC pulses. We also observe that by increasing the number of spatial diversity branches, the BER performance is improved due to the improvement in the SINR conditions.

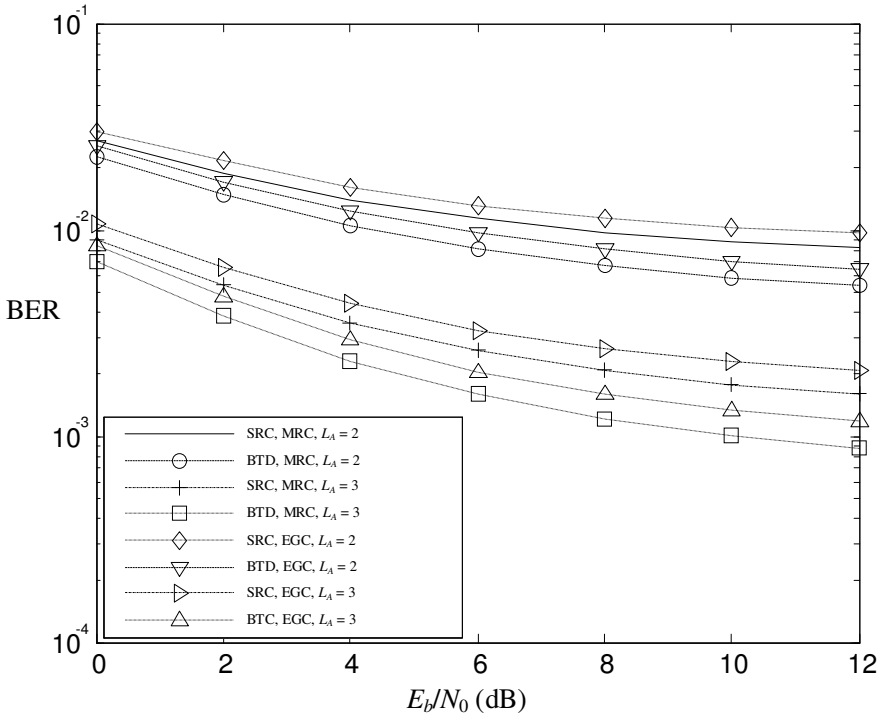

Figure 3.14: BER performance of two-dimensional systems, K_u =11, L_r = 3, $m_{1,l}$ = 6, $M_{1,l}$ = 12 and SJR= -10 dB.

In Fig. 3.15, we compare the BER performance of both the single-dimensional and two-dimensional diversity based systems. We consider both types of pulses and only MRC-based combining technique is considered. From Fig. 3.15, we observe that the system with two-dimensional diversity outperforms the one with multipath diversity. We also observe that the system with BTD pulse outperforms the one with SRC pulse for both

types of diversity schemes. Thus, by combining multipath and spatial diversity schemes, a noticeable improvement in the BER performance can be achieved.

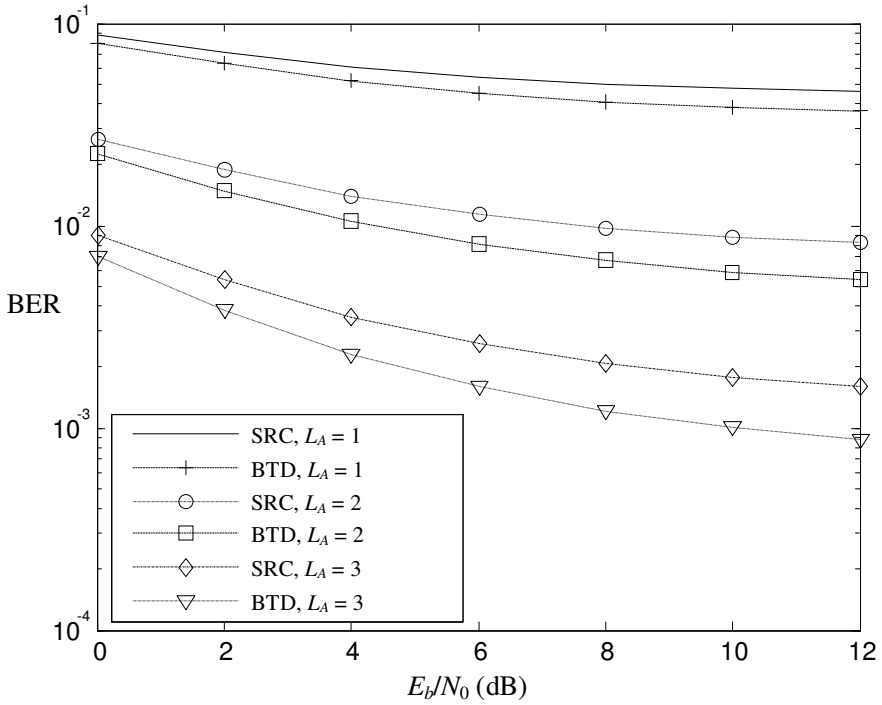

Figure 3.15: BER performance comparison of single-dimensional and two-dimensional systems with MRC, K_u =11, L_r = 3, $m_{1,l}$ = 6, $M_{1,l}$ = 12 and SJR= -10 dB.

In Fig. 3.16, we compare the BER performance under various shadowing conditions. Only BTD pulse is employed. Two-dimensional diversity scheme with MRC-based system is considered. It is observed that the presence of shadowing degrades the BER performance. However, by increasing the number of spatial branches, the BER performance can be further improved. In Fig. 3.17, we present the BER performance of single-dimensional and two-dimensional systems versus the number of users in the system. Only BTD pulse is considered and SJR is fixed at -10 dB. We consider both MRC and EGC based systems. We fix the number of multipath diversity branches at L_r = 5. From Fig. 3.17, we observe that as the system load increases, the BER performance degrades. The reason of such behavior is due to increase in the MAI power.

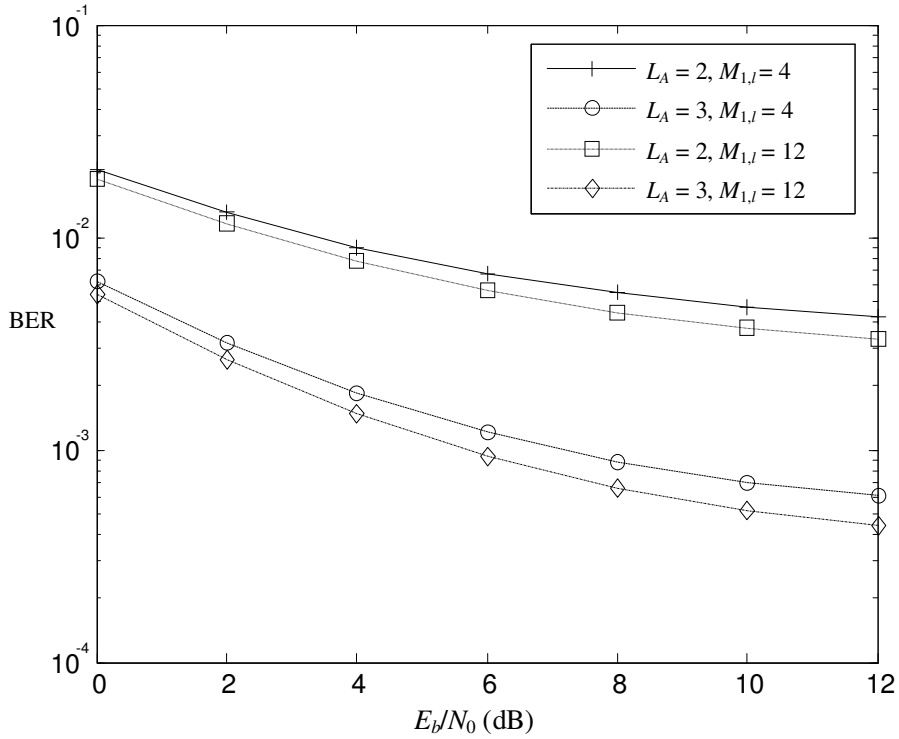

Figure 3.16: BER performance comparison of two-dimensional systems under various shadowing conditions with MRC, BTD pulse, K_u = 11, L_r = 3, $m_{1,l}$ = 6 and SJR = -5 dB.

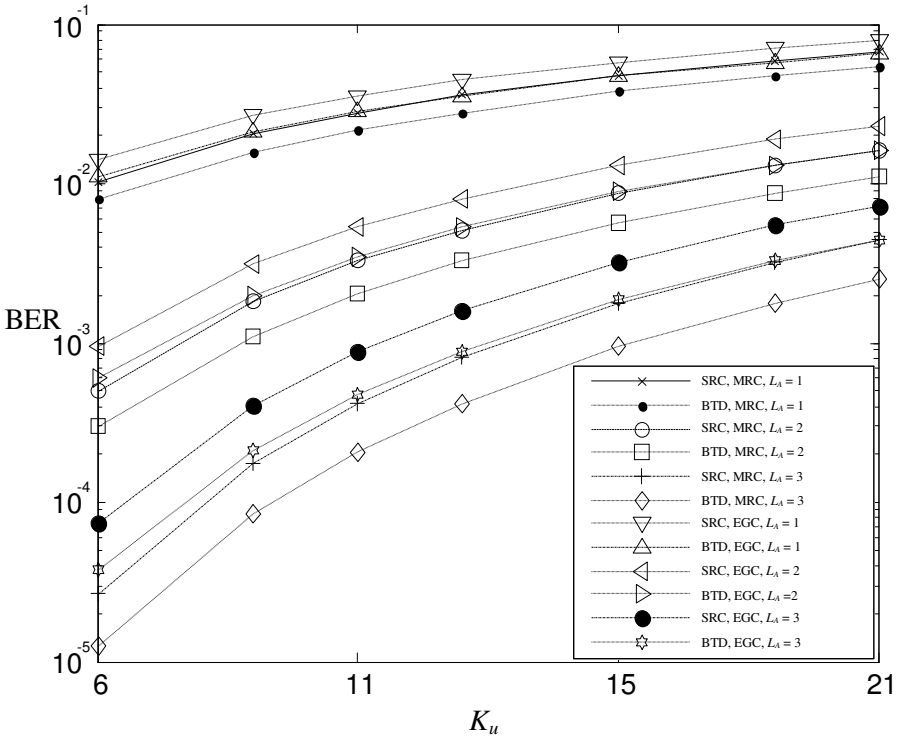

Figure 3.17: BER performance of single-dimensional and two-dimensional systems with various system loads, BTD pulse, L_r = 5, $m_{1,l}$ = 2, $M_{1,l}$ = 12, E_b/N_0 = 10 dB and SJR = -10 dB.

Furthermore, we also observe that the systems with MRC-based combining technique, BTD pulse shape and the highest number of diversity branches, i.e., L_A = 3, show best BER performance. In Fig. 3.18, we analyze BER performance with various shadowing and load conditions. We consider both types of diversity-combining techniques as well as both types of pulses. From Fig. 3.18, it is clear that under various MAI and shadowing conditions, systems employing BTD pulse and MRC show the best BER performance.

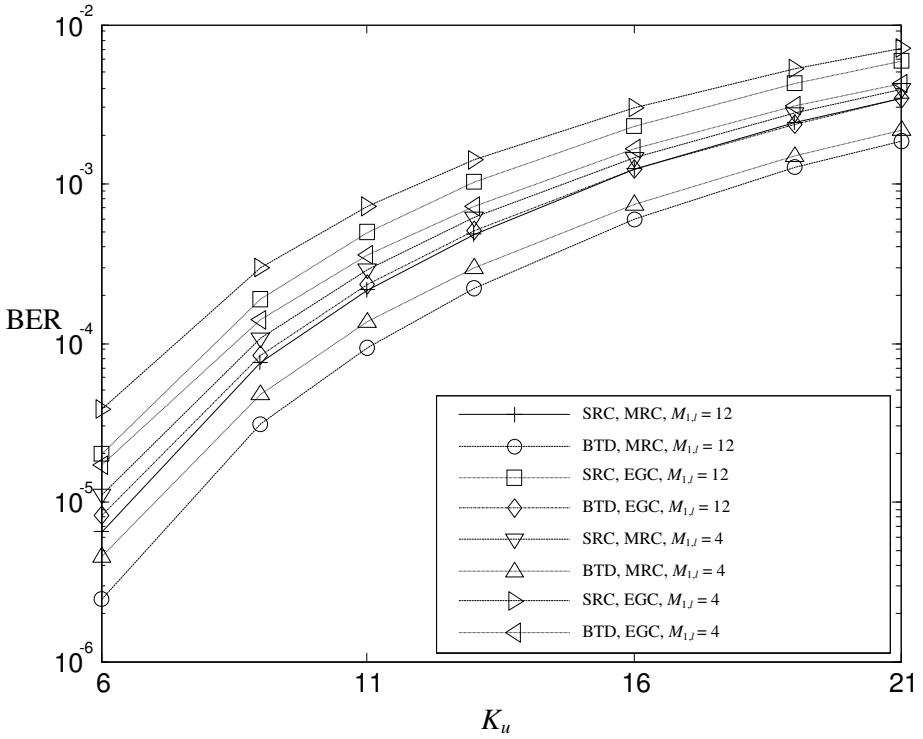

Figure 3.18: BER performance of two-dimensional systems, L_r = 5, L_A = 3, $m_{1,l}$ = 2, E_b/N_0 = 10 dB and SJR = -5 dB.

In Fig. 3.19, we compare the BER performance of single-dimensional and two-dimensional systems with both types of pulse shapes while keeping other system parameters fixed. We fix E_b/N_0 at 10 dB and SJR at -10 dB. From Fig. 3.19, we observe that the combination of spatial and multipath diversity techniques can effectively combat the fading as well as interference.

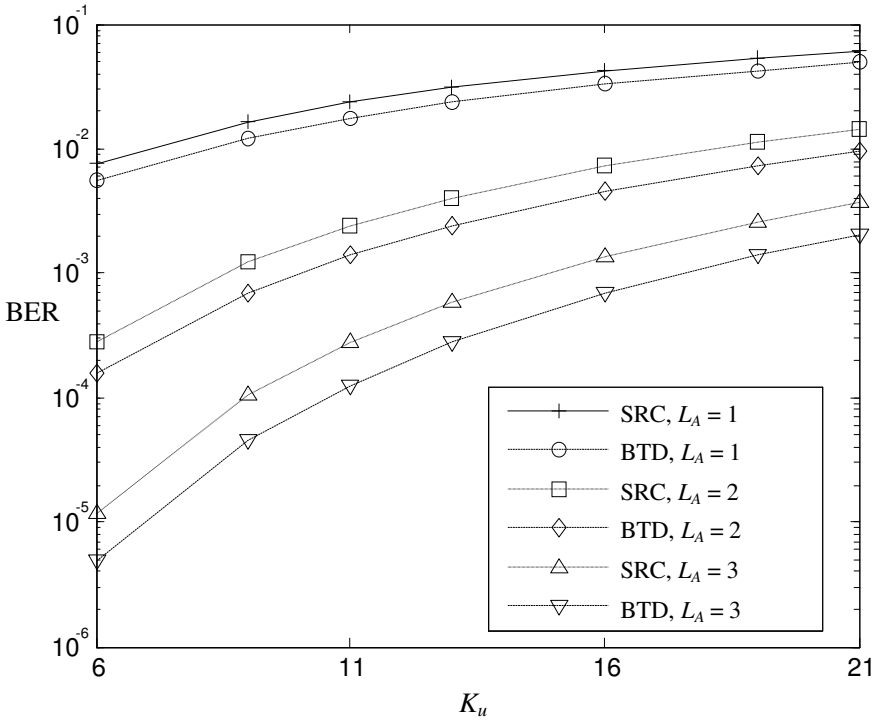

Figure 3.19: BER performance of single-dimensional and two-dimensional systems for both types of pulses with MRC, $L_r = 5$, $m_{1,l} = 5$, $M_{1,l} = 12$, $E_b/N_0 = 10$ dB and SJR = -10 dB.

In Fig. 3.20, BER results of two-dimensional systems with both types of pulse shapes are plotted against various SJR levels. We have fixed E_b/N_0 at 10 dB. From the figure, it is clear that by increasing the number of diversity branches, the BER performance is improved. Also, as we increase the diversity level of the system, the gap between the BER plots of the BTD-based systems and the SRC-based systems increases. In Fig. 3.21, we observe improvement in the BER performance with both types of pulse shapes as the number of multipath diversity branches is increased while keeping the number of spatial diversity branches, interference powers, and channel fading and shadowing parameters unchanged.

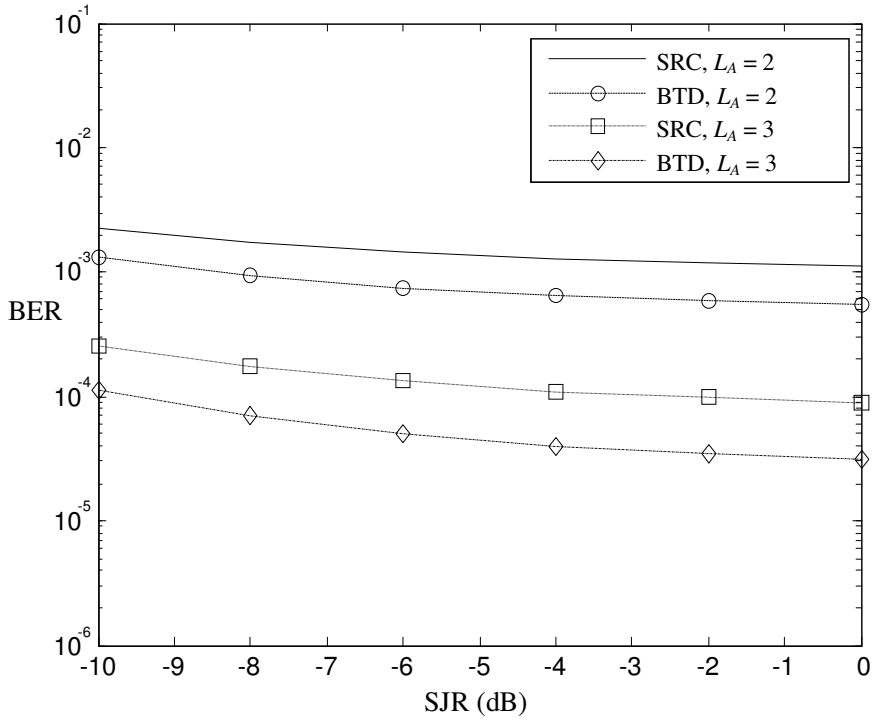

Figure 3.20: BER performance of two-dimensional MRC-based systems with various jamming power conditions, $K_u = 11$, $L_r = 5$, $m_{1,l} = 7$, $M_{1,l} = 12$ and $E_b/N_0 = 10$ dB.

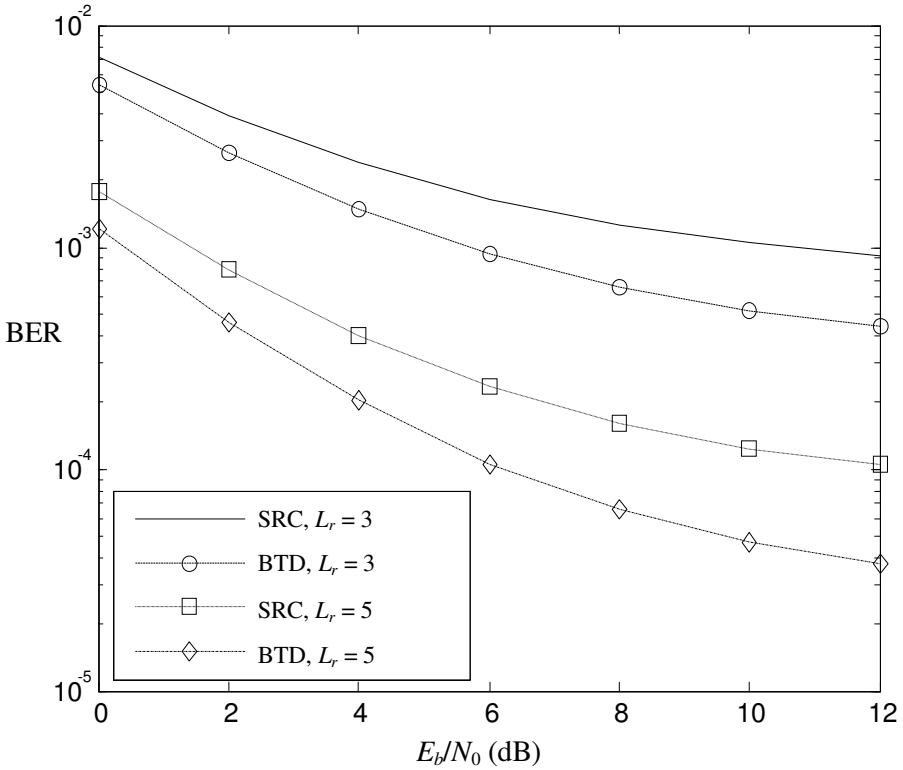

Figure 3.21: BER performance of two-dimensional MRC-based systems with various number of multipath diversity branches, $K_u = 11$, $L_A = 3$, $m_{1,l} = 6$, $M_{1,l} = 12$ and SJR = -10 dB.

3.5 Conclusion

In this chapter, we have presented the BER performance analyses of band-limited asynchronous DS-CDMA systems over generalized-K fading channels in the presence of MTJ, MAI and AWGN. Both flat and frequency-selective multipath fading conditions have been considered. With the help of our theoretical BER expressions, various scenarios of small-scale fading and shadowing for the band-limited DS-CDMA systems are analyzed. We have shown that various combinations of wireless channel fading and shadowing can be easily included in the BER analysis by incorporating the generalized-K distribution without much increase in the mathematical complexity. With the help of our BER expressions, we have studied the performance of various systems under low BER ranges, where simulation is time consuming. From our numerical analysis, we observe that band-limited DS-CDMA systems with BTD pulses demonstrate better BER performance as compared to the ones with SRC pulses under various conditions of shadowing and fading due to its better correlation properties. Moreover, we also observe that under frequency-selective multipath channels, the two-dimensional diversity based receiver gives better BER performance as compared to the one that incorporates only multipath diversity. This is because the receivers employing two-dimensional diversity scheme incorporate both spatial as well as the multipath diversity to combat shadowing and the small-scale fading effects, and thus improve the system SINR conditions. We also observe that the presence of MTJ and MAI in the system introduces a noise floor at high levels of E_b/N_0. We observe that for the smaller values of M and m, the BER performance is degraded. However, for the large values of M and m, improvement in BER

performance is observed due to less severe fading and shadowing conditions of the wireless channel.

Chapter 4

BER Analysis for Decorrelator-Based Multiuser Detector

In this chapter, we investigate the BER performance of decorrelator-based multiuser receivers for asynchronous band-limited DS-CDMA systems. We focus on the BER performance over frequency-selective multipath fading channels. Multipath diversity schemes based on MRC and EGC techniques are employed to combat fading effects. Our analytical expressions are valid for arbitrary diversity levels and fading parameters with both types of diversity-combining techniques. The remainder of this chapter is organized as follows. In Section 4.1, we present a brief overview of the previous work and the contributions of our work. In Section 4.2, analytical BER expressions of EGC and MRC based schemes are presented. Numerical results and conclusions are given in Sections 4.3 and 4.4, respectively.

4.1 Introduction

The BER performance of multiuser detection techniques for DS-CDMA systems has been extensively studied in the literature [10]-[12]. Various optimal and sub-optimal multiuser detectors have been proposed to suppress MAI and alleviate the near-far problem [48]. However, the complexity of the receiver using optimal multiuser detection is very high and the complexity exponentially increases with the number of the users [12]. The computational complexity of the optimum multiuser receivers prompted the development

of high performance sub-optimal receivers with practical complexity [48]-[52]. Consequently, sub-optimal linear detectors with a good tradeoff between complexity and performance have been proposed in the literature [48]-[57]. Among such receivers, the decorrelator detector [48] is perhaps the simplest in structure and is reasonably easy to implement [55]. In addition to its simplicity, the decorrelator-based system does not require the knowledge of the received signal strengths. The BER performance of the decorrelator is independent of the interferer's received energies, and hence is near-far resistant [48]. Various schemes have been studied in the literature for DS-CDMA systems employing decorrelator-based detection over multipath fading channels [54]-[57]. However, most of the systems in the literature have employed rectangular pulse shape [6]. Therefore, in this chapter, we analyze the BER performance of band-limited DS-CDMA systems incorporating decorrelator-based schemes. We incorporate generalized-K distribution in order to analyze the BER performance under various channel shadowing and fading conditions. We extend the BER analysis of band-limited DS-CDMA systems as discussed in previous chapter to the case of decorrelator-based schemes. We compare the BER performance of both SRC and BTD based systems under various channel shadowing and fading conditions. Analytical BER expressions are derived based on the Gaussian approximation technique. Various fading and shadowing scenarios of multipath generalized-K channel are analyzed with the decorrelator-based scheme. Furthermore, based on the principles of MRC and EGC techniques, we consider both single-dimensional and two-dimensional diversity schemes in our BER analysis. With the help of our theoretical BER expressions, various scenarios of small-scale fading, shadowing and MTJ for the decorrelator-based band-limited DS-CDMA systems are analyzed.

4.2 System Model and BER Analysis

4.2.1 System Model

We consider an asynchronous band-limited DS-CDMA system with K_u active users. The desired signal is assumed to undergo independent multipath frequency-selective generalized-K fading in the presence of MTJ and AWGN. We assume binary phase-shift keying (BPSK) as the modulation scheme in our analysis. The low-pass equivalent representation of channel impulse response encountered by the k-th user with L_p resolvable multipaths is considered here. We assume a negative exponentially decaying multipath intensity profile (MIP) as described in Section 3.3.1. The detector consists of a bank of $K_u \times L_p$ filters matched to the delayed versions of the users' signature waveforms. The l-th branch received signal after co-phasing is [15]

$$r_l(t) = \sum_{k=1}^{K_u}\sum_{l=1}^{L_p} A_k X_{k,l} \cos\left(2\pi f_S t + \theta_{k,l}\right) \sum_{n=-\infty}^{\infty} d_{\lfloor n/N \rfloor}^{(k)} c_n^{(k)} h\left(t - \tau_k - lT_C - nT_C\right) + I_l(t) + n_l(t) \tag{4.1}$$

where $I_l(t)$ is the MTJ term and $n_l(t)$ is the AWGN term with two-sided power spectral density (PSD) $N_0/2$. The MTJ term in (4.1) follows the same form as described by (3.2) in Section 3.2.1. The parameters $d_{\lfloor n/N \rfloor}^{(k)}$, $c_n^{(k)}$, $\theta_{k,l}$, N, T_C, T_b, A_k, τ_k, $h(t)$ and f_S follow the same definitions as described in Section 3.2.1. Moreover, $X_{k,l}$ is the independent generalized-K random fading variable for the k-th user in the l-th multipath. The matrix representation of the output from the bank of matched filters is [48]

$$\mathbf{y} = \mathbf{RACd} + \mathbf{n} + \mathbf{I}_{MTJ} \tag{4.2}$$

where $\mathbf{n}$ and $\mathbf{I}_{MTJ}$ are $K_u L_p \times 1$ Gaussian noise and MTJ column vectors, respectively. The vectors $\mathbf{n}$ and $\mathbf{I}_{MTJ}$ consist of the correlation terms of Gaussian noise and MTJ signals with the band-limited pulse template $h(t)$ from all $K_u L_p$ matched filters [16]. The diagonal matrices $\mathbf{A}$ and $\mathbf{C}$ in (4.2) are defined as $\mathbf{A} = \text{diag}\left[A_1\mathbf{I}_{L_p},\ldots,A_{K_u}\mathbf{I}_{L_p}\right]$ where $\mathbf{I}_{L_p}$ is an $L_p \times L_p$ identity matrix and $\mathbf{C} = \text{diag}\left[X_{1,1},\ X_{1,2},\ \ldots,\ X_{K_u,L_p-1},\ X_{K_u,L_p}\right]$. The vector $\mathbf{d}$ in (4.2) is defined as $\mathbf{d} = \left[d^{(1)}\mathbf{1},\ldots,d^{(K_u)}\mathbf{1}\right]^{\mathrm{T}}$, where $\mathbf{1}$ is a $1\times L_p$ vector of ones and $(.)^{\mathrm{T}}$ represents the transpose operation, hence, the dimension of vector $\mathbf{d}$ is $K_u L_p \times 1$. The matrix $\mathbf{R}$ is the $K_u L_p \times K_u L_p$ dimensional correlation matrix defined as [6]

$$\mathbf{R} = \begin{bmatrix} \boldsymbol{\psi}_{1,1} & \boldsymbol{\beta}_{1,2} & \boldsymbol{\beta}_{1,3} & \cdots & \boldsymbol{\beta}_{1,K_u} \\ \boldsymbol{\beta}_{2,1} & \boldsymbol{\psi}_{2,2} & \boldsymbol{\beta}_{2,3} & \cdots & \boldsymbol{\beta}_{2,K_u} \\ \vdots & \vdots & \vdots & \cdots & \vdots \\ \boldsymbol{\beta}_{K_u,1} & \boldsymbol{\beta}_{K_u,2} & \cdots & \cdots & \boldsymbol{\psi}_{K_u,K_u} \end{bmatrix}. \tag{4.3}$$

In (4.3), $\boldsymbol{\psi}_{y,y}$ is the self-correlation sub-matrix of dimension $L_p \times L_p$. It consists of correlation elements among the same *y*-th user from its various multipaths. The (*u,w*)-th element of the self-correlation sub-matrix is defined as [6], [15], [58]

$$\gamma_{u,w}^{y,y} = T_C \cos\left(\theta_{u,w}\right) \sum_{r=0}^{N-1} \sum_{v=0}^{N-1} c_r^{(u)}\ c_v^{(w)}\ g\left((r-v)T_C - (u-w)T_C\right) \tag{4.4}$$

where $c_r^{(u)} \in \{+1,-1\}$ and $c_v^{(w)} \in \{+1,-1\}$ are respectively the *r*-th and *v*-th chips of the random sequences corresponding to the (*u,w*)-th element of the sub-matrix. Also, $\theta_{u,w}$ is the random phase uniformly distributed over $[0,2\pi]$ for the (*u,w*)-th element of the sub-

matrix. Moreover, in (4.3), $\boldsymbol{\beta}_{y,z}$ is the cross-correlation sub-matrix and it consists of the correlation elements between the y-th and the z-th users. The (u,w)-th elements of the cross-correlation sub-matrix are defined as [6], [15], [58]

$$\beta_{u,w}^{y,z} = T_C \cos\left(\theta_{u,w}\right) \sum_{r=0}^{N-1} \sum_{v=0}^{N-1} c_r^{(u)} \, c_v^{(w)} \, g\left((r-v)T_C - (u-w)T_C - \tau_{y,z}\right). \tag{4.5}$$

In (4.5), the random variable $\tau_{y,z}$ represents the random time delay between the y-th and z-th users' chip and is uniformly distributed over $[0, T_C]$ [15]. The entries of the correlation matrix $\mathbf{R}$ can be determined numerically with the help of (4.4) and (4.5). The outputs from the bank of matched filters in (4.3) are then processed by the decorrelating stage as [48]

$$\mathbf{R}^{-1}\mathbf{y} = \mathbf{ACd} + \mathbf{R}^{-1}\mathbf{n} + \mathbf{R}^{-1}\mathbf{I}_{MTJ}. \tag{4.6}$$

In our following BER analysis for the EGC and MRC based systems, we assume bit "+1" is transmitted and $k = 1$ as the desired user. The entries of matrix $\mathbf{R}^{-1}$ can be determined numerically.

4.2.2 BER Analysis for Equal-Gain Combining

In this section, BER performance of a L_r-branch EGC receiver is analyzed, where $L_r \le L_p$. Based on the principle of EGC, we set the weighting parameter of each branch of the multipath diversity receiver to unity. Hence, the outputs from the decorrelator stage in (4.6) are coherently combined to form the final decision statistic. After some algebraic manipulations, the conditional SINR for the EGC-based system is [8]

$$SINR_{EGC} = \frac{\left(A_1 \sum_{l=1}^{L_r} X_{1,l} \right)^2}{\sigma^2_{\mathrm{N},EGC} + \sigma^2_{MTJ,EGC}}. \tag{4.7}$$

In (4.7), the MTJ term is assumed to follow Gaussian distribution with zero mean and variance $\sigma^2_{MTJ,\mathrm{EGC}}$. Also in (4.7), $\sigma^2_{\mathbf{N},\mathrm{EGC}}$ is the variance of the Gaussian noise term. These two variance terms are given by [48]

$$\sigma^2_{\mathrm{N,EGC}} = N_0 \sum_{l=1}^{L_r} \left[\left(\mathbf{R}^{-1} \right)^{\mathrm{T}} \right]_{l,l} \tag{4.8}$$

and

$$\sigma^2_{MTJ,\mathrm{EGC}} = \sum_{l=1}^{L_r} [\mathbf{M}]_{l,l}, \tag{4.9}$$

respectively, where the notation $[\mathbf{B}]_{x,y}$ represents the (x,y)-th component of matrix $\mathbf{B}$. In (4.9), the matrix $\mathbf{M}$ is defined as $\mathbf{M} = \mathbf{R}^{-1}\mathbf{X}\left(\mathbf{R}^{-1}\right)^{\mathrm{T}}$, where $\mathbf{X}$ is the MTJ correlation matrix. The MTJ correlation matrix $\mathbf{X}$ is defined in a similar manner as that of $\mathbf{R}$. The (u,w)-th entry of the MTJ cross-correlation sub-matrix is [6], [15], [48]

$$\begin{aligned} \varsigma^{y,z}_{u,w} &= \frac{T_C}{2} \sum_{i=1}^{J} \alpha_i^2 \mathrm{E}\left(\hat{\lambda}^2_{l,i} \right) G(\Delta f_i) \sum_{r=0}^{N-1} \sum_{v=0}^{N-1} c_r^{(u)} c_v^{(w)} \\ &\quad \times \cos\left[2\pi \Delta f_i \left\{ (r-v)T_C - (u-w)T_C - \tau_{y,z} \right\} - \theta_{u,w} \right] \\ &= T_C \sum_{i=1}^{J} \frac{\alpha_i^2 G(\Delta f_i) M_{(i)} m_{(i)}}{b^2_{(i)}} \sum_{r=0}^{N-1} \sum_{v=0}^{N-1} c_r^{(u)} c_v^{(w)} \\ &\quad \times \cos\left[2\pi \Delta f_i \left\{ (r-v)T_C - (u-w)T_C - \tau_{y,z} \right\} - \theta_{u,w} \right]. \end{aligned} \tag{4.10}$$

Similarly, the (u,w)-th entry of the MTJ self-correlation sub-matrix is

$$\chi_{u,w}^{y,y} = \frac{T_C}{2}\sum_{i=1}^{J}\alpha_i^2 \mathrm{E}\left(\hat{\lambda}_{l,i}^2\right) G\left(\Delta f_i\right) \sum_{r=0}^{N-1}\sum_{v=0}^{N-1} c_r^{(u)} c_v^{(w)}$$

$$\times \cos\left[2\pi\Delta f_i \left\{(r-v)T_C - (u-w)T_C\right\} - \theta_{u,w}\right]$$

$$= T_C \sum_{i=1}^{J} \frac{\alpha_i^2 G\left(\Delta f_i\right) M_{(i)} m_{(i)}}{b_{(i)}^2} \sum_{r=0}^{N-1}\sum_{v=0}^{N-1} c_r^{(u)} c_v^{(w)}$$

$$\times \cos\left[2\pi\Delta f_i \left\{(r-v)T_C - (u-w)T_C\right\} - \theta_{u,w}\right]. \tag{4.11}$$

In (4.10) and (4.11), the parameters α_i, $G\left(\Delta f_i\right)$, J, $M_{(i)}$, $m_{(i)}$, $b_{(i)}$, $\hat{\lambda}_{l,i}$ and Δf_i follow the same definition as in Section 3.2. The values of matrices **R** and **X** can be determined numerically. Here, we incorporate characteristic function with Gaussian approximation approach. Now, by assuming that all the fading variables are independent of each other, the final BER expression for the EGC case can be obtained by using the inversion formula technique as in Sections 3.2 and 3.3, and [47]

$$P_e \approx \frac{1}{2} - \frac{1}{\pi}\int_0^{\infty} \frac{\Phi_{\mathrm{N},EGC}(\omega)\Phi_{MTJ,EGC}(\omega)\Im\left(\Phi_{D,EGC}(\omega)\right)}{\omega}\, d\omega. \tag{4.12}$$

The integral in (4.12) can be evaluated by using any suitable numerical technique. Following the approach of Section 3.2.2, the characteristic function of the data term in (4.12) is given as

$$\Phi_{D,EGC}(\omega) = \prod_{l=1}^{L_r} \frac{\sqrt{\pi}\, 2^{2-2m_{1,l}}\, {b_{1,l}}^{2M_{1,l}} \Gamma(2M_{1,l}) \Gamma(2m_{1,l})}{\Gamma(M_{1,l}) \Gamma(m_{1,l}) \Gamma(\Theta_{1,l})}$$

$$\times \frac{\mu^{M_{1,l}}\, {}_2F_1(2M_{1,l}, \mathfrak{M}_{1,l}; \Theta_{1,l}; -\mu_{1,l})}{\left[{b_{1,l}}^2 + (A_1\omega)^2 \right]^{M_{1,l}}}, \tag{4.13}$$

where

$$\Theta_{1,l} = M_{1,l} + m_{1,l} + 1/2, \tag{4.14}$$

$$\mathfrak{M}_{1,l} = M_{1,l} - m_{1,l} + 1/2 \tag{4.15}$$

and

$$\mu_{1,l} = \exp\left[j2\tan^{-1}(A_1\omega / b_{1,l}) \right]. \tag{4.16}$$

In (4.14)-(4.16), $M_{1,l}$, $m_{1,l}$ and $b_{1,l}$ are the generalized-K parameters of the desired data term. In (4.12), MTJ and noise components are assumed to follow Gaussian distribution. Hence, the characteristic functions of the MTJ and Gaussian noise terms are [6], [48]

$$\Phi_{MTJ,EGC}(\omega) = \exp\left(-\frac{\omega^2}{2} \sum_{l=1}^{L_r} [\mathbf{M}]_{l,l} \right)$$

$$= \prod_{l=1}^{L_r} \exp\left(-\frac{\omega^2}{2} [\mathbf{M}]_{l,l} \right) \tag{4.17}$$

and

$$\Phi_{\mathrm{N},EGC}(\omega) = \exp\left(-\frac{\omega^2 N_0}{2} \sum_{l=1}^{L_r} \left[\left(\mathrm{R}^{-1} \right)^{\mathrm{T}} \right]_{l,l} \right)$$

$$= \prod_{l=1}^{L_r} \exp\left(-\frac{\omega^2 N_0}{2} \left[\left(\mathrm{R}^{-1} \right)^{\mathrm{T}} \right]_{l,l} \right), \tag{4.18}$$

respectively. We now consider a two-dimensional diversity system consisting of an array of L_A antennas or space diversity branches each followed by a decorrelator-based multipath receiver. The final BER expression for the two-dimensional diversity system by employing characteristic function with Gaussian approximation approach is [47]

$$P_e \approx \frac{1}{2} - \frac{1}{\pi}\int_0^{\infty} \frac{\Phi_{\mathrm{N},EGC,2\mathrm{D}}(\omega)\Phi_{MTJ,EGC,2\mathrm{D}}(\omega)\Im\left(\Phi_{D,EGC,2\mathrm{D}}(\omega)\right)}{\omega}\, d\omega. \tag{4.19}$$

In (4.19), the characteristic function of the data term is

$$\Phi_{D,EGC,2\mathrm{D}}(\omega) = \prod_{d=1}^{L_A}\prod_{l=1}^{L_r} \frac{\sqrt{\pi}\,2^{2-2m_{1,d,l}}\, b_{1,d,l}{}^{2M_{1,d,l}}\Gamma\left(2M_{1,d,l}\right)\Gamma\left(2m_{1,d,l}\right)}{\Gamma\left(M_{1,d,l}\right)\Gamma\left(m_{1,d,l}\right)\Gamma\left(\Theta_{1,d,l}\right)}$$

$$\times \frac{\mu^{M_{1,d,l}}\,{}_2F_1\left(2M_{1,d,l}, \mathfrak{M}_{1,d,l}; \Theta_{1,d,l}; -\mu_{1,d,l}\right)}{\left[b_{1,d,l}{}^2 + (A_1\omega)^2\right]^{M_{1,d,l}}}, \tag{4.20}$$

where

$$\Theta_{1,d,l} = M_{1,d,l} + m_{1,d,l} + 1/2, \tag{4.21}$$

$$\mathfrak{M}_{1,d,l} = M_{1,d,l} - m_{1,d,l} + 1/2, \tag{4.22}$$

and

$$\mu_{1,d,l} = \exp\left[\, j2\tan^{-1}\left(A_1\omega / b_{1,d,l}\right)\right]. \tag{4.23}$$

Furthermore, the characteristic functions of the MTJ and Gaussian noise terms can be expressed as

$$\Phi_{MTJ,EGC}(\omega) = \exp\left(-\frac{\omega^2}{2} L_A \sum_{l=1}^{L_r} [\mathbf{M}]_{l,l}\right)$$

$$= \prod_{l=1}^{L_r} \exp\left(-\frac{\omega^2}{2} L_A [\mathbf{M}]_{l,l}\right) \tag{4.24}$$

and

$$\Phi_{\mathrm{N},EGC}(\omega) = \exp\left(-\frac{\omega^2 N_0 L_A}{2}\sum_{l=1}^{L_r}\left[\left(\mathrm{R}^{-1}\right)^{\mathrm{T}}\right]_{l,l}\right)$$

$$= \prod_{l=1}^{L_r}\exp\left(-\frac{\omega^2 N_0 L_A}{2}\left[\left(\mathrm{R}^{-1}\right)^{\mathrm{T}}\right]_{l,l}\right) \tag{4.25}$$

respectively.

4.2.3 BER Analysis for Maximal-Ratio Combining

In this section, we use MRC as the diversity-combining technique. Based on the principle of MRC, we set the weighting parameter of each branch to be the corresponding fading variable, i.e., $X_{1,l}$ [8]. The outputs from the decorrelator stage in (4.6) are first weighted by their respective fading gains and are then coherently combined to form the final decision statistic. After some algebraic manipulations, the conditional SINR for the system is [6]

$$SINR_{MRC} = \frac{\left(A_1\sum_{l=1}^{L_r}X_{1,l}^2\right)^2}{\sigma_{\mathrm{N},MRC}^2+\sigma_{MTJ,MRC}^2} \tag{4.26}$$

where

$$\sigma_{\mathrm{N},MRC}^2 = N_0\sum_{l=1}^{L_r}\left[\left(\mathbf{R}^{-1}\right)^{\mathrm{T}}\right]_{l,l}X_{1,l}^2 \tag{4.27}$$

and

$$\sigma_{MTJ,MRC}^2 = \sum_{l=1}^{L_r}[\mathbf{M}]_{l,l}X_{1,l}^2. \tag{4.28}$$

In (4.26), we assume that AWGN and MTJ terms follow Gaussian distribution with zero mean and variances defined in (4.27) and (4.28), respectively. Here, we use the

characteristic function with Gaussian approximation technique. By the inversion formula, the final BER expression for the MRC case is given by [47]

$$P_e \approx \frac{1}{2} - \frac{1}{\pi}\int_0^{\infty} \frac{\Phi_{\mathrm{N},MRC}(\omega)\Phi_{MTJ,MRC}(\omega)\Im\left(\Phi_{D,MRC}(\omega)\right)}{\omega}\, d\omega. \tag{4.29}$$

The integral in (4.29) can be evaluated by using numerical technique. In (4.29), the characteristic function of the desired data term is [6], [46]

$$\begin{aligned}
\Phi_{D,MRC}(\omega) &= \prod_{l=1}^{L_r} \mathrm{E}\left\{\exp\left(j\omega A_1 X_{1,l}^2\right)\right\} \\
&= \prod_{l=1}^{L_r} \frac{b_{l,D}^{\,M_{l,D}+m_{l,D}}}{2^{M_{l,D}+m_{l,D}-2}\Gamma\left(m_{l,D}\right)\Gamma\left(M_{l,D}\right)} \\
&\quad \times \int_0^{\infty} x^{M_{l,D}+m_{l,D}-1} K_{M_{l,D}-m_{l,D}}\left(b_{l,D}x\right)\exp\left(j\omega x^2 A_1\right)dx \\
&= \prod_{l=1}^{L_r}\left(j\frac{b_{1,l}^2}{4A_1^2\omega}\right)^{1/2\left(M_{1,l}+m_{1,l}-1\right)} \times \exp\left(j\frac{b_{1,l}^2}{8A_1^2\omega}\right) \\
&\quad \times W_{-\frac{1}{2}\left(M_{1,l}+m_{1,l}-1\right),\frac{1}{2}\left(M_{1,l}-m_{1,l}\right)}\left(j\frac{b_{1,l}^2}{4A_1^2\omega}\right).
\end{aligned} \tag{4.30}$$

Finally, the characteristic functions of the Gaussian noise and MTJ terms are [6], [46]

$$\Phi_{\mathrm{N},MRC}(\omega) = \prod_{l=1}^{L_r} \mathrm{E}\left\{\exp\left(-\frac{\omega^2 N_0}{2}\left[\left(\mathbf{R}^{-1}\right)^{\mathrm{T}}\right]_{l,l} X_{1,l}^2\right)\right\}$$

$$= \prod_{l=1}^{L_r}\left(\frac{b_{1,l}^2}{2\omega^2 N_0\left[\left(\mathbf{R}^{-1}\right)^{\mathrm{T}}\right]_{l,l}}\right)^{1/2\left(M_{1,l}+m_{1,l}-1\right)} \times \exp\left(\frac{b_{1,l}^2}{4\omega^2 N_0\left[\left(\mathbf{R}^{-1}\right)^{\mathrm{T}}\right]_{l,l}}\right)$$

$$\times W_{-\frac{1}{2}\left(M_{1,l}+m_{1,l}-1\right),\frac{1}{2}\left(M_{1,l}-m_{1,l}\right)}\left(\frac{b_{1,l}^2}{2\omega^2 N_0\left[\left(\mathbf{R}^{-1}\right)^{\mathrm{T}}\right]_{l,l}}\right) \tag{4.31}$$

and

$$\Phi_{MTJ,MRC}(\omega) = \prod_{l=1}^{L_r} \mathrm{E}\left\{\exp\left(-\frac{\omega^2 [\mathbf{M}]_{l,l}}{2} X_{1,l}^2\right)\right\}$$

$$= \prod_{l=1}^{L_r}\left(\frac{b_{1,l}^2}{2\omega^2 [\mathbf{M}]_{l,l}}\right)^{1/2\left(M_{1,l}+m_{1,l}-1\right)} \times \exp\left(\frac{b_{1,l}^2}{4\omega^2 [\mathbf{M}]_{l,l}}\right)$$

$$\times W_{-\frac{1}{2}\left(M_{1,l}+m_{1,l}-1\right),\frac{1}{2}\left(M_{1,l}-m_{1,l}\right)}\left(\frac{b_{1,l}^2}{2\omega^2 [\mathbf{M}]_{l,l}}\right), \tag{4.32}$$

respectively. We now extend our analysis to two-dimensional diversity systems with L_A space diversity branches each followed by a decorrelator based receiver. The final BER expression for the two-dimensional diversity system is [8], [47]

$$P_e \approx \frac{1}{2} - \frac{1}{\pi}\int_0^{\infty} \frac{\Phi_{\mathrm{N},MRC,2\mathrm{D}}(\omega)\Phi_{MTJ,MRC,2\mathrm{D}}(\omega)\Im\left(\Phi_{D,MRC,2\mathrm{D}}(\omega)\right)}{\omega} d\omega. \tag{4.33}$$

In (4.33), the characteristic function of the data is [8], [46]

$$\Phi_{D,MRC,2\mathrm{D}}(\omega) = \prod_{d=1}^{L_A}\prod_{l=1}^{L_r}\left(j\frac{b_{1,d,l}^2}{4A_1^2\omega}\right)^{1/2\left(M_{1,d,l}+m_{1,d,l}-1\right)} \times\exp\left(j\frac{b_{1,d,l}^2}{8A_1^2\omega}\right)$$
$$\times W_{-\frac{1}{2}\left(M_{1,d,l}+m_{1,d,l}-1\right),\frac{1}{2}\left(M_{1,d,l}-m_{1,d,l}\right)}\left(j\frac{b_{1,d,l}^2}{4A_1^2\omega}\right). \tag{4.34}$$

Moreover, the characteristic functions of the Gaussian noise and MTJ terms in (4.33) are given by [8], [46]

$$\Phi_{\mathrm{N},MRC,2\mathrm{D}}(\omega) = \prod_{d=1}^{L_A}\prod_{l=1}^{L_r}\left(\frac{b_{1,d,l}^2}{2\omega^2 N_0\left[\left(\mathbf{R}^{-1}\right)^{\mathrm{T}}\right]_{l,l}}\right)^{1/2\left(M_{1,d,l}+m_{1,d,l}-1\right)} \exp\left(\frac{b_{1,d,l}^2}{4\omega^2 N_0\left[\left(\mathbf{R}^{-1}\right)^{\mathrm{T}}\right]_{l,l}}\right)$$
$$\times W_{-\frac{1}{2}\left(M_{1,d,l}+m_{1,d,l}-1\right),\frac{1}{2}\left(M_{1,d,l}-m_{1,d,l}\right)}\left(\frac{b_{1,d,l}^2}{2\omega^2 N_0\left[\left(\mathbf{R}^{-1}\right)^{\mathrm{T}}\right]_{l,l}}\right) \tag{4.35}$$

and

$$\Phi_{MTJ,MRC,2\mathrm{D}}(\omega) = \prod_{d=1}^{L_A}\prod_{l=1}^{L_r}\left(\frac{b_{1,d,l}^2}{2\omega^2\left[\mathbf{M}\right]_{l,l}}\right)^{1/2\left(M_{1,d,l}+m_{1,d,l}-1\right)} \exp\left(\frac{b_{1,d,l}^2}{4\omega^2\left[\mathbf{M}\right]_{l,l}}\right)$$
$$\times W_{-\frac{1}{2}\left(M_{1,d,l}+m_{1,d,l}-1\right),\frac{1}{2}\left(M_{1,d,l}-m_{1,d,l}\right)}\left(\frac{b_{1,d,l}^2}{2\omega^2\left[\mathbf{M}\right]_{l,l}}\right). \tag{4.36}$$

respectively. The entries of matrices $\mathbf{R}^{-1}$ and $\mathbf{M}$ can be determined numerically. Due to the complex nature of the problem considered in this chapter, the BER expressions presented cannot be further simplified analytically. Therefore, numerical techniques are required to generate numerical results. However, with the help of our BER expressions, we can analyze the BER performance under low BER ranges, where the simulation is time consuming.

4.3 Numerical Results and Discussions

In this section, we present numerical results based on the BER expressions presented in Section 4.2. Both SRC and BTD pulses are considered here. We assume $\beta = 1$, i.e., the excess bandwidth is 100%. We also assume perfect power control, though our results can be easily extended to non-uniform power scenarios. To be consistent, we consider $N = 31$ with random spreading sequences as in Section 3.4. However, our expressions are valid for any value of N. In Figs. 4.1 to 4.7, we consider $K_u = 5$ users in the system. We assume the total jamming power to be uniformly distributed among all jamming tones [6]. To be consistent, we consider similar condition for the MTJ as in Section 3.4, i.e., $J = 3$ jamming tones with shadowing parameter fixed at $M_{(i)} = 12$ for $i = 1$, 2 and 3, and the small-scale fading parameters for the three jamming tones are set at $m_{(1)} = 2$, $m_{(2)} = 1$ and $m_{(3)} = 4$. In Figs. 4.1 to 4.7, we consider $L_p = 3$, $L_r = 3$ and $\eta = 0.2$. We present the BER plots by averaging over various combinations of random spreading codes for each user. Furthermore, in our simulations, we also assume to have perfect knowledge of channel fading parameters at the receiver side in order to incorporate MRC. Furthermore, all random fading variables are assumed to be fixed for a bit duration in order to have a coherent reception. In addition, fading variables of all K_u users are assumed to be independent of each other and vary independently from one bit to another. The jamming tones are assumed to be uniformly distributed over the spectrum of the desired user and the total jamming power is assumed to be equally distributed among all jamming tones. In Fig. 4.1, analytical and simulation results are presented for both EGC and MRC based systems with BTD pulses. We fix SJR at -10 dB. We observe a close match between the

simulation and analytical results. This validates the BER expressions presented in Section 4.2. We observe that since we incorporate Gaussian approximation in our analytical analysis, therefore, there is a slight deviation between the analytical and simulation results. We also observe that the system with MRC shows better BER performance as compared to the one with EGC. Furthermore, we also observe flattening of the BER plots as E_b/N_0 value increases, due to the dominating effect of MTJ.

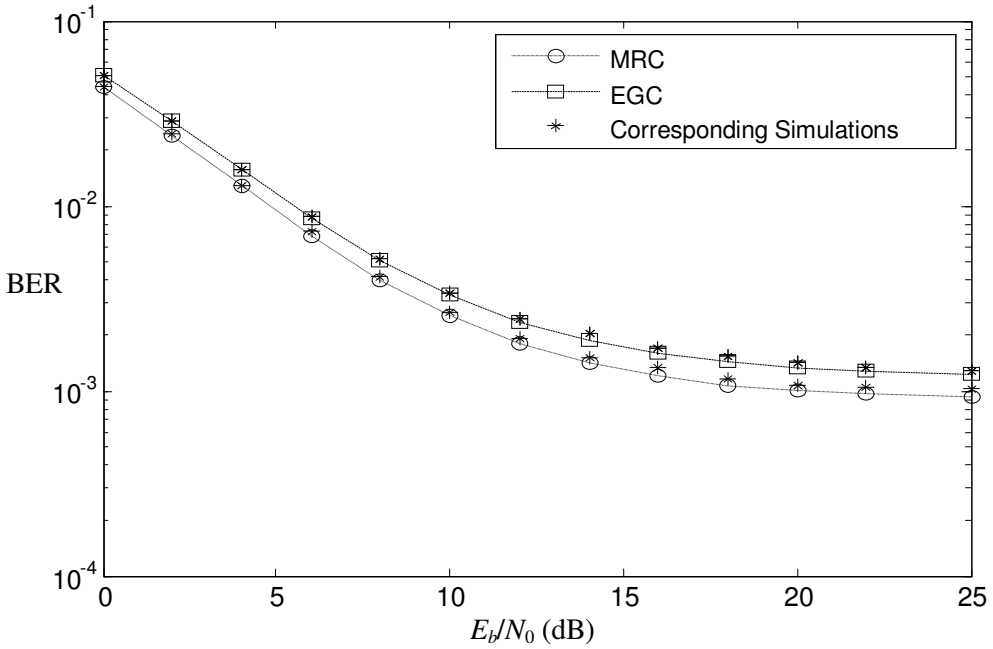

Figure 4.1: Comparison of analytical and simulation results for systems with BTD pulses, $m_{1,l} = 3$, $M_{1,l} = 4$, $L_A = 1$ and SJR = -10 dB.

In Fig. 4.2, we compare the BER performance of EGC and MRC based system with both types of band-limited pulses. From the figure, we observe that with both diversity-combining techniques and under identical scenarios of fading and jamming, systems with BTD pulse outperform the ones with SRC pulse. Hence, with the decorrelator-based systems, BTD pulse gives better BER performance due to its superior correlation properties. In Fig. 4.3, we compare BER performance of EGC and MRC based systems

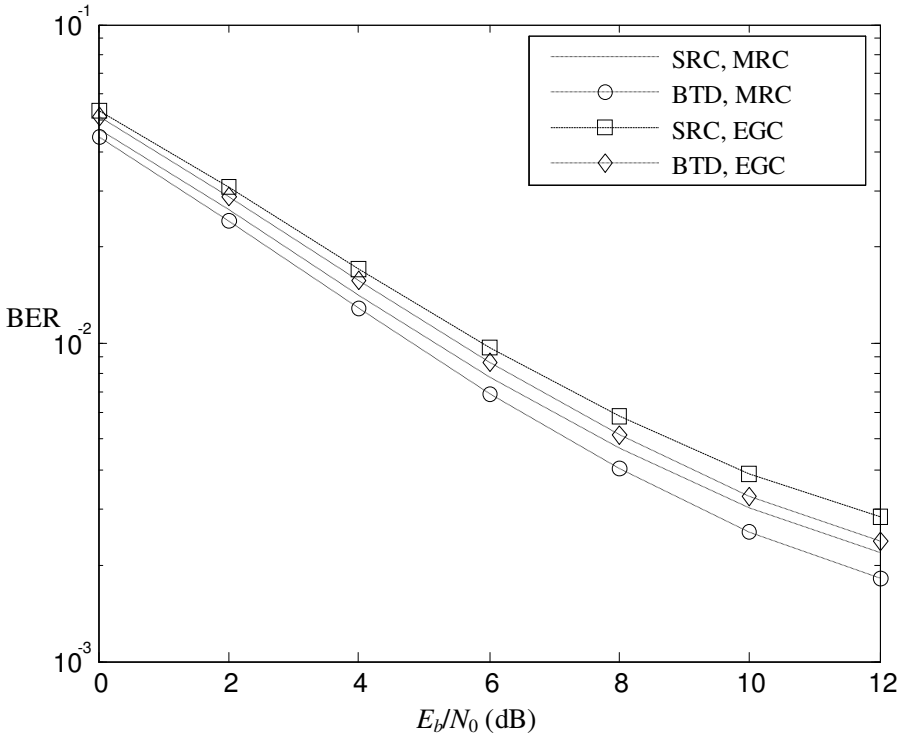

Figure 4.2: BER performance comparison of EGC and MRC based systems with two types of pulses, $m_{1,l} = 3$, $M_{1,l} = 4$, $L_A = 1$ and SJR = -10 dB.

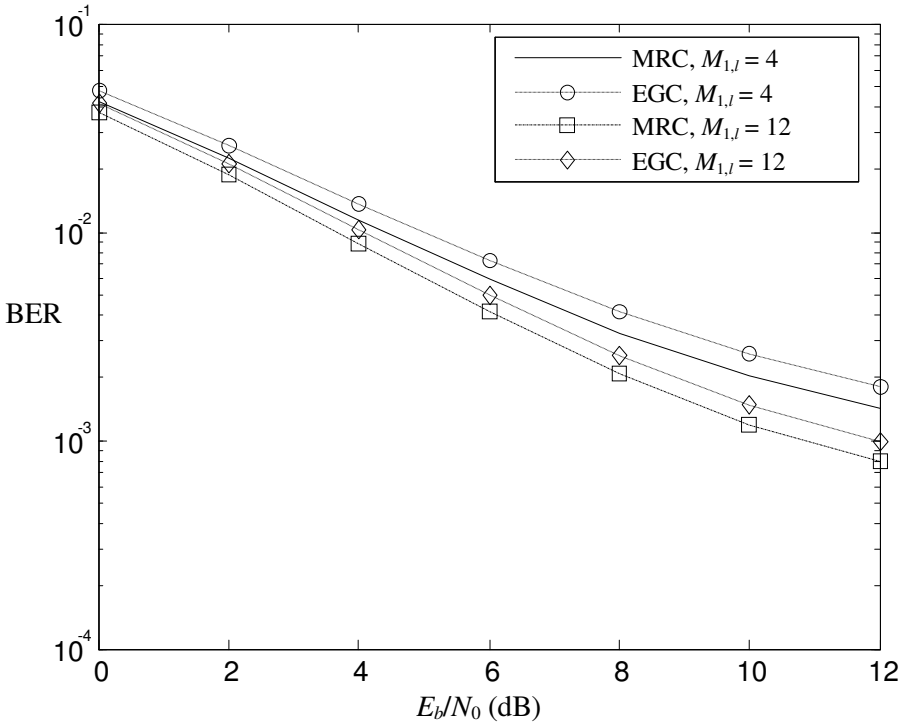

Figure 4.3: BER performance comparison of EGC and MRC based systems under various shadowing conditions with BTD pulses, $m_{1,l} = 4$, $L_A = 1$ and SJR = -10 dB.

under shadowing and negligible shadowing conditions. From Fig. 4.3, we observe that both EGC and MRC decorrelator-based systems show degradation in BER performance under shadowing conditions. This is because the overall system SINR suffers as the wireless channel exhibits severe shadowing conditions [8]. In Fig. 4.4, we analyze the effects of various small-scale fading parameters on the BER performance of MRC-based receiver. Only BTD pulse shape is considered. It can be observed that by increasing the small-scale fading parameter, the BER performance is improved due to the improved fading conditions of the wireless channel [20]. From Figs. 4.1 to 4.4, we observe that the BER curves show flattening effect at higher values of E_b/N_0. Such behavior is due to the presence of interference contributed by the MTJ.

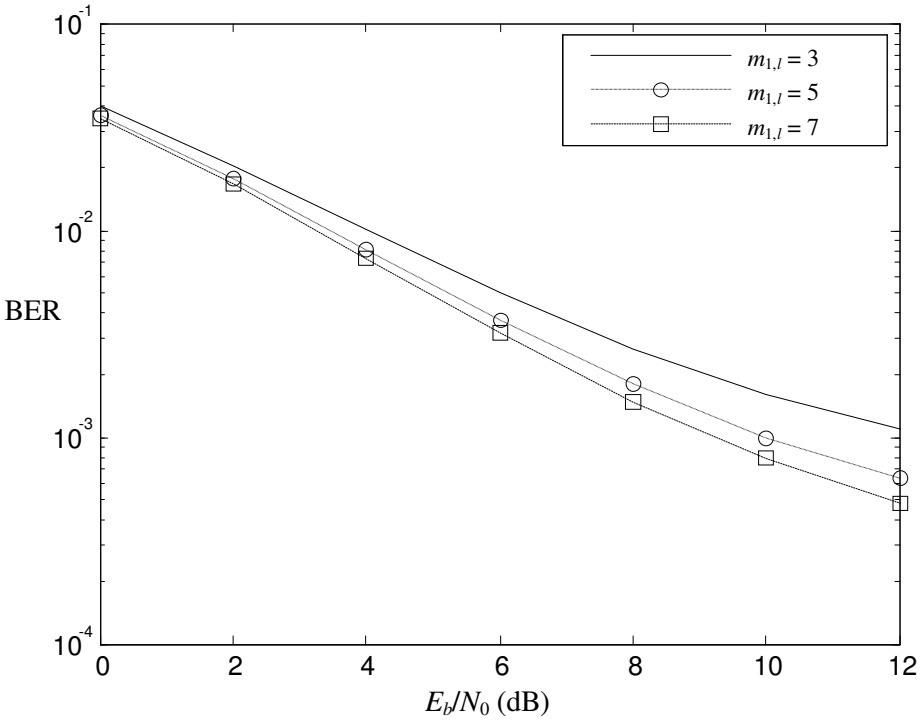

Figure 4.4: BER performance of MRC based systems with BTD pulse, $M_{1,l} = 12$, $L_A = 1$, SJR = -10 dB, and various small-scale fading parameters.

In Fig. 4.5, we compare the BER performance of systems with a decorrelator stage and the ones without it. From the figure, we observe that the systems with decorrelator

stage outperform the ones without it. We further observe that at high E_b/N_0 levels, due to the presence of MAI and MTJ, the systems without decorrelator stage show more flattening of the BER curves as compared to the ones with decorrelator stage. Thus, the presence of combined effects of the interference caused by MAI, self-interference and MTJ not only degrades the BER performance but also introduces a quicker flattening effect of BER plots. Hence, by introducing a decorrelator stage, we not only improve the BER performance but also reduce the flattening effects of the BER plot caused by the combined effects of interference.

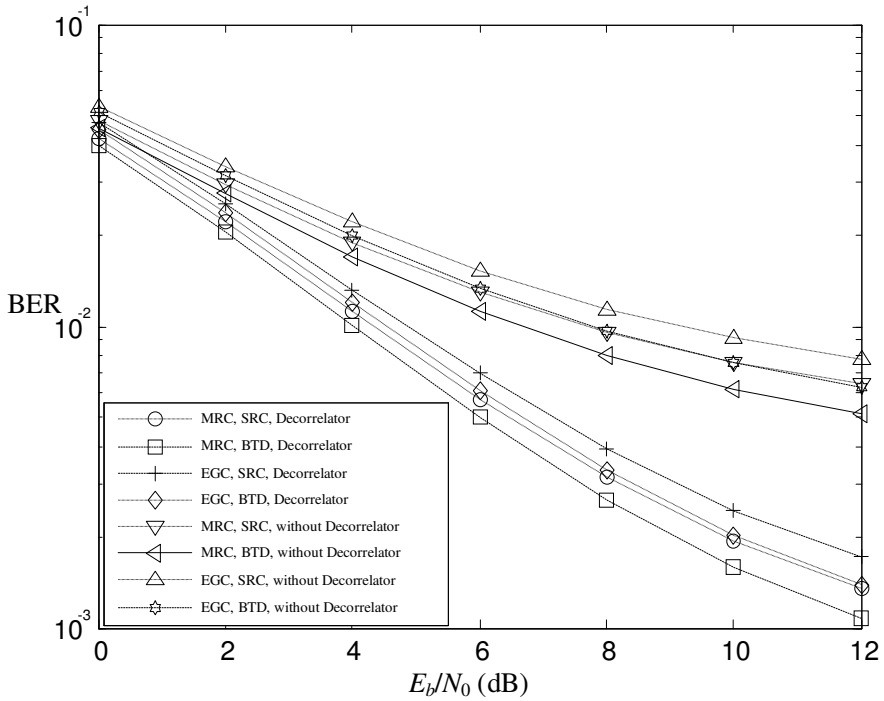

Figure 4.5: Performance comparison of systems with and without decorrelator stage, $m_{1,l} = 3$, $M_{1,l} = 12$, $L_A = 1$ and SJR = -10 dB.

In Fig. 4.6, we compare the BER performance of single-dimensional diversity scheme, i.e., multipath-only, and the two-dimensional diversity based systems. Both types of combining schemes as well as both pulse shapes are considered. From the figure, it is

clear that the band-limited systems with two-dimensional diversity scheme, i.e., the combination of space and multipath, outperform the ones with single-dimensional diversity. This is due to the improved SINR conditions under the two-dimensional scheme.

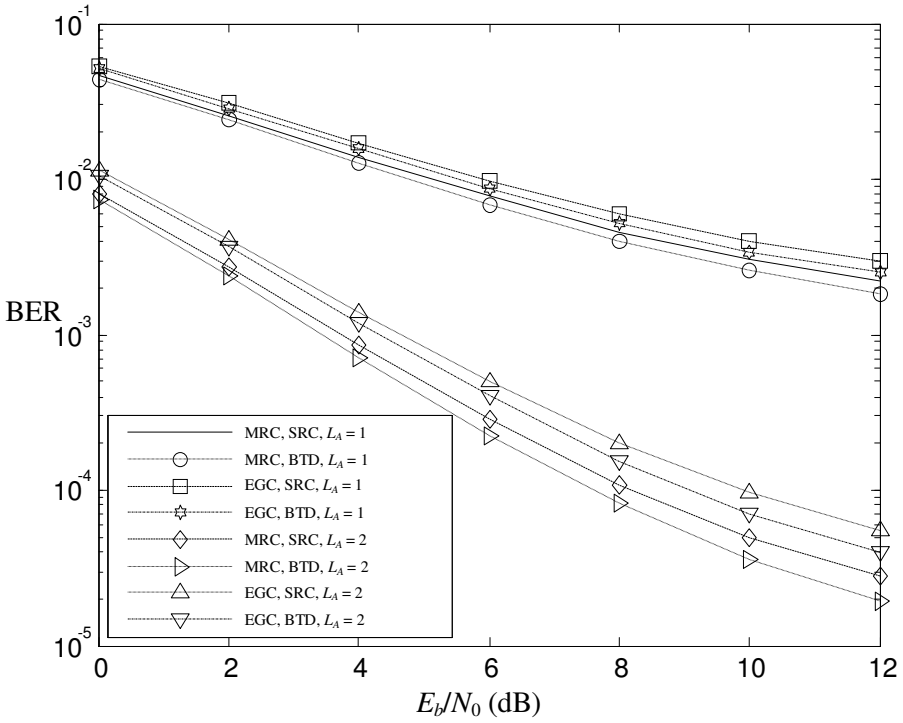

Figure 4.6: Performance comparison between single-dimensional and two-dimensional systems with $m_{1,l} = 2$, $M_{1,l} = 12$ and SJR = -10 dB.

We further observe that the BER plots do not show noticeable increase in the slopes with the increase of the diversity branches due to the presence of MTJ.

In Fig. 4.7, we analyze the effects of various jamming power conditions on the BER performance of the system. We consider a MRC-based two-dimensional diversity system with BTD pulse. From Fig. 4.7, we observe the BER performance is degraded when the jamming power is increased. We also notice an increase in the flattening of BER curves

for the systems under higher jamming power scenarios. In Fig. 4.8, we present the BER performance under various system load conditions. We consider a MRC-based system with L_A = 1, L_p = L_r = 2 and with BTD pulse shape. We fix E_b/N_0 at 14 dB and assume SJR to be -11 dB. From the figure, it can be observed that as load increases, BER performance degrades due to noise enhancement effects of the decorrelator. Furthermore, we also observe improvement in BER performance as the values of M and m are increased, i.e., when channel shadowing and fading conditions are improved. We observe this improvement in BER performance under various system loading conditions.

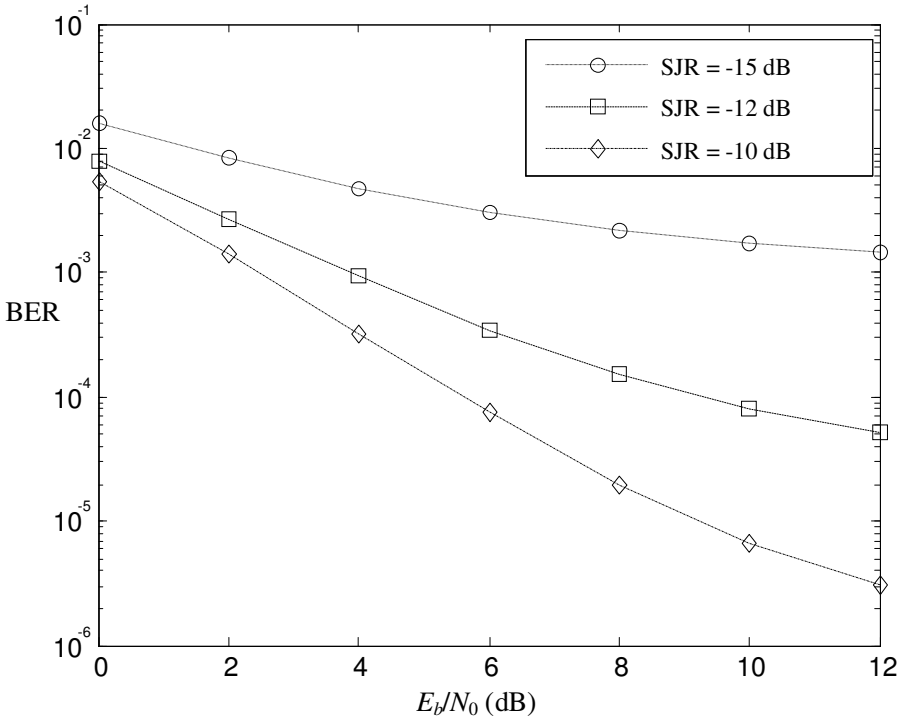

Figure 4.7: BER performance with various jamming power conditions for MRC based systems with BTD pulse, L_A = 2, $m_{1,l}$ = 5 and $M_{1,l}$ = 12.

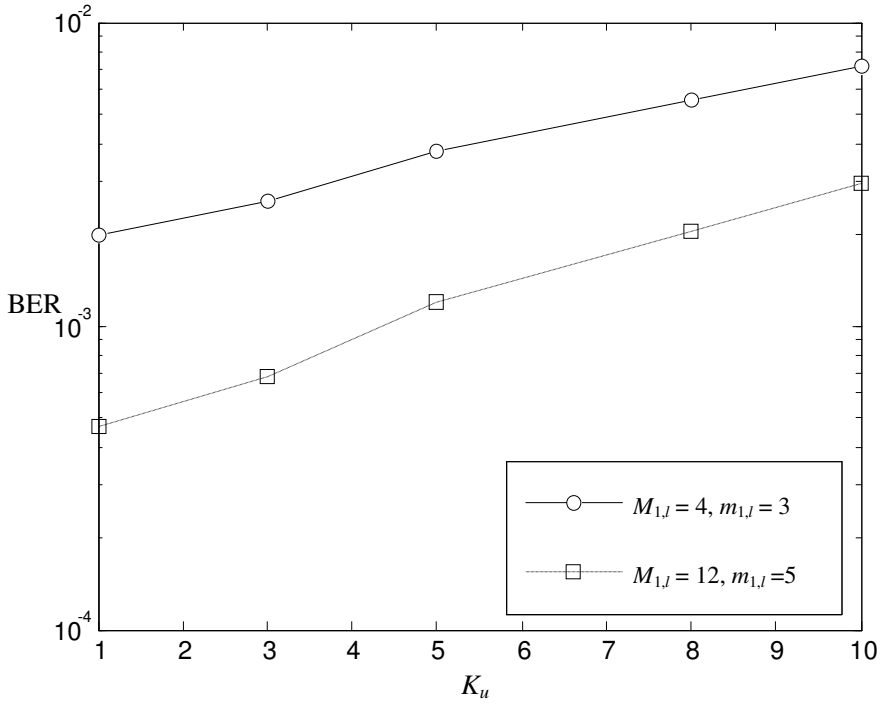

Figure 4.8: BER performance of MRC based systems, BTD pulse, $L_A = 1$, $L_p = L_r = 2$, E_b/N_0 = 14 dB and SJR = -11 dB.

4.4 Conclusion

In this chapter, we have presented the BER performance analyses of band-limited asynchronous DS-CDMA systems with decorrelator-based systems. Analytical BER expressions with the help of Gaussian approximation are presented as a function of generalized-*K* distribution parameters, number of multipaths and the number of space diversity branches at the receiver side. Due to the complexity of the problem considered in this chapter, our BER expressions cannot be further simplified by using analytical approaches. Hence, numerical techniques are incorporated to generate numerical results. However, with the help of our BER expressions, we have analyzed the BER performance under low BER ranges, where the simulation is time consuming. Numerical results have

shown that the systems with BTD pulses have demonstrated better BER performance as compared to the ones with SRC pulses under various scenarios of fading and shadowing. Moreover, we also observe that the two-dimensional diversity receivers outperform the multipath-only receivers. This is because the receivers employing two-dimensional diversity scheme incorporate both spatial as well as the multipath diversity to combat shadowing and the small-scale fading effects. It has also been observed that the presence of MTJ in the system introduces a noise floor at high levels of E_b/N_0. We have also shown that various combinations of wireless channel fading and shadowing can be easily analyzed by incorporating the generalized-K distribution.

Chapter 5

Performance Analysis of Multiuser Band-limited MIMO DS-CDMA Systems

In this chapter, we study the BER performance of space-time transmit diversity scheme for synchronous and asynchronous band-limited DS-CDMA systems over generalized-K flat as well as frequency-selective multipath fading channels. We consider a space-time system with two transmitter and multiple receiver antennas. Both slow and fast fading conditions are analyzed. It has been shown in the previous chapters that the systems with MRC-based combining technique outperform the ones with EGC, therefore, for the space-time transmit diversity scheme, we only incorporate MRC. However, our BER analysis can be easily extended to the EGC case as well. This chapter is organized as follows. In Section 5.1, we present an overview of the previous work and the contributions of our work. In Section 5.2, analytical BER analysis of the MRC-based scheme is presented for synchronous DS-CDMA systems with decorrelator and MMSE based system. In Section 5.3, we extend our analytical BER analysis to asynchronous DS-CDMA systems over frequency-selective multipath fading channels. Numerical results and conclusions are given in Sections 5.4 and 5.5, respectively.

5.1 Introduction

With the large demand for high data rate applications and improved signal quality over wireless channels, much research has been conducted to fulfill the promises of future wireless systems [34]. One solution to these problems resides in the use of multiple antennas at the transmitter and/or receiver sides, referred as multiple-input multiple-output (MIMO) systems. Space-time coding (STC) techniques that are based on MIMO systems were introduced in [34], where it was shown that they can provide both spatial diversity and coding gain. By exploiting the independent fading between channels of different transmitter and receiver antennas, spatial diversity can be achieved. One major class of STC is space-time trellis code (STTC) [34]. Although offering tremendous performance improvement over fading channels, STTC present major complexity issues. Another class of STC is referred to as space-time block code (STBC) [35]. These are known to provide the same system diversity but with much less complexity than STTC. An example of STBC was first introduced by Alamouti [36] as a simple space-time transmit diversity scheme, which is based on two transmitter and multiple receiver antennas. Within the framework of space-time coding, many researchers have recently focused on the application of such codes in DS-CDMA systems [59]-[63]. The authors in [23] proposed a space-time spreading scheme suitable for DS-CDMA systems over Rayleigh fast-fading channels. The scheme in [23] considers a space-time spreading technique where each user is assigned a pair of code sequences to provide the full temporal and spatial diversity of the system. In [23], space-time transmit diversity scheme for DS-CDMA systems was examined for Rayleigh flat-fading channels. In [64] and [65], the authors incorporated this scheme for DS-CDMA systems with linear multiuser

detection schemes over Rayleigh and Nakagami flat-fading channels, respectively. The underlying space-time system employed 2 transmitter and L_A receiver antennas. In [64], it has been shown that the full diversity orders of $2\times 2L_A$ for fast-fading and $2L_A$ for slow-fading channels can be achieved for the Rayleigh fading case. Recently, some efforts have aimed at the integration of STC with direct-sequence code-division multiple-access (DS-CDMA) systems over frequency-selective fading channels [37]. In [66], it was shown that for the space-time transmit diversity scheme with two transmitter antennas, one receiver antenna and L_p resolvable multipaths over a frequency-selective Rayleigh fast fading channel, a full diversity-order of $2\times 2L_p$ can be achieved with decorrelator detector. Motivated by [23] and [64]-[66], we perform BER analysis of this transmit diversity scheme for the case of band-limited DS-CDMA systems. We consider a synchronous as well as asynchronous band-limited DS-CDMA system over flat and frequency-selective generalized-K fading channels.

5.2 BER Performance of Synchronous Space-Time Multiuser Systems

We consider a synchronous band-limited DS-CDMA system with two transmitter and L_A receiver antennas. The transmitter employs STBC-based space-time spreading transmit diversity scheme as defined in [64]. A flat fast-fading channel is assumed in this section. There are K_u users transmitting data. Based on the encoder model described in [64], data bits are encoded with two spreading codes s_1 and s_2 for each user. The encoder produces codewords

$$d_1 s_1 + d_2 s_2 \tag{5.1}$$

and

$$d_1 s_2 - d_2 s_1 \tag{5.2}$$

where $d_1 \in \{+1, -1\}$ and $d_2 \in \{+1, -1\}$ are equal-probable data bits of duration T_b. These codewords are then transmitted from antenna 1 and 2, respectively, during the first transmission period. In the second transmission period, these codewords are switched with respect to the antenna order. We employ random non-orthogonal spreading codes [64] and use linear multiuser detection schemes to combat the MAI. BPSK is considered as the modulation technique. The transmitted signals are captured by each of the L_A receiver antennas in the presence of MTJ and AWGN. Each antenna has a pair of matched filters, matched to the spreading codes. The received signal of the *l*-th antenna after co-phasing, down-conversion and demodulation from each of the two matched filters can be written in a matrix form as [65]

$$\mathbf{Y}_v^l = \mathbf{RAH}_v^l \mathbf{d} + \mathbf{I}_v^l + \mathbf{N}_v^l \tag{5.3}$$

where the subscript $v = 0$ and 1 denotes the time instance t and $t + T_b$ respectively, $\mathbf{Y}_v^l$ is a $2K_u \times 1$ vector of the output from the matched filters, $\mathbf{R}$ is a $2K_u \times 2K_u$ cross-correlation matrix [64], $\mathbf{A}$ is the $2K_u \times 2K_u$ diagonal matrix containing all K_u users' amplitudes, $\mathbf{d}$ is the $2K_u \times 1$ vector containing bits d_1 and d_2 of all users, and $\mathbf{I}_v^l$, $\mathbf{N}_v^l$ are the $2K_u \times 1$ MTJ and Gaussian noise vectors, respectively. The channel matrix $\mathbf{H}_v^l$ is a $2K_u \times 2K_u$ diagonal matrix defined as [64]

$$\mathbf{H}_v^l = \text{diag}\left[\mathbf{h}_{v,1}^l, \ldots \mathbf{h}_{v,k}^l\right]. \tag{5.4}$$

The 2×2 matrices $\mathbf{h}_{v,k}^{l}$ are [64]

$$\mathbf{h}_{0,k}^{l}=\begin{bmatrix} x_{0,1,l,k} & -x_{0,2,l,k} \\ x_{0,2,l,k} & x_{0,1,l,k} \end{bmatrix} \tag{5.5}$$

and

$$\mathbf{h}_{1,k}^{l}=\begin{bmatrix} x_{1,2,l,k} & -x_{1,1,l,k} \\ x_{1,1,l,k} & x_{1,2,l,k} \end{bmatrix} \tag{5.6}$$

where the entry $x_{v,p,l,k}$ is an independent random variable that follows the generalized-K distribution, and the subscripts v, p, l and k indicate the time index, transmitter antenna, receiver antenna and the user, respectively. We assume user 1 as our desired user and $d_1=+1$ as the transmitted bit. We also assume various random variables to be independent of each other. Based on the assumption that we have perfect channel information at the receiver side, we incorporate MRC in our analysis. Now, by applying decorrelation operation on (5.3) and combining the outputs based on the principle of MRC as described in [64], the conditional SINR expression is [65]

$$SINR=\frac{\left(A_1/\sqrt{2}\right)^2\left(\sum_{l=1}^{L_A}\sum_{p=1}^{2}\sum_{v=0}^{1}x_{v,p,l}^2\right)^2}{\sigma_{\mathbf{N},decorr}^2+\sigma_{\mathbf{I},decorr}^2}. \tag{5.7}$$

In (5.7), A_1 denotes the signal amplitude of user 1. In (5.7), we assume MTJ term to have a Gaussian distribution with zero mean and variance $\sigma_{\mathbf{I},decorr}^2$. The variance terms of Gaussian noise and MTJ can be expressed as [65]

$$\sigma_{\mathbf{N},decorr}^2=N_0\left(\left[\mathbf{R}^{-1}\right]_{1,1}\left\{\sum_{l=1}^{L_A}\left(x_{0,1,l}^2+x_{1,2,l}^2\right)\right\}+\left[\mathbf{R}^{-1}\right]_{2,2}\left\{\sum_{l=1}^{L_A}\left(x_{0,2,l}^2+x_{1,1,l}^2\right)\right\}\right) \tag{5.8}$$

and

$$\sigma^2_{\mathbf{I},decorr} = \Lambda\left(\left[\mathbf{R}^{-1}\right]_{1,1}\left\{\sum_{l=1}^{L_A}\left(x^2_{0,1,l}+x^2_{1,2,l}\right)\right\}+\left[\mathbf{R}^{-1}\right]_{2,2}\left\{\sum_{l=1}^{L_A}\left(x^2_{0,2,l}+x^2_{1,1,l}\right)\right\}\right) \tag{5.9}$$

respectively. The parameter Λ is given as

$$\Lambda = 2\sum_{i=1}^{J}\left(\frac{\alpha_i^2 G\left(\Delta f_i\right) M_{(i)} m_{(i)}}{b^2_{(i)}}\right). \tag{5.10}$$

We will use the characteristic function approach to obtain the final unconditional BER expression. Based on expressions (5.7)-(5.9) and by using the Gaussian nature of noise and MTJ, we can obtain the BER expression by using the inversion formula as [19]

$$P_e \approx \frac{1}{2}-\frac{1}{\pi}\int_0^{\infty}\frac{\Phi_{noise}\left(\omega\right)\Phi_{MTJ}\left(\omega\right)\Im\left(\Phi_{data}\left(\omega\right)\right)}{\omega}d\omega. \tag{5.11}$$

The integral in (5.11) can be computed by using any suitable numerical technique. The unconditional characteristic function of the Gaussian noise is defined as

$$\Phi_{noise}\left(\omega\right) = \prod_{l=1}^{L_A}\left(\Phi^{noise}_{0,1,l}\left(\omega\right)\Phi^{noise}_{1,2,l}\left(\omega\right)\Phi^{noise}_{0,2,l}\left(\omega\right)\Phi^{noise}_{1,1,l}\left(\omega\right)\right) \tag{5.12}$$

where

$$\Phi^{noise}_{\rho}\left(\omega\right) = \left(\frac{b^2_{\rho}}{2\omega^2 N_0\left[\mathbf{R}^{-1}\right]_{1,1}}\right)^{1/2\left(M_{\rho}+m_{\rho}-1\right)}\exp\left(\frac{b^2_{\rho}}{4\omega^2 N_0\left[\mathbf{R}^{-1}\right]_{1,1}}\right) \times W_{-\frac{1}{2}\left(M_{\rho}+m_{\rho}-1\right),\frac{1}{2}\left(M_{\rho}-m_{\rho}\right)}\left(\frac{b^2_{\rho}}{2\omega^2 N_0\left[\mathbf{R}^{-1}\right]_{1,1}}\right). \tag{5.13}$$

In (5.13), $\rho = \{0,1,l\}$, $\{1,2,l\}$, $\{0,2,l\}$ or $\{1,1,l\}$ for $\Phi^{noise}_{0,1,l}\left(\omega\right)$, $\Phi^{noise}_{1,2,l}\left(\omega\right)$, $\Phi^{noise}_{0,2,l}\left(\omega\right)$ or $\Phi^{noise}_{1,1,l}\left(\omega\right)$, respectively. The entries of matrix $\mathbf{R}^{-1}$ can be determined numerically. Now, the unconditional characteristic function of the MTJ term is

$$\Phi_{MTJ}\left(\omega\right) = \prod_{l=1}^{L_A}\left(\Phi^{MTJ}_{0,1,l}\left(\omega\right)\Phi^{MTJ}_{1,2,l}\left(\omega\right)\Phi^{MTJ}_{0,2,l}\left(\omega\right)\Phi^{MTJ}_{1,1,l}\left(\omega\right)\right) \tag{5.14}$$

where $\Phi_{0,1,l}^{MTJ}(\omega)$, $\Phi_{1,2,l}^{MTJ}(\omega)$, $\Phi_{0,2,l}^{MTJ}(\omega)$, and $\Phi_{1,1,l}^{MTJ}(\omega)$ can be easily obtained from $\Phi_{0,1,l}^{noise}(\omega)$, $\Phi_{1,2,l}^{noise}(\omega)$, $\Phi_{0,2,l}^{noise}(\omega)$, and $\Phi_{1,1,l}^{noise}(\omega)$ by replacing the term N_0 with Λ in each of them. Finally, the unconditional characteristic function of the required data term can be obtained as [46]

$$\Phi_{data}(\omega)=\prod_{l=1}^{L_A}\prod_{p=1}^{2}\prod_{v=0}^{1}\left(j\frac{\sqrt{2}b_{v,p,l}^2}{4A_1\omega}\right)^{1/2\left(M_{v,p,l}+m_{v,p,l}-1\right)}\exp\left(j\frac{\sqrt{2}b_{v,p,l}^2}{8A_1\omega}\right)$$
$$\times W_{-\frac{1}{2}\left(M_{v,p,l}+m_{v,p,l}-1\right),\frac{1}{2}\left(M_{v,p,l}-m_{v,p,l}\right)}\left(j\frac{\sqrt{2}b_{v,p,l}^2}{4A_1\omega}\right). \quad (5.15)$$

Furthermore, we observe that the BER expression in (5.15) is valid for any arbitrary fading and shadowing parameters. It should also be noted that (5.7)-(5.15) can be applied to the slow-fading case by assuming fixed channel fading coefficients over a duration of at least two consecutive symbols [64], i.e., $x_{0,1,l}=x_{1,1,l}$.

In the following, we consider a special case under slow and flat fading conditions in the absence of shadowing effects, i.e., when $M\to\infty$. Under slow-fading conditions the channel fading coefficients are assumed to be fixed over a duration of at least two consecutive symbols, i.e., $x_{0,1,l}=x_{1,1,l}$. Furthermore, the generalized-K fading channel can be described as the Nakagami-m fading channel in the absence of shadowing conditions [20]. We further assume random fading variables of the desired user's signal in various branches of the receiver to be identically distributed as well as independent. Hence, similar to the approach in Section 3.2.3, the PDF of the random fading variable $X_{L_A}=\sum_{l=1}^{L_A}\sum_{p=1}^{2}x_{p,l}^2=\sum_{l=1}^{L_A}\left(x_{2,l}^2+x_{1,l}^2\right)$ is [43]

$$f_{X_{L_A}}(x) = \frac{1}{\Gamma(2mL_A)}\left(\frac{m}{\mathrm{E}\left(X_1^2\right)}\right)^{2mL_A} \exp\left(\frac{-m}{\mathrm{E}\left(X_1^2\right)}\right) x^{2mL_A-1}, \qquad \text{for } x > 0. \tag{5.16}$$

By using (5.16), the unconditional BER expression based on the Gaussian approximation is [43]

$$P_e \approx \int_0^{\infty} Q\left(\sqrt{2C_M X_{L_A}}\right) f_{X_{L_A}}(x)\, dx$$

$$P_e \approx \frac{\Gamma\left(2mL_A + \frac{1}{2}\right)}{4\sqrt{\pi} mL_A \Gamma(2mL_A)}\left[\frac{m}{C_M\ \mathrm{E}\left(X_1^2\right)}\right]^{2mL_A}$$

$$\times\, {}_2F_1\left(2mL_A, 2mL_A + \frac{1}{2}; 2mL_A + 1; \frac{-m}{C_M\ \mathrm{E}\left(X_1^2\right)}\right) \tag{5.17}$$

where the parameter C_M in (5.17) is defined as $C_M = \dfrac{(A_1)^2}{2(\Lambda + N_0)\left(\left[\mathbf{R}^{-1}\right]_{1,1} + \left[\mathbf{R}^{-1}\right]_{2,2}\right)}$, and m is the small-scale fading parameter. The simplified BER expression in (5.17) is valid for arbitrary number of branches as well as arbitrary values of small-scale fading parameter m.

Now, due to the noise enhancement effects of the decorrelator [6], minimum mean-square error (MMSE) multiuser detector is also incorporated in this section to improve the overall BER performance. We can obtain the MMSE matrix by using the standard Wiener solution as [48]

$$\mathbf{V}_v^l = \mathbf{A}^{\mathrm{T}}\mathbf{H}_v^l \left(\mathbf{H}_v^l\right)^{\mathrm{T}} \mathbf{R}^{\mathrm{T}}\left[\mathbf{R}\ \mathbf{H}_v^l \mathbf{A}\mathbf{A}^{\mathrm{T}} \left(\mathbf{H}_v^l\right)^{\mathrm{T}} \mathbf{R}^{\mathrm{T}} + N_0\mathbf{R} + \Lambda\mathbf{R}\right]^{-1}. \tag{5.18}$$

The outputs from the bank of matched filters in (5.3) are processed by the MMSE stage as [6]

$$\mathbf{V}_v^l \mathbf{Y}_v^l = \mathbf{V}_v^l \mathbf{R} \mathbf{A} \mathbf{H}_v^l \mathbf{d} + \mathbf{V}_v^l \mathbf{I}_v^l + \mathbf{V}_v^l \mathbf{N}_v^l. \tag{5.19}$$

Now, by assuming that we have perfect channel information at the receiver side [6], the outputs in (5.19) are then weighted by their respective independent fading gains and are combined based on the principle of MRC. With user 1 as our desired user and $d_1 = +1$ as the transmitted bit, the BER expression based on Gaussian approximation is [48]

$$P_e \approx \mathrm{E}\left(Q\left(\frac{\sum_{l=1}^{L_A} \lambda_l}{\sqrt{\sum_{l=1}^{L_A} \left(\varphi_{l,\mathbf{N}} + \varphi_{l,\mathbf{M}} \right)}} \right) \right) \tag{5.20}$$

where various parameters in (5.20) are given as,

$$\lambda_l = \left(x_{0,1,l} \left[\mathbf{V}_0^l \mathbf{R} \mathbf{A} \mathbf{H}_0^l \mathbf{d} \right]_1 + x_{0,2,l} \left[\mathbf{V}_0^l \mathbf{R} \mathbf{A} \mathbf{H}_0^l \mathbf{d} \right]_2 + x_{1,2,l} \left[\mathbf{V}_1^l \mathbf{R} \mathbf{A} \mathbf{H}_1^l \mathbf{d} \right]_1 + x_{1,1,l} \left[\mathbf{V}_1^l \mathbf{R} \mathbf{A} \mathbf{H}_1^l \mathbf{d} \right]_2 \right),$$

$$\varphi_{l,\mathbf{N}} = \left[\left(x_{0,1,l} \right)^2 N_0 \mathbf{V}_0^l \mathbf{R} \left(\mathbf{V}_0^l \right)^{\mathrm{T}} \right]_{1,1} + \left[\left(x_{0,2,l} \right)^2 N_0 \mathbf{V}_0^l \mathbf{R} \left(\mathbf{V}_0^l \right)^{\mathrm{T}} \right]_{2,2}$$

$$+ \left[\left(x_{1,1,l} \right)^2 N_0 \mathbf{V}_1^l \mathbf{R} \left(\mathbf{V}_1^l \right)^{\mathrm{T}} \right]_{2,2} + \left[\left(x_{1,2,l} \right)^2 N_0 \mathbf{V}_1^l \mathbf{R} \left(\mathbf{V}_1^l \right)^{\mathrm{T}} \right]_{1,1},$$

and

$$\varphi_{l,\mathbf{M}} = \left[\left(x_{0,1,l} \right)^2 \Lambda \mathbf{V}_0^l \mathbf{R} \left(\mathbf{V}_0^l \right)^{\mathrm{T}} \right]_{1,1} + \left[\left(x_{0,2,l} \right)^2 \Lambda \mathbf{V}_0^l \mathbf{R} \left(\mathbf{V}_0^l \right)^{\mathrm{T}} \right]_{2,2}$$

$$+ \left[\left(x_{1,1,l} \right)^2 \Lambda \mathbf{V}_1^l \mathbf{R} \left(\mathbf{V}_1^l \right)^{\mathrm{T}} \right]_{2,2} + \left[\left(x_{1,2,l} \right)^2 \Lambda \mathbf{V}_1^l \mathbf{R} \left(\mathbf{V}_1^l \right)^{\mathrm{T}} \right]_{1,1}.$$

Note that the notation $\left[\mathbf{d} \right]_l$ represents the l-th entry of the vector $\mathbf{d}$ and $\mathrm{E}(.)$ represents expectation. It should also be noted that numerical techniques will be required to solve (5.20). It can be observed from above analysis that MMSE-based multiuser receiver improves BER performance by taking into consideration the effects of noise and MTJ.

However, BER performance improvement is achieved at the expanse of more complicated system design.

5.3 BER Analysis of Asynchronous Space-Time Multiuser Systems over Frequency-Selective Multipath Channels

We consider an asynchronous band-limited DS-CDMA system with K_u users. A similar space-time spreading system as in Section 5.2 is assumed in this section. A fast frequency-selective fading channel with L_p resolvable paths is assumed here, where fading coefficients are assumed to change independently from one symbol to another [66]. We assume random spreading codes and use a linear decorrelator detector to compensate for the interference arising from signal cross correlations. At the receiver side, each l_A-th antenna has a bank of $2L_r$ filters matched to the delayed versions of the desired user signal, where $L_r \le L_p$. After down-conversion and demodulation, the signal for the l_A-th receive antenna can be written in a matrix form as [66]

$$\mathbf{Y}_v^{l_A} = \mathbf{RAH}_v^{l_A}\mathbf{d} + \mathbf{I}_v^{l_A} + \mathbf{N}_v^{l_A} \tag{5.21}$$

where $\mathbf{Y}_v^{l_A}$ is a $2L_pK_u \times 1$ vector of the output from the matched filters, $\mathbf{R}$ is a $2L_pK_u \times 2L_pK_u$ cross-correlation matrix whose (x,y)-th entry is [15]

$$\beta_{x,y}^{p,q} = T_c \cos\left(\theta_{x,y}\right) \sum_{n=0}^{N-1}\sum_{v=0}^{N-1} c_n^{(x)}\, c_v^{(y)}\, g\left((n-v)T_c - (q-p)T_c - \tau_k\right). \tag{5.22}$$

In (5.22), the parameters p and q represent multipath indexes, τ_k represents the time delay of the k-th user and is uniformly distributed over $[0, T_c]$ [15]. Also, $\theta_{x,y}$ is the random phase uniformly distributed over $[0, 2\pi]$ for the (x,y)-th element of the cross-

correlation matrix. In addition, $c_n^{(x)} \in \{+1,-1\}$ and $c_v^{(y)} \in \{+1,-1\}$ are respectively the n-th and v-th chips of the random sequences corresponding to the (x,y)-th element of the correlation matrix. The matrix $\mathbf{A}$ is a $2L_pK_u \times 2L_pK_u$ diagonal matrix containing K_u users' amplitudes, $\mathbf{d}$ is a $2L_pK_u \times 1$ vector containing data bits of K_u users, and $\mathbf{I}_v^{l_A}$ and $\mathbf{N}_v^{l_A}$ are $2L_pK_u \times 1$ MTJ and Gaussian noise vectors, respectively. The channel matrix $\mathbf{H}_v^{l_A}$ is a $2L_pK_u \times 2L_pK_u$ diagonal matrix defined as [64], [66]

$$\mathbf{H}_v^{l_A} = \text{diag}\left[\mathbf{h}_{v,1,1}^{l_A},\ldots,\mathbf{h}_{v,L_p,1}^{l_A},\ldots,\mathbf{h}_{v,1,k}^{l_A},\ldots,\mathbf{h}_{v,L_p,k}^{l_A}\right]. \tag{5.23}$$

The 2×2 matrices $\mathbf{h}_{v,l_p,k}^{l_A}$ are [64], [66]

$$\mathbf{h}_{0,l_p,k}^{l_A} = \begin{bmatrix} x_{0,1,l_p,l_A,k} & -x_{0,2,l_p,l_A,k} \\ x_{0,2,l_p,l_A,k} & x_{0,1,l_p,l_A,k} \end{bmatrix} \tag{5.24}$$

and

$$\mathbf{h}_{1,l_p,k}^{l_A} = \begin{bmatrix} x_{1,2,l_p,l_A,k} & -x_{1,1,l_p,l_A,k} \\ x_{1,1,l_p,l_A,k} & x_{1,2,l_p,l_A,k} \end{bmatrix} \tag{5.25}$$

where the entry $x_{v,p,l_p,l_A,k}$ represents the independent generalized-K random fading parameter, the subscripts v, p, l_p, l_A and k indicate the indexes of time, transmitter antenna, multipath, receiver antenna and the user, respectively. We assume various fading variables to be independent of each other in our BER analysis. We also assume user 1 as our desired user and $d_1 = +1$ is the desired bit. Thus, we will drop the subscript for the user in the subsequent part of our discussion. We first apply the decorrelation operation on (5.21) and then combine the outputs from the decorrelator stage based on the MRC

technique. With the help of [64]-[66] and after some algebraic manipulations, the conditional SINR expression can be obtained as

$$SINR_{v,p,l_r,l_A} = \frac{\left(A_1/\sqrt{2}\right)^2 \left(\sum_{v=0}^{1} \sum_{p=1}^{2} \sum_{l_r=1}^{L_r} \sum_{l_A=1}^{L_A} x^2_{v,p,l_r,l_A} \right)^2}{\sigma^2_{\mathbf{N},decorr} + \sigma^2_{MTJ,decorr}} \tag{5.26}$$

where A_1 is the amplitude of the desired user's signal. Here, we assume the MTJ term to follow Gaussian distribution with zero mean and variance of $\sigma^2_{MTJ,decorr}$. In (5.26), the variance terms of Gaussian noise and MTJ can be expressed as

$$\sigma^2_{\mathbf{N},decorr} = N_0 \sum_{l_r=1}^{L_r} \left(\left[\left(\mathbf{R}^{-1} \right)^{\mathrm{T}} \right]_{2l_r-1,2l_r-1} \times \delta \; + \; \left[\left(\mathbf{R}^{-1} \right)^{\mathrm{T}} \right]_{2l_r,2l_r} \times \partial \right) \tag{5.27}$$

and

$$\sigma^2_{MTJ,decorr} = \sum_{l_r=1}^{L_r} \left(\left[\mathbf{M} \right]_{2l_r-1,2l_r-1} \times \delta \; + \; \left[\mathbf{M} \right]_{2l_r,2l_r} \times \partial \right) \tag{5.28}$$

respectively, where

$$\delta = \sum_{l_A=1}^{L_A} \left(x^2_{0,1,l_r,l_A} + x^2_{1,2,l_r,l_A} \right) \tag{5.29}$$

and

$$\partial = \sum_{l_A=1}^{L_A} \left(x^2_{0,2,l_r,l_A} + x^2_{1,1,l_r,l_A} \right). \tag{5.30}$$

Furthermore, $\mathbf{M} = \mathbf{R}^{-1}\mathbf{X}\left(\mathbf{R}^{-1}\right)^{\mathrm{T}}$ where $\mathbf{X}$ is the MTJ correlation matrix whose (x,y)-th entry for (p,q)-th multipath is [15]

$$\psi^{p,q}_{x,y} = \Lambda T_c \sum_{n=0}^{N-1} \sum_{v=0}^{N-1} c_n^{(x)} c_v^{(y)} \cos\left[2\pi \Delta f_i \left\{ (n-v)T_c - (q-p)T_c - \tau_k \right\} - \theta_{x,y} \right], \tag{5.31}$$

where

$$\Lambda = 2\sum_{i=1}^{J}\left(\frac{\alpha_i^2 G(\Delta f_i) M_{(i)} m_{(i)}}{b_{(i)}^2}\right). \tag{5.32}$$

In order to derive the unconditional BER expression, we use the following inversion formula [19]

$$P_e \approx \frac{1}{2} - \frac{1}{\pi}\int_0^{\infty} \frac{\Phi_{noise}(\omega)\Phi_{MTJ}(\omega)\Im\left(\Phi_{data}(\omega)\right)}{\omega}\, d\omega. \tag{5.33}$$

The unconditional characteristic function of Gaussian noise in (5.33) is given as [6]

$$\Phi_{noise}(\omega) = \prod_{l_A=1}^{L_A}\prod_{l_r=1}^{L_r}\left(\Phi_{0,1,l_r,l_A}^{noise}(\omega)\ \Phi_{1,2,l_r,l_A}^{noise}(\omega)\ \Phi_{0,2,l_r,l_A}^{noise}(\omega)\ \Phi_{1,1,l_r,l_A}^{noise}(\omega)\right). \tag{5.34}$$

Similarly, the characteristic function for the MTJ term in (5.33) can be written as [6]

$$\Phi_{MTJ}(\omega) = \prod_{l_A=1}^{L_A}\prod_{l_r=1}^{L_r}\left(\Phi_{0,1,l_r,l_A}^{MTJ}(\omega)\ \Phi_{1,2,l_r,l_A}^{MTJ}(\omega)\ \Phi_{0,2,l_r,l_A}^{MTJ}(\omega)\ \Phi_{1,1,l_r,l_A}^{MTJ}(\omega)\right). \tag{5.35}$$

In (5.34), the characteristic functions $\Phi_{0,1,l_r,l_A}^{noise}(\omega)$, $\Phi_{1,1,l_r,l_A}^{noise}(\omega)$, $\Phi_{0,2,l_r,l_A}^{noise}(\omega)$ and $\Phi_{1,2,l_r,l_A}^{noise}(\omega)$ are defined as

$$\Phi_{\beta}^{noise}(\omega) = \left(\frac{b_\beta^2}{2\omega^2 N_0\left[\left(\mathbf{R}^{-1}\right)^{\mathrm{T}}\right]_\gamma}\right)^{1/2\left(M_\beta+m_\beta-1\right)} \exp\left(\frac{b_\beta^2}{4\omega^2 N_0\left[\left(\mathbf{R}^{-1}\right)^{\mathrm{T}}\right]_\gamma}\right)$$

$$\times W_{-\frac{1}{2}\left(M_\beta+m_\beta-1\right),\frac{1}{2}\left(M_\beta-m_\beta\right)}\left(\frac{b_\beta^2}{2\omega^2 N_0\left[\left(\mathbf{R}^{-1}\right)^{\mathrm{T}}\right]_\gamma}\right). \tag{5.36}$$

Note that in (5.36), $\beta = 0,1,l_r,l_A$ and $\gamma = 2l_r - 1, 2l_r - 1$ for $\Phi_{0,1,l_r,l_A}^{noise}(\omega)$, $\beta = 1,1,l_r,l_A$ and $\gamma = 2l_r, 2l_r$ for $\Phi_{1,1,l_r,l_A}^{noise}(\omega)$, $\beta = 0,2,l_r,l_A$ and $\gamma = 2l_r, 2l_r$ for $\Phi_{0,2,l_r,l_A}^{noise}(\omega)$ and lastly $\beta = 1,2,l_r,l_A$ and $\gamma = 2l_r - 1, 2l_r - 1$ for $\Phi_{1,2,l_r,l_A}^{noise}(\omega)$. The characteristic functions for the

MTJ terms $\Phi^{MTJ}_{0,1,l_r,l_A}(\omega)$, $\Phi^{MTJ}_{1,2,l_r,l_A}(\omega)$, $\Phi^{MTJ}_{0,2,l_r,l_A}(\omega)$ and $\Phi^{MTJ}_{1,1,l_r,l_A}(\omega)$ can be similarly obtained from $\Phi^{noise}_{0,1,l_r,l_A}(\omega)$, $\Phi^{noise}_{1,2,l_r,l_A}(\omega)$, $\Phi^{noise}_{0,2,l_r,l_A}(\omega)$ and $\Phi^{noise}_{1,1,l_r,l_A}(\omega)$ by replacing $N_0\left[\left(\mathbf{R}^{-1}\right)^{\mathrm{T}}\right]_\gamma$ with $[\mathbf{M}]_\gamma$. Finally, the characteristic function of the required data term in (5.33) can be shown as [8]

$$\Phi_{data}(\omega)=\prod_{l_A=1}^{L_A}\prod_{l_r=1}^{L_r}\prod_{p=1}^{2}\prod_{v=0}^{1}\left(j\frac{\sqrt{2}b^2_{v,p,l_r,l_A}}{4A_1\omega}\right)^{1/2\left(M_{v,p,l_r,l_A}+m_{v,p,l_r,l_A}-1\right)}\exp\left(j\frac{\sqrt{2}b^2_{v,p,l_r,l_A}}{8A_1\omega}\right)$$

$$\times W_{-\frac{1}{2}\left(M_{v,p,l_r,l_A}+m_{v,p,l_r,l_A}-1\right),\frac{1}{2}\left(M_{v,p,l_r,l_A}-m_{v,p,l_r,l_A}\right)}\left(j\frac{\sqrt{2}b^2_{v,p,l_r,l_A}}{4A_1\omega}\right). \quad (5.37)$$

In (5.37), b_{v,p,l_r,l_A}, M_{v,p,l_r,l_A}, and m_{v,p,l_r,l_A} are the generalized-K parameters of the independent random variables x_{v,p,l_r,l_A}. The entries of the matrices $\mathbf{R}^{-1}$ and $\mathbf{X}$ can be determined numerically. It should be noted that (5.33)-(5.37) are also applicable for the slow-fading case by assuming fixed channel fading coefficients over a duration of at least two consecutive symbols [64], i.e., $x_{0,1,l_r,l_A}=x_{1,1,l_r,l_A}$.

5.4 Numerical Results and Discussions

In this section, BER results are presented under various conditions of fading and shadowing. In the analytical and simulation results, we assume the excess bandwidth of the band-limited pulse is assumed to be 100%. We also assume perfect power control, although our results can be extended to non-uniform power cases. We consider random spreading codes with a processing gain of N = 31 and BPSK as the modulation scheme. Our BER analysis can be extended for any value of N as well. We only incorporate BTD

band-limited pulse shape in our numerical results. We assume total jamming power to be uniformly distributed among all jamming tones. We consider similar condition for the MTJ as in previous chapters, i.e., $J = 3$ jamming tones with shadowing parameter fixed at $M_{(i)} = 12$ for $i = 1, 2$ and 3, and the small-scale fading parameters for the three jamming tones are set at $m_{(1)} = 2$, $m_{(2)} = 1$ and $m_{(3)} = 4$. Furthermore, in our simulations, we assume random fading variables of all K_u users to be independent of each other. We also assume various channel fading variables to be perfectly known at the receiver side in order to incorporate MRC. The channel is assumed to be fast fading where the fading coefficients are fixed for the duration of one symbol. The total jamming power is assumed to be equally distributed among all jamming tones. We present the BER plots by averaging over various distinct combinations of random codes for each user. In Figs. 5.1 to 5.8, BER results are presented for the case of MIMO synchronous systems over flat-fading channels with $K_u = 5$. In Figs. 5.9 to 5.14, we analyze MIMO asynchronous case over frequency-selective multipath channel. Both cases of fast and slow fading conditions are analyzed. In Fig. 5.1, analytical and simulation BER results are plotted against E_b/N_0 over a fast-fading channel. We notice a close match between the two results, thus validating our theoretical analysis. In addition, we also observe a slight deviation between analytical and simulation results due to the Gaussian approximation. We further observe that when the small-scale fading parameter, m, is increased, system BER performance is improved. This is due to the fact that for higher values of m, the system is experiencing less severe fading effects of the wireless channel. Furthermore, we also observe flattening of the BER plots as E_b/N_0 value increases, due to the increase in the MTJ effects. In Fig. 5.2, we compare the BER performance under various shadowing conditions while

keeping the small-scale fading parameter fixed. From Fig. 5.2, we observe that the presence of shadowing degrades BER performance. When the shadowing parameter M is increased, we observe that the BER performance is improved. The reason of such behavior is due to the fact that at higher values of M, system is under less severe shadowing effects and thus has better SINR condition.

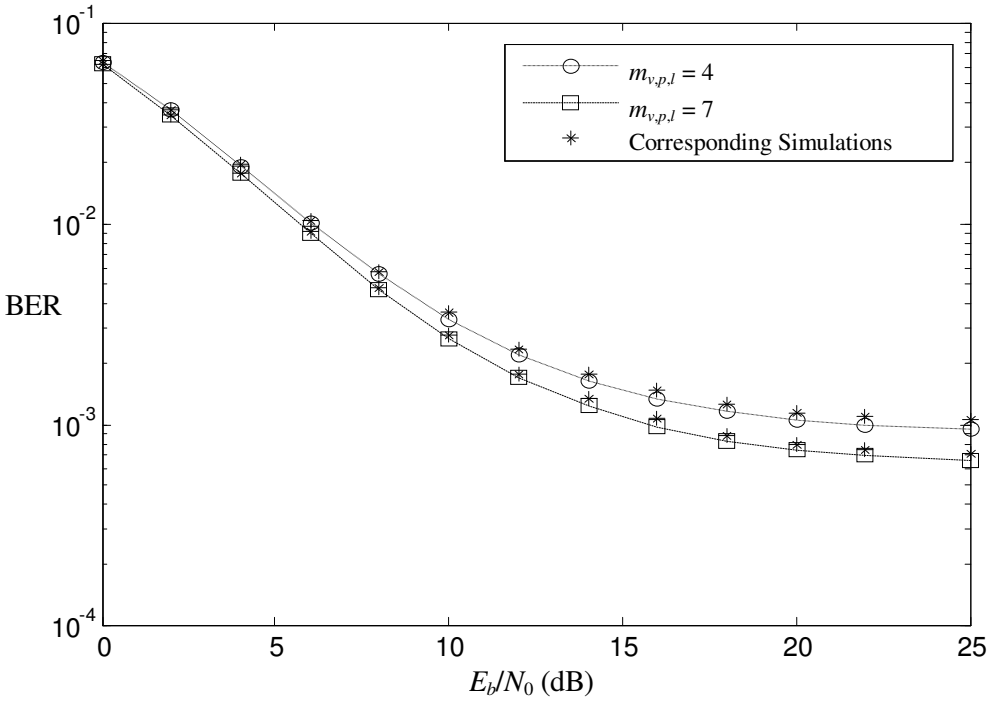

Figure 5.1: Comparison of analytical and simulation results over a fast-fading channel with $M_{v,p,l}$ = 12, L_A = 1 and SJR = -10 dB.

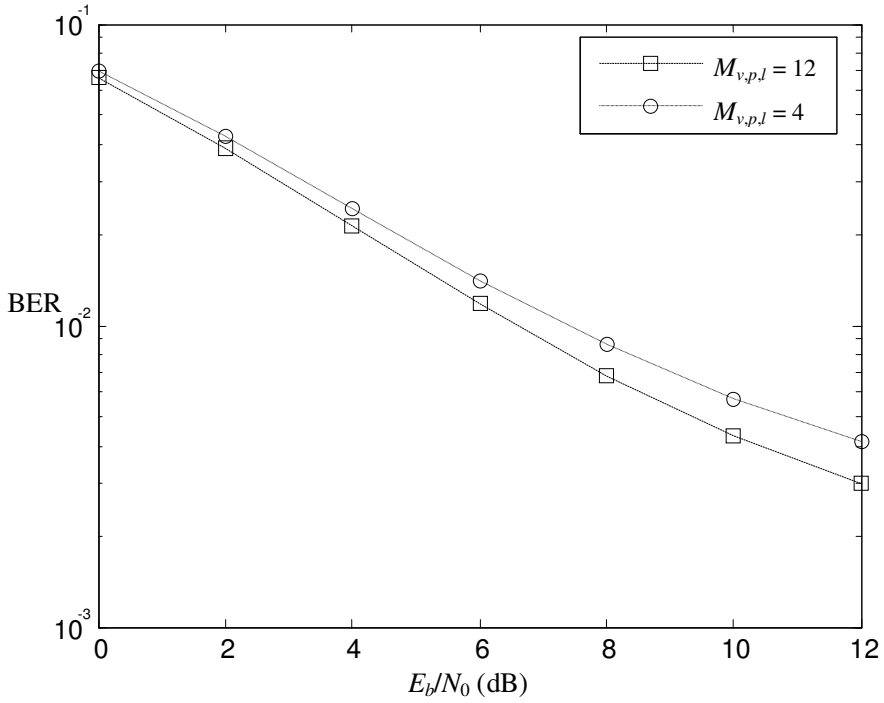

Figure 5.2: BER performance under various shadowing conditions over a fast-fading channel with $m_{v,p,l}$ = 3, L_A = 1 and SJR = -10 dB.

In Fig. 5.3, we compare the BER performance with various number of receiver antennas. From the figure, we observe that as we increase the number of receiver antennas, better BER performance can be achieved due to improved SINR conditions. In Fig. 5.4, we compare the BER performance under slow- and fast-fading conditions. We observe that the systems with fast-fading conditions show better BER performance as compared to the ones with slow-fading conditions. This is due to the fact that the receiver can exploit fast-fading conditions to improve SINR of the system. We also observe such scenario with both shadowing and less shadowing effects.

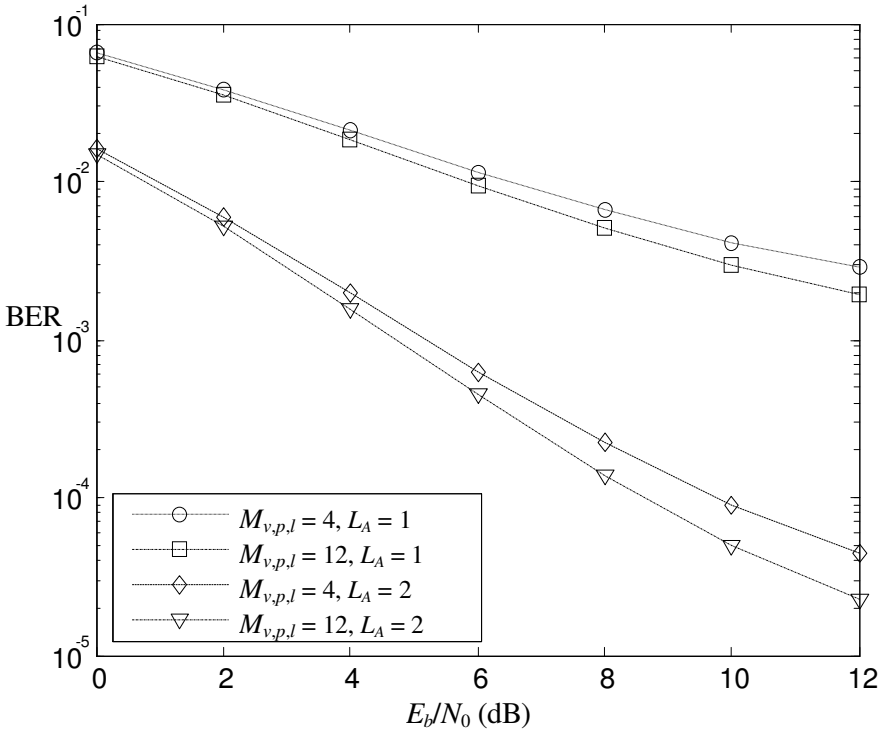

Figure 5.3: BER performance with various number of receiver antennas over a fast-fading channel with $m_{v,p,l}$ = 7 and SJR = -10 dB.

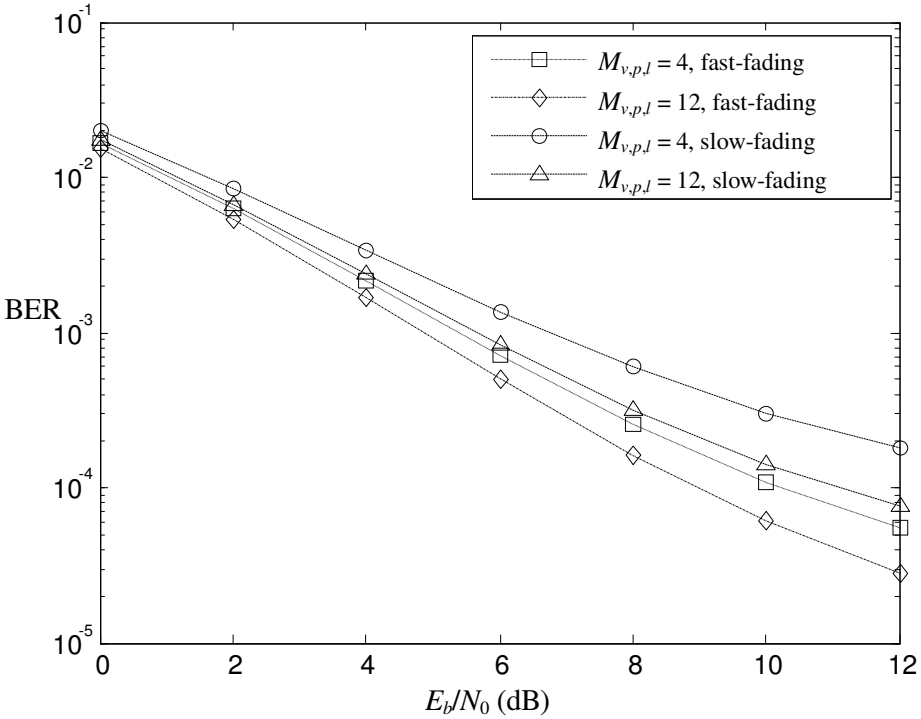

Figure 5.4: Comparison of BER performance under slow- and fast-fading conditions with L_A = 2, $m_{v,p,l}$ = 5 and SJR = -10 dB.

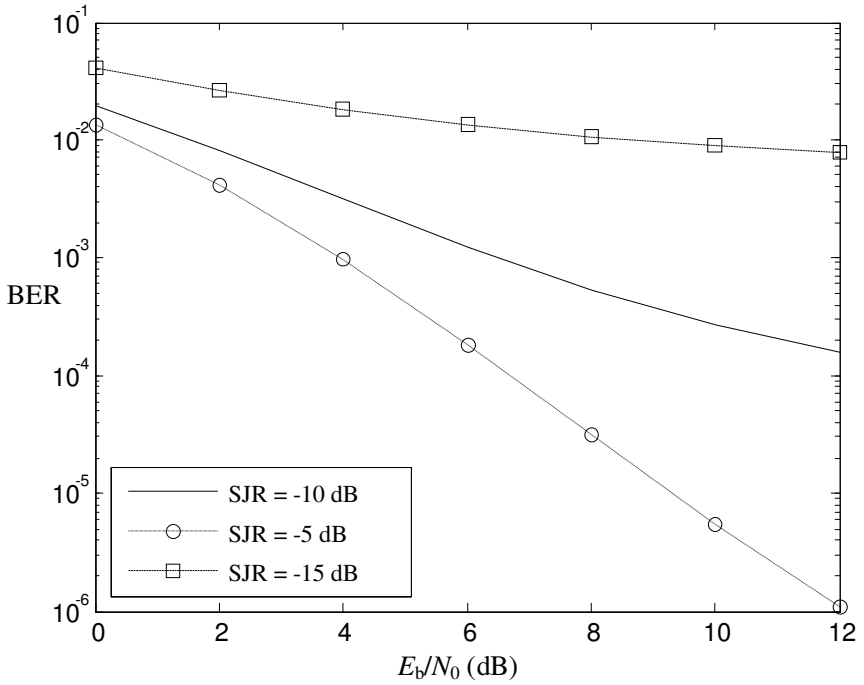

Figure 5.5: BER performance under various jamming conditions over a slow-fading channel with $M_{v,p,l} = 12$, $L_A = 2$ and $m_{v,p,l} = 3$.

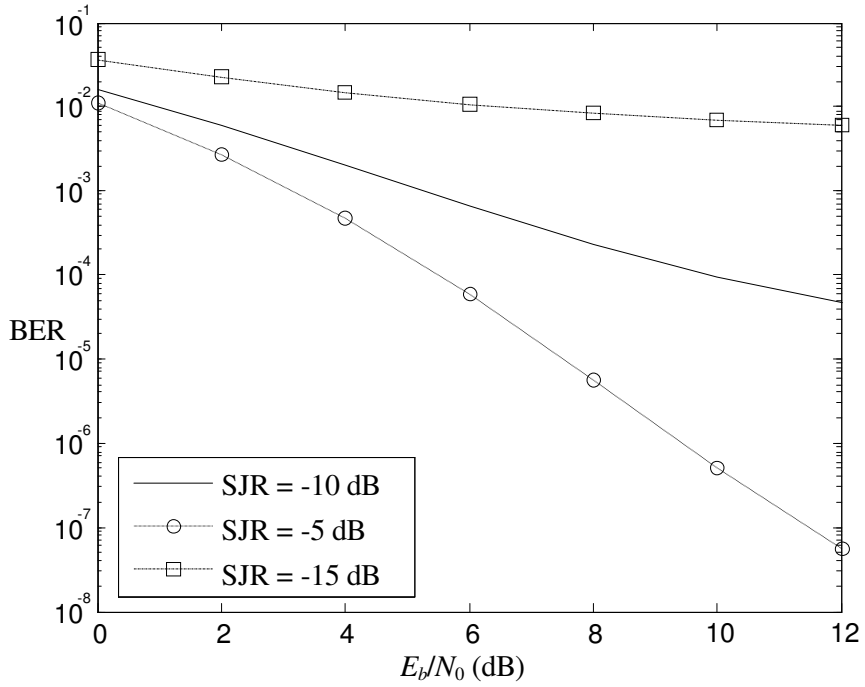

Figure 5.6: BER performance under various jamming conditions with a fast-fading channel, $M_{v,p,l} = 12$, $L_A = 2$ and $m_{v,p,l} = 3$.

In Figs. 5.5 and 5.6, we compare the BER performance under various jamming power conditions for slow- and fast-fading channels, respectively. From these two figures, we observe that both types of systems suffer BER performance degradation under higher jamming power conditions. We further observe a flattening effect of BER plots due to irreducible noise floor introduced by the MTJ. In Fig. 5.7, we compare BER performance over a fast-fading channel with various jamming power and small-scale fading conditions. From Fig. 5.7, we observe that under weaker jamming conditions, BER plots show less flattening effects. We further observe an improvement in BER performance under less severe fading conditions as well, i.e., under larger value of m. In Fig. 5.8, we present BER results of systems with decorrelator and MMSE based detectors under fast-fading conditions. We compare the BER performance of both systems with SJR = -11 dB and SJR = -7 dB. We observe that the MMSE detector outperforms the decorrelator detector due to the fact that the MMSE matrix includes the effects of all types of interference in the system without affecting the diversity order. However, such improvement in performance is achieved at the cost of higher complicated system design. We also observe that the BER performance of decorrelator and MMSE based systems does not converge at high values of E_b/N_0. This is because at higher E_b/N_0 values, the MTJ term becomes dominant. We further observe degradation in the BER performance of both decorrelator and MMSE based systems as jamming condition gets severe. We also observe noticeable flattening of the BER plots for both systems under worse jamming conditions.

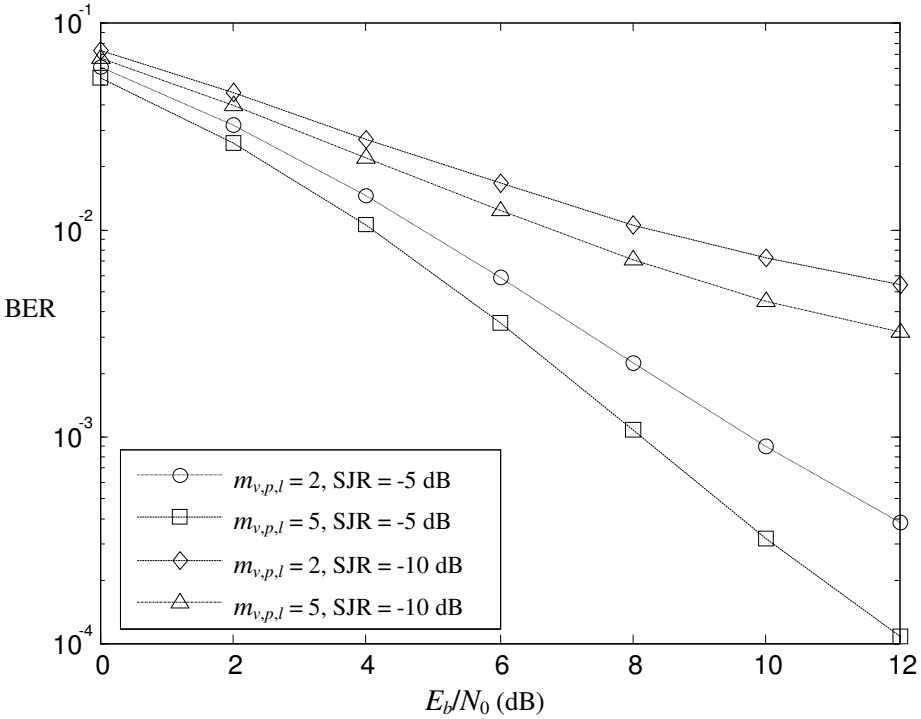

Figure 5.7: Comparison of BER performance over a fast-fading channel with various small-scale fading parameters, $M_{v,p,l}$ = 4 and L_A = 1.

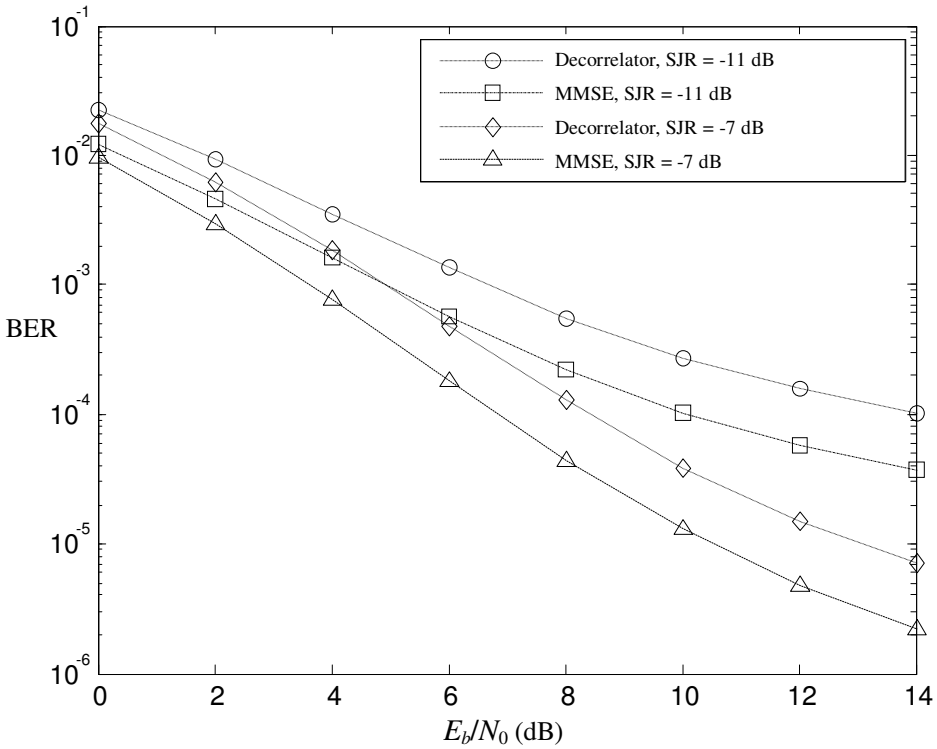

Figure 5.8: Comparison of BER performance of decorrelator and MMSE based receivers over a fast-fading channel, $M_{v,p,l}$ = 12, $m_{v,p,l}$ = 6 and L_A = 1.

For the asynchronous case, we assume similar conditions for the MTJ as for the synchronous case. Random spreading codes with $N = 31$ and BPSK modulation is considered. BTD band-limited pulse shape with excess bandwidth of 100% is employed. We assume $K_u = 3$, $L_p = 3$, $L_r = 2$, $\eta = 0.2$ and perfect power control. In Fig. 5.9, analytical and simulation BER results are plotted against E_b/N_0 over a fast-fading channel. We observe that there is a slight deviation between the two results, thus validating our theoretical analysis. Note that the slight deviation between analytical and simulation results is due to the Gaussian approximation adopted in our theoretical analysis. Moreover, we also observe that with higher value of small-scale fading parameter of the desired user, i.e., m_1, the system BER performance is improved due to better channel fading conditions. In Fig. 5.10, we compare BER performance under various shadowing conditions of the desired user, i.e., M_1, while keeping the other parameters unchanged. It is clear from Fig. 5.10 that the system BER performance degrades under shadowing conditions due to worse SINR conditions. In Fig. 5.11, we compare the BER performance under both slow and fast fading conditions. We observe that the systems with fast-fading show better BER performance as compared to the ones with slow-fading conditions. This is due to the fact that the receiver can exploit fast-fading conditions to improve BER performance. In Fig. 5.12, we compare the BER performance with various jamming power conditions. We fix small-scale fading and shadowing parameters of the system at, $m_1 = 2$ and $M_1 = 4$, respectively. We observe from Fig. 5.12 that BER performance improves when SJR is varied from -10 dB to -5 dB due to weaker jamming power. We further observe a noticeable flattening effect of BER plots at higher jamming power conditions. We observe that the system BER performance degrades noticeably when

jamming conditions get severe. It is due to the fact that when jamming gets severe system SINR conditions degrade. From the figure, we also observe a noticeable flattening of BER plots under the condition of high jamming power and high E_b/N_0 levels. The flattening effect is caused by the irreducible noise floor introduced by the MTJ at higher values of E_b/N_0, because the jamming power becomes dominant at higher E_b/N_0 values. Thus, presence of jamming not only degrades the BER performance but also introduces an irreducible noise floor.

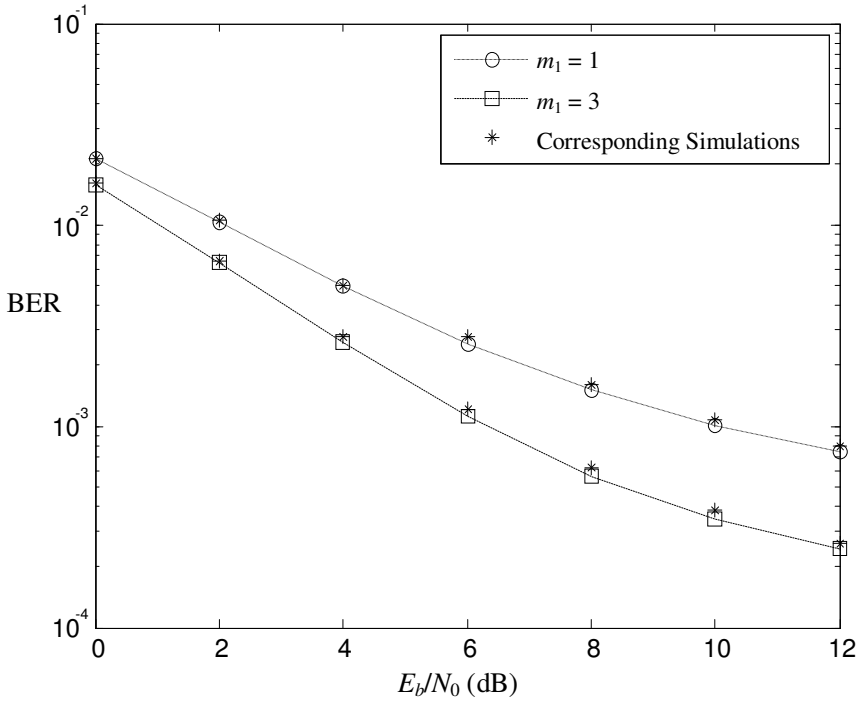

Figure 5.9: Comparisons of analytical and simulation results over a frequency-selective multipath fast-fading channel with $M_1 = 4$, $L_A = 1$ and SJR = -10 dB.

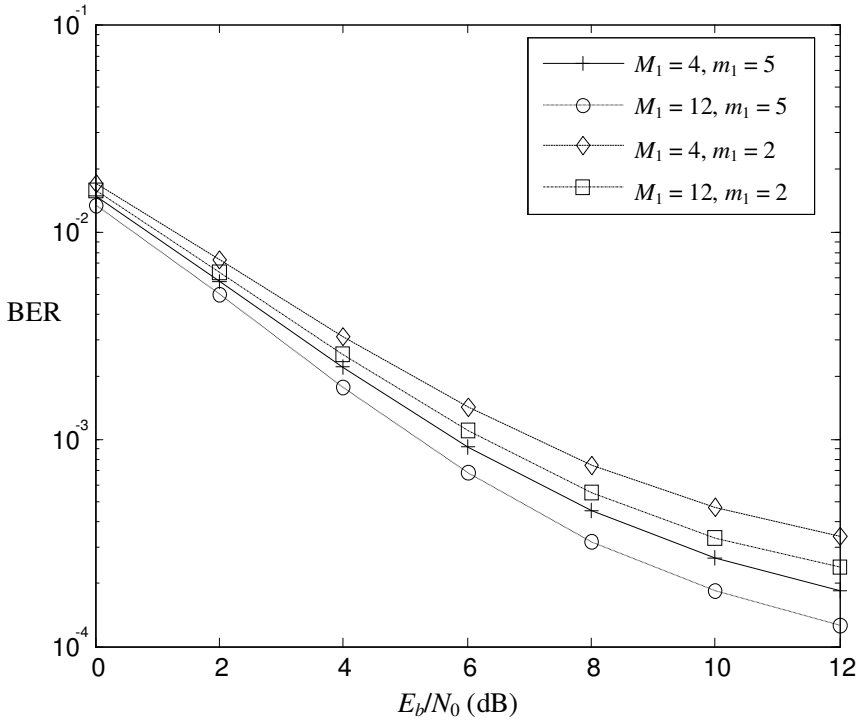

Figure 5.10: BER performance over a fast-fading channel with various combinations of fading parameters, $L_A = 1$ and SJR = -10 dB.

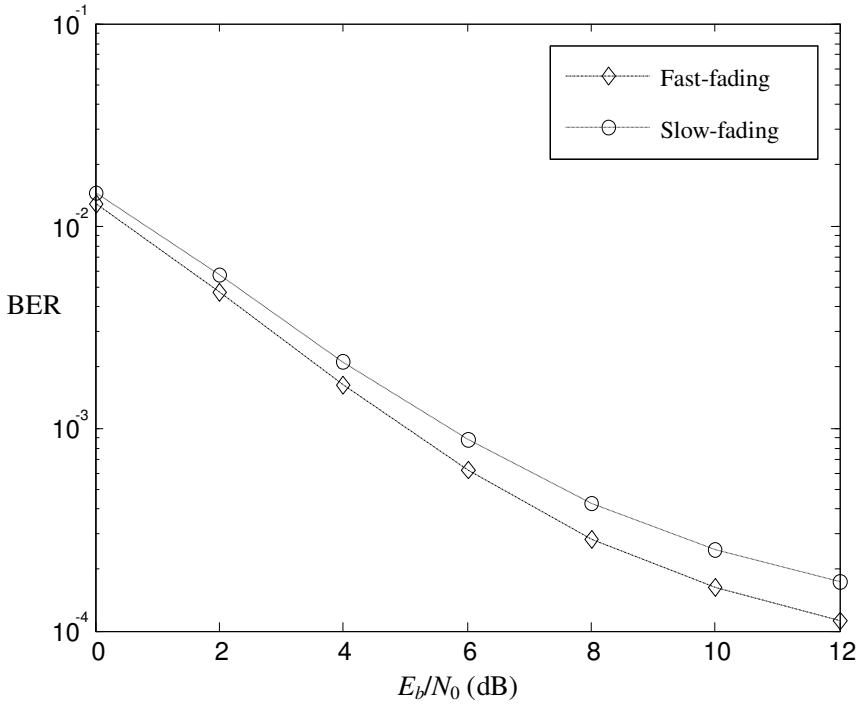

Figure 5.11: BER performance under both slow- and fast-fading conditions with $M_1 = 12$, $m_1 = 7$, $L_A = 1$ and SJR = -10 dB.

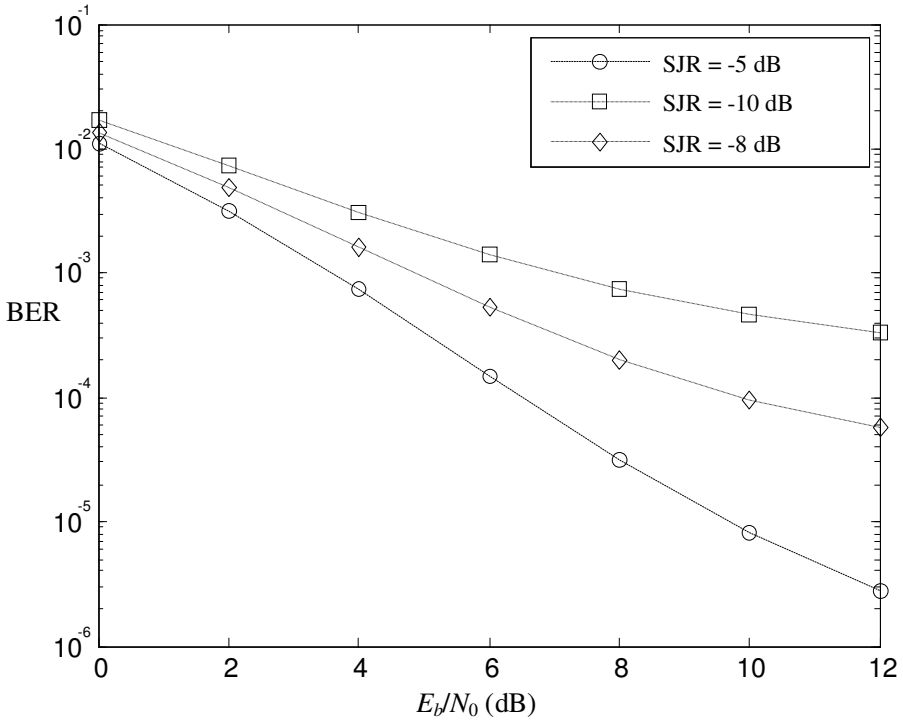

Figure 5.12: BER performance over a fast-fading channel with different SJR levels, $m_1 = 2$, $M_1 = 4$ and $L_A = 1$.

In Fig. 5.13, we compare the BER performance with various number of receiver antennas under various SJR conditions. We observe from Fig. 5.13 that the system BER performance improves as the spatial diversity level increases from $L_A = 1$ to $L_A = 2$. This is because when the number of spatial diversity branches is increased, the system SINR improves and thus the BER performance of the system is improved. In Fig. 5.14, we compare the BER performance with various jamming power conditions for the system with spatial diversity $L_A = 2$. We consider a fast-fading channel with $m_1 = 3$ and $M_1 = 12$. From the figure, we again observe that the BER performance of systems under less severe jamming effects, show less flattening of the BER plots as well as less SINR degradation. However, the systems under severe jamming conditions show visible flattening of the BER plots and the worsening of the system SINR.

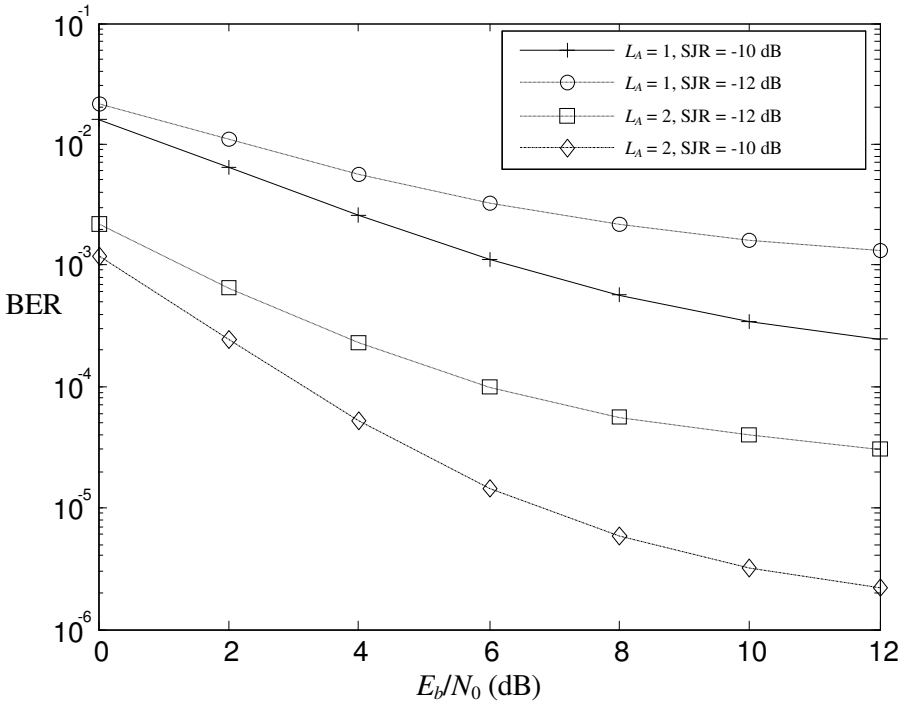

Figure 5.13: BER performance over a fast-fading channel with various combinations of receiver antennas and SJR conditions, $m_1 = 3$ and $M_1 = 4$.

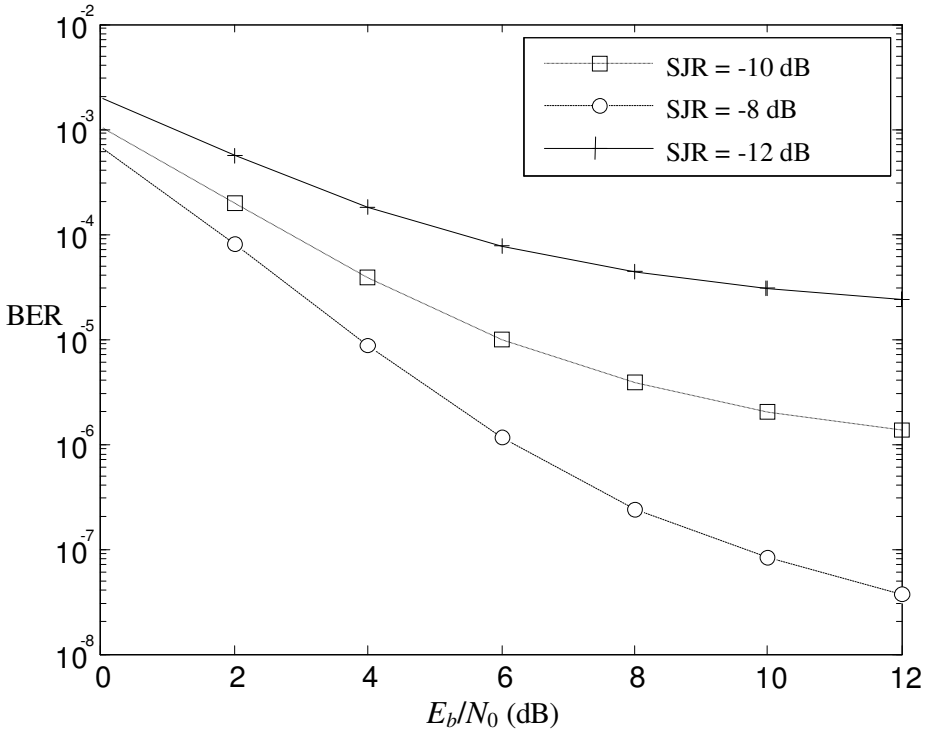

Figure 5.14: BER performance over a fast-fading channel with various jamming conditions, $L_A = 2, m_1 = 3$ and $M_1 = 12$.

5.5 Conclusion

In this chapter, a transmit diversity scheme for band-limited DS-CDMA systems based on space-time spreading has been investigated. We have studied the BER performance of decorrelator and MMSE based systems for slow- and fast-fading channels. Flat and frequency-selective multipath generalized-K fading channels are considered. Analytical BER expressions have been presented as a function of the number of receiver antennas and the characteristics of the multipath fading channel. Due to complexity of the problem considered in this chapter, final BER expressions cannot be further simplified with the help of analytical approaches. Therefore, numerical techniques are used to present numerical results. However, with the help of our BER expressions, we have analyzed the BER performance under low BER ranges, where the simulations are time consuming. Numerical results have shown that the systems under fast-fading show better BER performance for various scenarios of channel fading and shadowing as compared to the systems under slow-fading conditions. We also observe that the MMSE-based scheme shows better BER performance as compared to the one with decorrelator at the expense of more complicated system design. We further observe that the presence of MTJ introduces an irreducible noise floor to the BER plots at higher values of E_b/N_0. However, better BER performance can be achieved by increasing the number of receiver antennas. In addition, we have also observed that the system can exploit both temporal and spatial diversity over a multipath fading channel to combat fading and shadowing conditions.

Chapter 6

Conclusion and Future Work

In this chapter, we present conclusion of our research and the possible direction for the future work.

6.1 Conclusion

In this research, we have analyzed the BER performance of band-limited DS-CDMA systems under composite shadowing and small-scale fading conditions. We have presented analytical BER expressions for these systems under various fading and shadowing conditions using the generalized-*K* fading model. The generalized-*K* model has the advantages of simplicity, accuracy and mathematical tractability when compared with other distributions. In our numerical analysis, we have compared and analyzed the BER performance of various band-limited DS-CDMA systems incorporating two types of band-limited pulse shapes, namely, SRC and BTD, under various conditions of shadowing and small-scale fading. Additional scenario includes interference caused by MTJ, MAI and AWGN.

We first present BER expressions for the case of conventional matched-filter based systems. We consider systems under flat and frequency-selective multipath fading conditions. Systems employing MRC and EGC diversity-combining schemes are considered. Diversity systems based on space, multipath, and the combination of two, i.e., space and multipath, are analyzed. From our numerical analysis, we observe that the

systems with BTD pulse shape outperform the ones with SRC pulse. We further observe that the systems employing two-dimensional diversity outperform the ones with multipath-only diversity. Moreover, we observe that by employing the generalized-*K* distribution, channels with shadowing and small-scale fading effects can be easily analyzed. From the BER plots, we notice that the presence of MTJ and MAI introduces a flattening effect on the BER plots at higher values of SNR. Furthermore, systems based on MRC diversity-combining technique have been shown to outperform the ones with EGC under various scenarios of channel shadowing and fading effects.

Following that, we have extended our BER analysis to the case of linear decorrelator based systems. We consider a frequency-selective multipath fading channel. Both single and two-dimensional diversity schemes have been studied. We incorporate both EGC and MRC based systems. From our numerical analysis, we observe that the decorrelator-based systems outperform the ones without it. We also observe that with decorrelator, systems with BTD pulse outperform the ones with SRC pulse. Moreover, we also observe that the two-dimensional diversity receivers outperform the ones incorporating multipath-only receivers due to the improvement of the overall SINR conditions.

Lastly, we have also extended our BER analysis to the case of MIMO systems, incorporating space-time spreading transmit diversity scheme. We consider MIMO systems with 2-transmitter and multiple receiver antennas. Both the decorrelator and MMSE based MUD schemes are analyzed for the flat-fading case. However, only decorrelator-based system is employed for the asynchronous frequency-selective multipath scenario. Flat as well as frequency-selective multipath fading channels are considered. The systems over both slow and fast fading channels are analyzed. From our

numerical analysis, we observe that the space-time spreading based temporal and spatial diversity technique can exploit both temporal and spatial diversity to enhance system SINR. Numerical results have also shown that the systems under fast-fading condition show better BER performance than the systems under slow-fading condition with various scenarios of fading and shadowing. Now, due to the complexity of the problem considered in this work, various BER expressions presented can only be solved by using numerical techniques. However, as shown in Sections 3.4, 4.3 and 5.4, with the help of our BER expressions, various scenarios of small-scale fading and shadowing for the band-limited DS-CDMA systems can be analyzed. In addition, the derived theoretical expressions allow us to study the performance of the system under low BER ranges, where simulation is time consuming.

6.2 Suggestions for Future Work

In this research, we have considered MIMO asynchronous band-limited DS-CDMA systems with decorrelator-based multiuser detection (MUD) scheme. Analysis of such MIMO systems can be further extended for the linear minimum mean-squared error (MMSE) based systems over frequency-selective multipath fading channels. BER performance of such MMSE-based MIMO systems with jamming can be studied over frequency-selective slow and fast fading channels. Furthermore, we can employ diversity systems based on the adaptive weight adjustments for the combining technique at the receiver side. Implementation of such receiver requires the knowledge of channel parameters as well as that of the interferer. Such an adaptive technique can be incorporated based on the parameters of the fading channel as well as jamming or interference, to optimize the SINR conditions [8].

In addition, by adopting the technique introduced in [67], it is possible to study MIMO band-limited DS-CDMA systems employing convolutional coding technique with MMSE instead of decorrelator-based MUD scheme. BER performance improvement for such MIMO systems over frequency-selective multipath fading channels with interference can be studied. Adaptive gains for the diversity receiver with convolutional coding technique can be employed to maximize SINR conditions. So far in our study, we only consider DS-CDMA systems where weighting is done at the receiver side. In [68], DS-CDMA systems based on the space-time multiuser transmitter precoding have been analyzed. Such scheme can be incorporated in our system such that the transmitter precoding not only takes into consideration the effects of multiuser interference, but jamming as well. BER performance of such band-limited DS-CDMA systems involving multiple transmitter and receiver antennas can be considered such that the transmitted signal is adaptively precoded at the transmitter side to simultaneously combat fading and interference conditions. In this work, we mainly focus on uncorrelated fading channels. This BER analysis can be further extended for the correlated fading scenarios with jamming and various types of diversity-combining techniques [8]. Furthermore, in this research, we analyze BER performance of band-limited DS-CDMA systems over generalized-K channels with the help of Gaussian approximation technique due to its simplicity. BER analysis of such systems can be further extended by employing the improved Gaussian approximation based techniques.

Author's Publication List

1 H. Mehdi, K. C. Teh, and K. H. Li, "Analysis of MIMO band-limited DS-CDMA systems in the presence of multitone jamming over generalized-*K* fading channels," *IEEE Trans. Veh. Technol.*, vol. 58, pp. 3825-3829, Sept. 2009.

2 H. Mehdi, K. C. Teh, and K. H. Li, "Analysis of BPSK modulated asynchronous band-limited DS-CDMA systems with diversity receivers over generalized-*K* fading channels," *IET Commun.*, vol. 3, pp. 1498-1508, Sept. 2009.

3 H. Mehdi, K. C. Teh, and K. H. Li, "Analysis of asynchronous band-Limited DS-CDMA with MMSE multiuser detector over generalized-*K* fading channels," *Wireless Personal Commun.*, accepted for publication.

4 H. Mehdi, K. C. Teh, and K. H. Li, "Effect of chip waveforms on the performance of DS-SS in the presence of multitone jamming over generalized-*K* fading channels," in *Proc. IEEE 6th International Conference on Information, Communications & Signal Processing,* 2007, 10-13 Dec. 2007, pp. 1-5.

5 H. Mehdi, K. C. Teh, and K. H. Li, "Performance analysis of asynchronous band-limited DS-CDMA systems in generalized-*K* fading with multitone jamming," in *Proc. IEEE 6th International Conference on Information, Communications & Signal Processing,* 2007, 10-13 Dec. 2007, pp. 1-5.

References

[1] A. K. Salkintzis, G. Dimitriadis, D. Skyrianoglou, N. Passas, and N. Pavlidou, "Seamless continuity of real-time video across UMTS and WLAN networks: Challenges and performance evaluation," *IEEE Wireless Commun. Mag.*, vol. 12, pp. 8-18, June 2005.

[2] A. K. Salkintzis, "Interworking techniques and architectures for WLAN/3G integration toward 4G mobile data networks," *IEEE Wireless Commun. Magazine*, vol. 11, pp. 50-61, June 2004.

[3] J. G. McNeff, "The global positioning system," *IEEE Trans. Microwave Theory and Techniques*, vol. 50, pp. 645-652, Mar. 2002.

[4] A. Papathanassiou, A. K. Salkintzis, and P. T. Mathiopoulos, "A comparison study of the uplink performance of W-CDMA and OFDM for mobile multimedia communications via LEO satellites," *IEEE Personal Commun.*, vol. 8, pp. 35-43, June 2001.

[5] L. B. Milstein, "Wideband code division multiple access," *IEEE J. Select. Areas Commun.*, vol. 18, pp. 1344-1354, Aug. 2000.

[6] J. G. Proakis, *Digital Communiations*, 4th ed. New York: McGrawHill, 2001.

[7] H. Honkasalo, K. Pehkonen, M. T. Niemi, and A. T. Leino, "WCDMA and WLAN for 3G and beyond," *IEEE Wireless Commun. Mag.*, vol. 9, pp. 14-18, Apr. 2002.

[8] M. K. Simon and M. S. Alouini, *Digital Communication Over Fading Channels*. New York: John Wiley & Sons, 2000.

[9] M. Aljerjawi and W. Hamouda, "Performance analysis of space-time diversity in multiuser CDMA systems over fading channels," *Proc. ICC'06*, June 2006, pp. 5622-5627.

[10] S. Verdu, "Minimum probability of error for asynchronous Gaussian multiple access channels," *IEEE Trans. Inform. Theory*, vol. 32, pp. 85-96, Jan. 1986.

[11] R. Lupas and S. Verdu, "Linear multiuser detectors for synchronous code-division multiple-access channels," *IEEE Trans. Inform. Theory*, vol. 35, pp. 123-136, Jan. 1989.

[12] Z. Xie, R. T. Short, and C. K. Rushforth, "A family of suboptimum detectors for coherent multi-user communications," *IEEE J. Select. Areas Commun.*, vol. 8, pp. 683-690, May 1990.

[13] H. H. Nguyen, "An improved design of chip waveforms for band-limited DS-CDMA systems," *IEEE Trans. Veh. Technol.*, vol. 53, pp. 1379-1386, Sept. 2004.

[14] P. I. Dallas and F. N. Pavlidou, "Innovative chip waveforms in microcellular DS/CDMA packet mobile radio," *IEEE Trans. Commun.*, vol. 44, pp. 1413-1416, Nov. 1996.

[15] N. C. Beaulieu and K. Sivanesan, "BER performance of band-limited DS-CDMA systems in Nakagami fading," *IEEE Trans. Commun.*, vol. 54, pp. 2075-2084, Nov. 2006.

[16] Y. C. Yoon, "An improved Gaussian approximation for probability of bit-error analysis of asynchronous band-limited DS-CDMA systems with BPSK spreading," *IEEE Trans. Wireless Commun.*, vol. 1, pp. 373-382, July 2002.

[17] G. Zang and C. Ling "Performance evaluation for band-limited DS-CDMA systems based on simplified improved Gaussian approximation," *IEEE Trans. Commun.*, vol. 51, pp. 1204-1213, July 2003.

[18] L. B. Milstein, S. Davidovici, and D. L. Schilling, "The effect of multiple-tone interfering signals on a direct sequence spread spectrum communication system," *IEEE Trans. Commun.*, vol. 30, pp. 436-446, Mar. 1982.

[19] A. Giorgetti, M. Chiani, and M. Z. Win, "The effect of narrowband interference on wideband wireless communication systems," *IEEE Trans. Commun.*, vol. 53, pp. 2139-2149, Dec. 2005.

[20] P. M. Shankar, "Error rates in generalized shadowed fading channels," *Wireless Personal Commun.*, vol. 28, pp. 233–238, Feb. 2004.

[21] I. M. Kostic, "Analytical approach to performance analysis for channel subject to shadowing and fading," *IEE Proc. Commun.*, vol. 152, pp. 821-827, Dec. 2005.

[22] N. C. Beaulieu, C. C. Tan, and M. O. Damen, "A "better than" Nyquist pulse," *IEEE Commun. Lett.*, vol. 5, no. 9, pp. 367-368, Sept. 2001.

[23] W. Hamouda and M. Aljerjawi, "A transmit diversity scheme using space–time spreading for DS-CDMA systems in Rayleigh fading channels," *Proc. IEEE Veh. Technol. Conf.*, Sept. 2005, pp. 147-151.

[24] T. Eng and L. B. Milstein, "Coherent DS-CDMA performance in Nakagami multipath fading," *IEEE Trans. Commun.*, vol. 43, pp. 1134-1143, Feb./Mar./Apr. 1995.

[25] A. A. Abu-Dayya and N. C. Beaulieu, "Micro- and macrodiversity NCFSK (DPSK) on shadowed Nakagami-fading channels," *IEEE Trans. Commun.*, vol. 42, pp. 2693-2702, Sept. 1994.

[26] C. Tellambura, A. J. Mueller, and V. K. Bhargava, "Analysis of M-ary phase-shift keying with diversity reception for land mobile satellite channels," *IEEE Trans. Veh. Technol.*, vol. 46, pp. 910-922, Nov. 1997.

[27] A. Abdi and M. Kaveh, "On the utility of the gamma PDF in modeling shadow fading (slow fading)," in *Proc. IEEE 49th VTC*, vol. 3, May 16-20, 1999, pp. 2308-2312.

[28] P. S. Bithas, N. C. Sagias, P. T. Mathiopoulos, G. K. Karagiannidis, and A. A. Rontogiannis, "On the performance analysis of digital communications over generalized-*K* fading channels," *IEEE Commun. Lett.*, vol. 10, pp. 353-355, May 2006.

[29] A. Abdi and M. Kaveh, "Comparison of DPSK and MSK bit error rates for *K* and Rayleigh-lognormal fading distributions," *IEEE Commun. Lett.*, vol. 4, pp. 122-124, Apr. 2000.

[30] T. Piboongungon, V. A. Aalo, C.-D. Iskander, and G. P. Efthymoglou, "Bivariate generalized gamma distribution with arbitrary fading parameters," *Electron. Lett.*, vol. 41, pp. 709-710, June 2005.

[31] N. C. Sagias, G. K. Karagiannidis, P. T. Mathiopoulos, and T. A. Tsiftsis, "On the performance analysis of equal-gain diversity receivers over generalized gamma fading channels," *IEEE Trans. Wireless Commun.*, vol. 5, pp. 2967-2975, Oct. 2006.

[32] D. Dardari and G. Pasolini, "Simple and accurate models for error probability evaluation of IEEE 802.11 DS-SS physical interface in the presence of Bluetooth interference," in *Proc. IEEE Global Telecommun. Conf.*, Taipei, Taiwan, R.O.C., vol. 1, Nov. 2002, pp. 201-206.

[33] G. J. Foschini and M. J. Gans, "On limits of wireless communication in a fading environment when using multiple antennas," *Wireless Personal Commun.*, vol. 6, pp. 311-335, Mar. 1998.

[34] V. Tarokh, N. Seshadri, and A. R. Calderbank, "Space-time codes for high data rate wireless communication: Performance criterion and code construction," *IEEE Trans. Inform. Theory*, vol. 44, pp. 774-765, Mar. 1998.

[35] V. Tarokh, H. Jafarkhani, and A. R. Calderbank, "Space-time block codes from orthogonal designs," *IEEE Trans. Inform. Theory*, vol. 45, pp. 1456-1467, July 1999.

[36] S. M. Alamouti, "A simple transmit diversity technique for wireless communications," *IEEE J. Select. Areas Commun.*, vol. 16, pp. 1451-1458, Oct. 1998.

[37] B. Hochwald, T. Marzetta, and C. Papadias, "A transmitter diversity scheme for wideband CDMA systems based on space-time spreading," *IEEE J. Select. Areas Commun.*, vol. 19, pp. 1451-1458, Jan. 2001.

[38] G. L. Stuber, *Principles of Mobile Communication*, 2nd ed. Norwell, MA: Kluwer, 2001.

[39] C. Kchao and G. L. Stuber, "Analysis of a direct-sequence spread spectrum cellular radio system," *IEEE Trans. Commun.*, vol. 41, pp. 1507-1516, Oct. 1993.

[40] E. Ozturk, "Performance analysis of asynchronous direct sequence code division multiple access for general chip waveforms over multi-path Rayleigh fading channels," *IET Commun*., vol. 1, pp. 570-576, Aug. 2007.

[41] H. Wei and L. Hanzo, "On the uplink performance of band-limited DS-CDMA systems using RAKE-receiver over Nakagami-m channels," in *Proc*. 5-th *IEE Conf. on* 3G *Mobile Communication Technologies* 2004, pp. 312-316.

[42] K. Sivanesan and N. C. Beaulieu, "Accurate BER analysis of bandlimited DS-CDMA system with EGC and SC diversity over Nakagami fading channels," in *Proc*. *IEEE WCNC* 2005, vol. 2, 2005, pp. 956-960.

[43] K. Sivanesan and N. C. Beaulieu, "Performance analysis of bandlimited DS-CDMA systems with diversity receivers over Nakagami fading channels," in *Proc*. *IEEE MILCOM* 2004, vol. 3, 2004, pp.1206-1212.

[44] H. Wei, L. L. Yang, and L. Hanzo, "On the performance of band-limited asynchronous DS-CDMA over Nakagami-*m* channels," *IEEE Trans. Wireless Commun*., vol. 5, pp. 1586-1593, July 2006.

[45] R. H. Dou and L. B. Milstein, "Error probability bounds and approximations for DS spread-spectrum communication systems with multiple tone or multiple access interference," *IEEE Trans. Commun.*, vol. 32, pp. 493-502, May 1984.

[46] I. S. Gradshteyn and I. M. Ryzhik, *Table of Integrals, Series, and Products*, 6-th ed. San Diego: Academic Press, 2000.

[47] J. Gil-Pelaez, "Note on the inversion theorem," *Biometrika*, vol. 38, pp. 481-482, Dec. 1951.

[48] S. Verdu, *Multiuser Detection*. Cambridge, U.K.: Cambridge Univ. Press, 1998.

[49] D. S. Chen and S. Roy, "An adaptive multiuser receiver for CDMA systems," *IEEE J. Select. Areas Commun.*, vol. 12, pp. 808-816, June 1994.

[50] A. Duel-Hallen, "Decision-feedback multiuser detector synchronous for code-division multiple access channel," *IEEE Trans. Commun.*, vol. 41, pp. 285-290, Feb. 1993.

[51] R. Lupas and S. Verdu, "Near-far resistance of multiuser detectors in asynchronous channels," *IEEE Trans. Commun.*, vol. 38, pp. 496-508, Apr. 1990.

[52] M. K. Varanasi and B. Aazhang, "Near-optimum detection in synchronous code-division multiple-access systems," *IEEE Trans. Commun.*, vol. 39, pp. 725-736, May 1991.

[53] U. Madhow and M. L. Honig, "MMSE interference suppression for direct-sequence spread-spectrum CDMA," *IEEE Trans. Commun.*, vol. 42, pp. 3178-3188, Dec. 1994.

[54] Z. Zvonar and D. Brady, "Suboptimal multiuser detector for frequency selective Rayleigh fading synchronous CDMA channels," *IEEE Trans. Commun.*, pp. 154-157, vol. 43, Feb.-Mar.-Apr. 1995.

[55] Z. Zvonar and D. Brady, "Linear multipath-decorrelating receivers for CDMA frequency-selective fading channels," *IEEE Trans. Commun.*, pp. 650-653, vol. 44, June 1996.

[56] Z. Zvonar, "Combined multiuser detection and diversity reception for wireless CDMA systems," *IEEE Trans. Veh. Technol.*, pp. 205-211, vol. 45, Feb. 1996.

[57] M. Stojanovic and Z. Zvonar, "Performance of multiuser diversity reception in Rayleigh fading CDMA channels," *Trans. Commun.*, pp. 356-359, vol. 47, Mar. 1996.

[58] R. Song and S. H. Leung, "Second order polynomial class of chip waveforms for band-limited DS-CDMA systems," *Wireless Personal Commun.*, vol. 43, pp. 655-663, Oct. 2007.

[59] R. Michael, R. A. Soni, and R. D. Benning, "Transmit diversity for combined 2G and 3G CDMA systems," *IEEE Trans. Commun.*, vol. 52, pp. 1648-1653, Oct. 2004.

[60] L. Yang, "MIMO-assisted space-code-division multiple-access: Linear detectors and performance over multipath fading channels," *IEEE J. Select. Areas Commun.*, vol. 24, pp. 121-131, Jan. 2006.

[61] K. C. B. Wavegedara, D. V. Djonin, and V. K. Bhargava, "Space-time coded CDMA uplink transmission with MUI-free receptions," *IEEE Trans. on Wireless Commun.*, vol. 4, pp. 3095-3105, Nov. 2005.

[62] P. Chiang, D. Lin, and H. Li, "Performance analysis of two-branch space-time block-coded DS-CDMA systems in time-varying multipath Rayleigh fading channels," *IEEE Trans. Veh. Technol.*, vol. 56, pp. 975-986, Mar. 2007.

[63] M. H. Taghavi and B. H. Khalaj, "Interference suppression for space-time coded CDMA via decision-feedback equalization," *IEEE Trans. Veh. Technol.*, vol. 55, pp. 200-206, Jan. 2006.

[64] M. Aljerjawi and W. Hamouda, "Performance analysis of multiuser DS-CDMA in MIMO systems over Rayleigh fading channels," *IEEE Trans. Veh. Technol.*, vol. 57, pp. 1480-1493, May 2008.

[65] A. L. Sacramento and W. Hamouda, "Multiuser decorrelator detectors in MIMO CDMA systems over Nakagami fading channels," *IEEE Trans. on Wireless Commun.*, vol. 8, pp. 1944-1952, Apr. 2009.

[66] A. Assra, W. Hamouda, and A. Youssef, "Space-time spreading and diversity in asynchronous CDMA systems over frequency-selective fading channels," in *Proc. IEEE GLOBECOM* 07, 2007, pp. 1514-1518.

[67] A. L. Sacramento and W. Hamouda, "Performance of multiuser-coded CDMA systems with transmit diversity over Nakagami-*m* fading channels," *IEEE Trans. Veh. Technol.*, vol. 58, pp. 2279 - 2287, June 2008.

[68] S. Guncavdi and A. Duel-Hallen, "Space-time pre-RAKE multiuser transmitter precoding for DS-CDMA systems," in *Proc. IEEE 58th Vehicular Technology Conf.*, vol. 4, 2003, pp. 2411 - 2415.